The Sol–Gel Process

LARRY L. HENCH* and JON K. WEST

Department of Materials Science and Engineering, Advanced Materials Research Center, University of Florida, Gainesville, Florida 32611

Received May 16, 1989 (Revised Manuscript Received October 27, 1989)

Contents

Larry L. Hench is a Graduate Research Professor in the Department of Materials Science and Engineering at the University of Florida, where he has taught since 1964 after receiving B.S. (1961) and Ph.D. (1964) degrees in Ceramic Engineering at The Ohio State University. He is the Director of the Bioglass Research Center and Co-Director of the Advanced Materials Research Center at the University of Florida. He has published more than 250 research articles and is the coauthor or coeditor of 12 books in the fields of biomaterials, ceramic processing, ceramic characterization, glass surfaces, electronic ceramics, nuclear waste disposal, and sol–gel processing.

Jon K. West received his Ph.D. at the University of Florida in 1979 while working full time as an engineering manager with the Battery Business Department of General Electric Co. His current position is Associate-in-Engineering with the Department of Materials Science and Engineering at the University of Florida. His work in sol–gel silica includes mechanical testing, process control and instrumentation, and theoretical studies based on molecular orbital calculations. He is the author of eight publications including the recently published textbook *Principles of Electronic Ceramics*, by Hench and West, from John Wiley & Sons.

I. Introduction

Interest in the sol–gel processing of inorganic ceramic and glass materials began as early as the mid-1800s with Ebelman[1,2] and Graham's[3] studies on silica gels. These early investigators observed that the hydrolysis of tetraethyl orthosilicate (TEOS), $Si(OC_2H_5)_4$, under acidic conditions yielded SiO_2 in the form of a "glass-like material".[1] Fibers could be drawn from the viscous gel, and even monolithic optical lenses[2] or composites formed.[2] However, extremely long drying times of 1 year or more were necessary to avoid the silica gels fracturing into a fine powder, and consequently there was little technological interest.

For a period from the late 1800s through the 1920s gels became of considerable interest to chemists stimulated by the phenomenon of Liesegang Rings[4,5] formed from gels. Many noted chemists, including Ostwald[6] and Lord Rayleigh,[7] investigated the problem of the periodic precipitation phenomena that lead to the formation of Liesegang rings and the growth of crystals from gels. A huge volume of descriptive literature resulted from these studies[8–10] but a relatively sparse understanding of the physical–chemical principles.[5]

Roy and co-workers[11–14] recognized the potential for achieving very high levels of chemical homogeneity in colloidal gels and used the sol–gel method in the 1950s and 1960s to synthesize a large number of novel ceramic oxide compositions, involving Al, Si, Ti, Zr, etc., that could not be made using traditional ceramic powder methods. During the same period Iler's pioneering work in silica chemistry[15] led to the commercial development of colloidal silica powders, Du Pont's colloidal Ludox spheres. Stober et al.[16] extended Iler's findings to show that using ammonia as a catalyst for the TEOS hydrolysis reaction could control both the morphology and size of the powders, yielding the so-called Stober spherical silica powder.

The final size of the spherical silica powder is a function of the initial concentration of water and ammonia, the type of silicon alkoxide (methyl, ethyl, pentyl, esters, etc.) and alcohol (methyl, ethyl, butyl, pentyl) mixture used,[16] and reactant temperature.[17] An example of a typical colloidal silica powder is shown in Figure 1a, made by the Stober process, and its uniform distribution of particle sizes is shown in Figure 1b from Khadikar and Sacks work.[18]

0009-2665/90/0790-0031$09.50/0

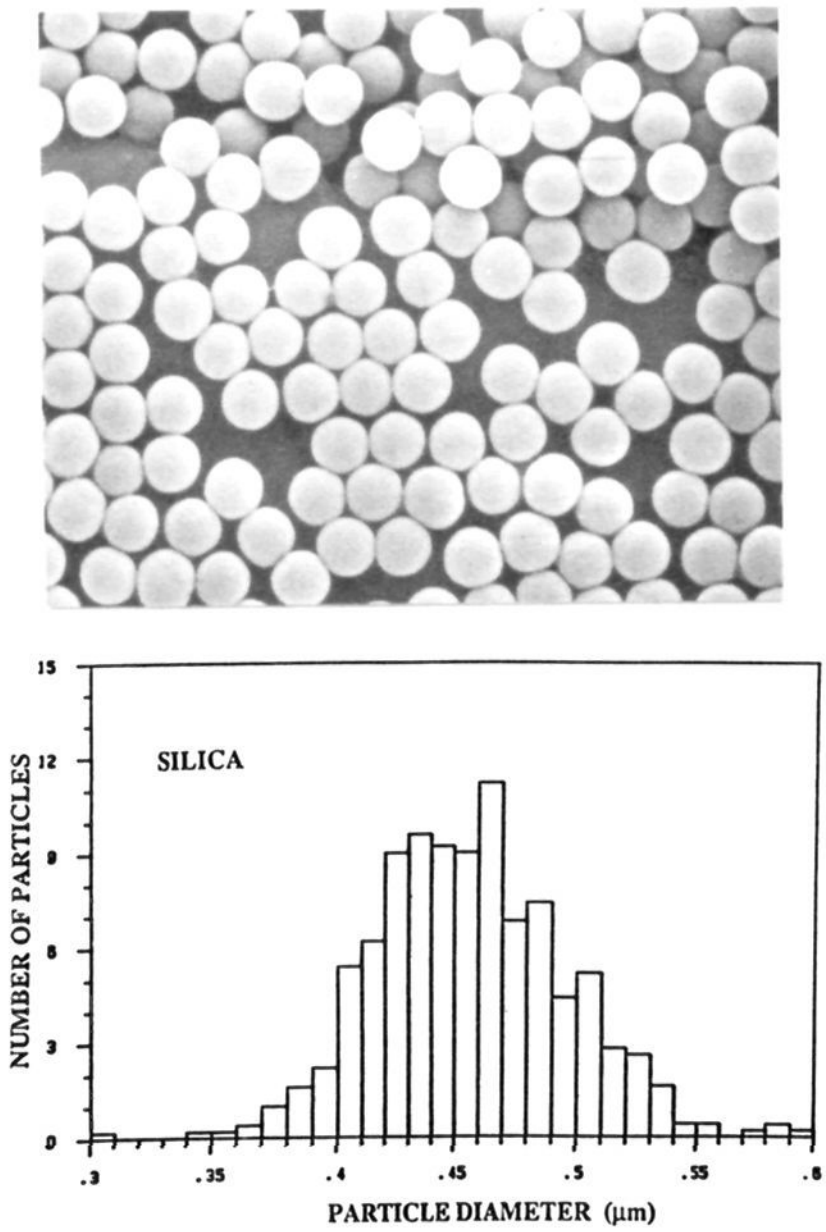

Figure 1. Top: SEM of Stober spherical silica powders. Bottom: Histogram (number of particles in a given diameter class versus particle diameter) of a typical batch of Stober spherical silica powders. Reprinted from ref 18; copyright 1988 University of Florida.

Overbeek[19,20] and Sugimoto[21] showed that nucleation of particles in a very short time followed by growth without supersaturation will yield monodispersed colloidal oxide particles. Matijevic and co-workers[22-25] have employed these concepts to produce an enormous range of colloidal powders with controlled size and morphologies, including oxides (TiO_2, α-Fe_2O_3, Fe_3O_4, $BaTiO_3$, CeO_2), hydroxides (AlOOH, FeOOH, $Cr(OH)_3$), carbonates ($Cd(OH)CO_3$), $Ce_2O(CO_3)_2$, Ce(III)/Y HCO_3), sulfides (CdS, ZnS), metals (Fe(III), Ni, Co), and various mixed phases or composites (Ni, Co, Sr ferrites), sulfides (Zn, CdS), (Pb, CdS), and coated particles (Fe_3O_4 with $Al(OH)_3$ or $Cr(OH)_3$).

The controlled hydrolysis of alkoxides has also been used to produce submicrometer TiO_2,[26] doped TiO_2,[27] ZrO_2,[28] and doped ZrO_2,[28] doped SiO_2,[29] $SrTiO_3$,[30] and even cordierite[30] powders.

Emulsions have been employed to produce spherical powders of mixed cation oxides, such as yttrium aluminum garnets (YAG), and many other systems such as reviewed in Hardy et al.[30]

Sol–gel powder processes have also been applied to fissile elements[31] where spray-formed sols of UO_2 and UO_2–PuO_2 were formed as rigid gel spheres during passage through a column of heated liquid.

Both glass and polycrystalline ceramic fibers have been prepared by using the sol–gel method. Compositions include TiO_2–SiO_2 and ZrO_2–SiO_2 glass fibers,[32] high-purity SiO_2 waveguide fibers,[33-38] Al_2O_3, ZrO_2, ThO_2, MgO, TiO_2, $ZrSiO_4$, and $3Al_2O_3 \cdot 2SiO_2$ fibers.[39-44] Abrasive grains based upon sol–gel-derived alumina are important commercial products.[44]

A variety of coatings and films have also been developed by using sol–gel methods. Of particular importance are the antireflection coatings of indium tin oxide (ITO) and related compositions applied to glass window panes to improve insulation characteristics.[45-47] Other work on sol–gel coatings is reviewed by Schroeder,[48] Mackenzie,[49,50] and Wenzel.[51] Mackenzie's reviews[49,50] include many other applications of the sol–gel process, proven, possible, and potential.

The motivation for sol–gel processing is primarily the potentially higher purity and homogeneity and the lower processing temperatures associated with sol–gels compared with traditional glass melting or ceramic powder methods. Mackenzie[49,50] summarizes a number of potential advantages and disadvantages and the relative economics of sol–gel methods in general. Hench and colleagues[52-54] compare quantitatively the merits of sol–gel-derived silica optics over the alternative high-temperature processing methods.

During the past decade there has been an enormous growth in the interest in the sol–gel process. This growth has been stimulated by several factors. On the basis of Kistler's early work,[55] several teams have produced very low density silica monoliths, called aerogels, by hypercritical point drying.[56] Zarzycki, Prassas, and Phalippou[57,58] demonstrated that hypercritical point drying of silica gels could yield large fully dense silica glass monoliths. Yoldas[59] showed that large monolithic pieces of alumina could be made by sol–gel methods. These demonstrations of potentially practical routes for production of new materials with unique properties coincided with the growing recognition that powder processing of materials had inherent limitations in homogeneity due to difficulty in controlling agglomeration.[60]

The first of a series of International Conferences on Ultrastructure Processing was held in 1983 to establish a scientific basis for the chemical-based processing of a new generation of advanced materials for structural, electrical, optical, and optoelectronic applications. Support by the Directorate of Chemical and Atmospheric Sciences of the Air Force Office of Scientific Research (AFOSR) for the Ultrastructure Conferences in 1983,[61] 1985,[62] 1987,[63] and 1989[64] and the Materials Research Society Better Ceramics Through Chemistry annual meetings in alternate years in 1984,[65] 1986,[66] and 1988[63] has provided constant stimulation for the field. In addition, AFOSR has provided a stable financial base of support for a number of university programs in sol–gel science throughout the 1980s under the technical monitoring of D. R. Ulrich.

The primary goal in these conferences and the AFOSR research and development program was to establish a scientific foundation for a new era in the manufacture of advanced, high-technology ceramics, glasses, and composites. For millennia, ceramics have been made with basically the same technology. Powders, either natural or man-made, have been shaped into objects and subsequently densified at temperatures close to their liquidus. The technology of making glass has also remained fundamentally the same since prehistory. Particles are melted, homogenized, and shaped

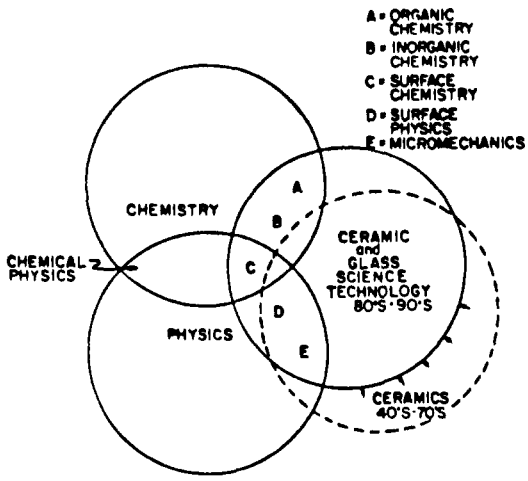

Figure 2. Change in the roles of physics and chemistry as ceramics move toward ultrastructure processing. Reprinted from ref 61; copyright 1984 Wiley.

into objects from the liquid.

The goal of sol–gel processing and ultrastructure processing in general is to control the surfaces and interfaces of materials during the earliest stages of production.[61] Long-term reliability of a material is usually limited by localized variations in the physical chemistry of the surface and interfaces within the material. The emphasis on ultrastructure processing is on limiting and controlling physical chemical variability by the production of uniquely homogeneous structures or producing extremely fine-scale (10–100 nm) second phases. Creating controlled surface compositional gradients and achieving unique physical properties by combining inorganic and organic materials are also goals of ultrastructure processing.

The concept of molecular manipulation of the processing of ceramics, glasses, and composites requires an application of chemical principles unprecedented in the history of ceramics. Modern ceramics are primarily the products of applied physics, as indicated in Figure 2. During the past decade there has been enormous progress made in the shifting of the emphasis of ceramic science to include a larger overlap with chemistry, as also illustrated in Figure 2.[61] The extensive literature represented by the conference proceedings cited above[61-67] contains excellent examples of this shift toward chemical-based processing in materials science.

Another essential factor for the increased scientific understanding of the sol–gel process is the availability of new analytical and calculational techniques capable of investigating on a nanometer scale the chemical processes of hydrolysis, polycondensation, syneresis, dehydration, and densification of materials. Many of the concepts of molecular control of sol–gel processes are a result of the use of nuclear magnetic resonance (NMR), X-ray small-angle scattering (XSAS), Raman spectroscopy, X-ray photoelectron spectroscopy (XPS), differential scanning calorimetry (DSC), dielectric relaxation spectroscopy (DRS), etc., that have been developed during the past three decades.

The difference between the modern development of sol–gel-derived materials, such as gel–silica optics,[52-54] and the classical work of Ebelman[1,2] is that now drying of the monolithic silica optics can be achieved in days rather than years. The primary problem that had to be overcome was cracking during drying due to the large shrinkage that occurs when pore liquids are removed from the gels. For small cross sections, such as in powders, coatings, or fibers, drying stresses are small and can be accommodated by the material. For monolithic objects greater than about 1 cm in diameter, drying stresses developed in ambient atmospheres can introduce catastrophic fracture. To prevent fracture during drying, it is essential to control the chemistry of each step of the sol–gel process carefully. Likewise, to densify a dried gel monolith, it is essential to control the chemistry of the pore network prior to and during pore closure. The objective of this review is to describe the chemistry of the seven steps of the sol–gel process that can yield monoliths under ambient pressures. This review also describes how sol–gel-derived monoliths can be processed to result in fully dense components or with precisely controlled and chemically stable porosities. Most detail exists for SiO_2, and therefore the emphasis in this review is on silica sol–gel processing. The processing of silica monoliths by alkoxide methods will be compared with more traditional colloidal sol–gel methods.

The reader interested in the sol–gel processing of compositional systems other than SiO_2 or coatings, fibers, powders, or aerogels is referred to the Conference Proceedings cited above[61-67] as well as an International Workshop on Sol–Gel Processing[68] and special conferences chaired by Sanders and Klein[69] and Fricke.[56]

Klein's volume on sol–gel technology,[69] emphasizing thin films, fibers, hollow glass microspheres, and specialty shapes, illustrates many potential applications of this field. A textbook on sol–gel science has recently been completed by Brinker and Scherer.[70] Other general reviews on earlier work include those by Klein,[71] Sakka and Kamiya,[72] Mukherjee,[73] Sakka,[74,75] and of course Iler[15,76] and Okkerse.[77]

II. Sol–Gel Process Steps: An Overview

Three approaches are used to make sol–gel monoliths: method 1, gelation of a solution of colloidal powders; method 2, hydrolysis and polycondensation of alkoxide or nitrate precursors followed by hypercritical drying of gels; method 3, hydrolysis and polycondensation of alkoxide precursors followed by aging and drying under ambient atmospheres.

Sols are dispersions of colloidal particles in a liquid. *Colloids* are solid particles with diameters of 1–100 nm.[78] A *gel* is a interconnected, rigid network with pores of submicrometer dimensions and polymeric chains whose average length is greater than a micrometer. The term "gel" embraces a diversity of combinations of substances that can be classified in four categories as discussed by Flory:[79] (1) well-ordered lamellar structures; (2) covalent polymeric networks, completely disordered; (3) polymer networks formed through physical aggregation, predominantly disordered; (4) particular disordered structures.

A silica gel may be formed by network growth from an array of discrete colloidal particles (method 1) or by formation of an interconnected 3-D network by the simultaneous hydrolysis and polycondensation of an organometallic precursor (methods 2 and 3). When the pore liquid is removed as a gas phase from the interconnected solid gel network under hypercritical conditions (critical-point drying, method 2), the network

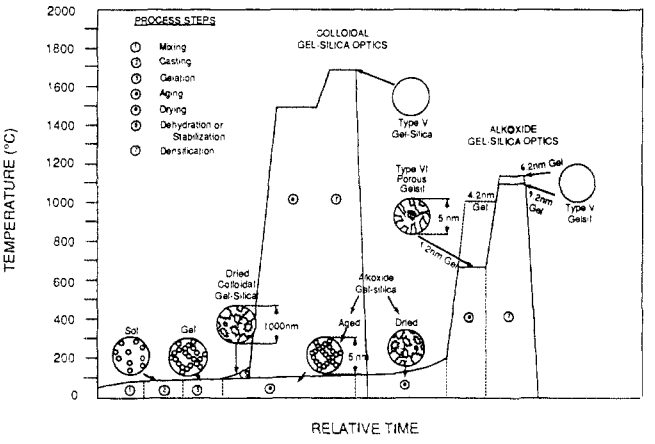

Figure 3. Gel-silica glass process sequence.

does not collapse and a low density *aerogel* is produced. Aerogels can have pore volumes as large as 98% and densities as low as 80 kg/m^3.[59,80]

When the pore liquid is removed at or near ambient pressure by thermal evaporation (called *drying*, used in methods 1 and 3) and shrinkage occurs, the monolith is termed a *xerogel*. If the pore liquid is primarily alcohol based, the monolith is often termed an *alcogel*. The generic term *gel* usually applies to either xerogels or alcogels, whereas aerogels are usually designated as such. A gel is defined as *dried* when the physically adsorbed water is completely evacuated. This occurs between 100 and 180 °C.

The surface area of dried gels made by method 3 is very large (>400 m^2/g), and the average pore radius is very small (<10 nm). Larger pore radii can be produced by thermal treatment,[220] by chemical washing during aging,[237] or by additions of HF to the sol.[323] The small pore radii can lead to large capillary pressures (eq 1) during drying or when the dried gel is exposed to liquids as described by Laplace's equation, discussed by Zarzycki,[81] and developed extensively by Scherer[70,82-88] for the drying of gels:

$$\Delta p = 2\gamma(\cos\theta)/r \qquad (1)$$

where Δp = the pressure difference in the capillaries, γ = specific surface energy of the vapor–liquid interface, θ = contact angle, and r = pore radius.

A dried gel still contains a very large concentration of chemisorbed hydroxyls on the surface of the pores. Thermal treatment in the range 500–800 °C desorbs the hydroxyls and thereby decreases the contact angle and the sensitivity of the gel to rehydration stresses, resulting in a *stabilized gel.*

Heat treatment of a gel at elevated temperatures substantially reduces the number of pores and their connectivity due to viscous-phase sintering. This is termed *densification.* The density of the monolith increases and the volume fraction of porosity decreases during sintering. The porous gel is transformed to a dense glass when all pores are eliminated. Densification is complete at 1250–1500 °C for gels made by method 1 and as low as 1000 °C for gels made by method 3.[299] The densification temperature decreases as the pore radius decreases and surface area of the gels increases, as illustrated in Figure 3. Silica glass made by densification of porous silica gel is amorphous and nearly equivalent in structure and density to vitreous silica made by fusing quartz crystals or sintering of SiO_2 powders made by chemical vapor deposition (CVD) of $SiCl_4$.[52-54]

The processing steps involved in making sol–gel-derived silica monoliths for methods 1–3 are compared below. A schematic illustration of these seven steps is given in Figure 3 for methods 1 and 3.

Step 1: *Mixing.* In method 1 a suspension of colloidal powders, or sol, is formed by mechanical mixing of colloidal particles in water at a pH that prevents precipitation, as discussed in detail by Iler.[15,76] In methods 2 and 3 a liquid alkoxide precursor, such as $Si(OR)_4$, where R is CH_3, C_2H_5, or C_3H_7, is hydrolyzed by mixing with water (eq 2).

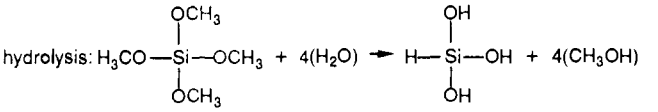

$$\text{TMOS} + 4(H_2O) \rightarrow Si(OH)_4 + 4(CH_3OH) \qquad (2)$$

The hydrated silica tetrahedra interact in a condensation reaction (eq 3), forming ≡Si—O—Si≡ bonds.

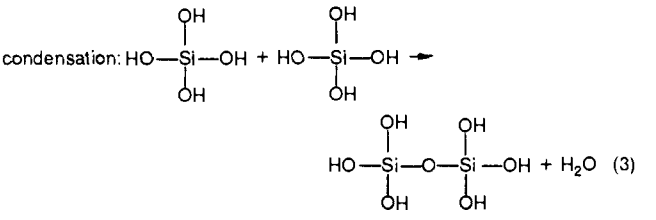

Linkage of additional ≡Si—OH tetrahedra occurs as a polycondensation reaction (eq 4) and eventually results in a SiO_2 network. The H_2O and alcohol expelled from the reaction remains in the pores of the network.

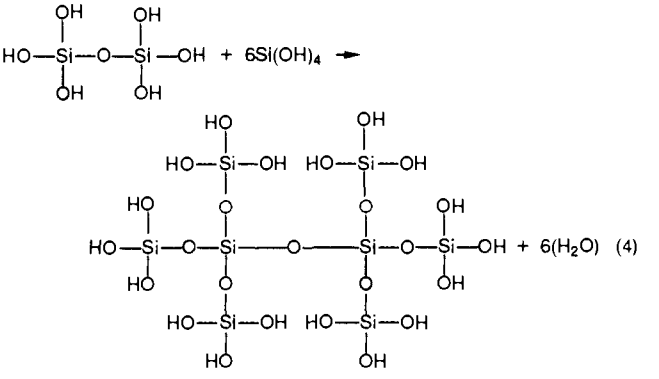

The hydrolysis and polycondensation reactions initiate at numerous sites within the TMOS + H_2O solution as mixing occurs. When sufficient interconnected Si–O–Si bonds are formed in a region, they respond cooperatively as colloidal (submicrometer) particles or a sol. The size of the sol particles and the cross-linking within the particles (i.e., density) depend upon the pH and R ratio ($R = [H_2O]/[Si(OR)_4]$) among other variables discussed in a later section.

Step 2: *Casting.* Since the sol is a low-viscosity liquid, it can be cast into a mold. The mold must be selected to avoid adhesion of the gel.

Step 3: *Gelation.* With time the colloidal particles and condensed silica species link together to become a three-dimensional network. The physical characteristics of the gel network depend greatly upon the size of particles and extent of cross-linking prior to gelation. At gelation, the viscosity increases sharply, and a solid object results in the shape of the mold. With appro-

priate control of the time-dependent change of viscosity of the sol, fibers can be pulled or spun as gelation occurs.

Step 4: *Aging*. Aging of a gel, also called *syneresis*, involves maintaining the cast object for a period of time, hours to days, completely immersed in liquid. During aging, polycondensation continues along with localized solution and reprecipitation of the gel network, which increases the thickness of interparticle necks and decreases the porosity. The strength of the gel thereby increases with aging. An aged gel must develop sufficient strength to resist cracking during drying.

Step 5: *Drying*. During drying the liquid is removed from the interconnected pore network. Large capillary stresses can develop during drying when the pores are small (<20 nm). These stresses will cause the gels to crack catastrophically unless the drying process is controlled by decreasing the liquid surface energy by addition of surfactants or elimination of very small pores (method 1), by hypercritical evaporation, which avoids the solid–liquid interface (method 2), or by obtaining monodisperse pore sizes by controlling the rates of hydrolysis and condensation (method 3).

After hypercritical drying (method 1) the aerogel has a very low density and is a very good thermal insulation when sandwiched between glass plates and evacuated.[59]

Step 6: *Dehydration or Chemical Stabilization*. The removal of surface silanol (Si–OH) bonds from the pore network results in a chemically stable ultraporous solid. Porous gel–silica made in this manner by method 3 is optically transparent with interconnected porosity and has sufficient strength to be used as unique optical components when impregnated with optically active polymers such as fluors, wavelength shifters, dyes, or nonlinear polymers.[52,53]

Step 7: *Densification*. Heating the porous gel at high temperatures causes densification to occur. The pores are eliminated, and the density ultimately becomes equivalent to fused quartz or fused silica. The densification temperature depends considerably on the dimensions of the pore network, the connectivity of the pores, and surface area, as illustrated in Figure 3.[89] Alkoxide gels (method 3) have been densified as low as 1000 °C by Klein and Garvey,[299] whereas gels made by the commercial colloidal process developed by Shoup[90] require 1500–1720 °C. However, colloidal silica gels with very carefully controlled dense packing can also be densified at low temperatures of 1000 °C, as shown by Sacks and Tseng.[91,92] The purity and homogeneity of dense gel–silica made by method 3 are superior to other silica glass processing methods. The ability to produce optics with nearly theoretical limits of optical transmission, lower coefficients of thermal expansion, and greater homogeneity, along with net shape casting, represents major advances resulting from sol–gel processing of monoliths.[52,53]

Details of these seven sol–gel processing steps follow. The emphasis is on sol–gel-derived silica monoliths made by the alkoxide process (method 3) processed under ambient pressures.

III. Hydrolysis and Polycondensation

As shown in Figure 3 the structure of a gel is established at the time of gelation. Subsequent processes such as aging, drying, stabilization, and densification all depend upon the gel structure. Since it is the relative rates of hydrolysis (eq 2) and condensation (eq 3) that determine the structure of the gel, it is essential to understand the kinetics of the hydrolysis and condensation reactions and the ratio of their rate constants (k_H/k_C).

As discussed by Orcel et al.,[93-95] Hench and Orcel,[96] Klemperer et al.,[97,98] Scherer and Brinker,[70] and Artaki et al.,[99] many factors influence the kinetics of hydrolysis and condensation, and the systems are considerably more complex than represented by the simplified eqs 2–4. Many species are present in the solution, and furthermore, hydrolysis and polycondensation occur simultaneously. The variables of major importance are temperature, nature and concentration of electrolyte (acid, base), nature of the solvent, and type of alkoxide precursor. Pressure influences the gelation process also; k_H increases with pressure as shown by Artaki et al.,[100-102] but pressure is usually not a processing variable.

There are relatively few studies of the dependence of k_H and k_C on independent processing variables. In fact many studies have reported the variation of the gelation time, viscosity, or textural characteristics (e.g., specific surface area) of the gel as a function of experimental conditions without determining k_H or k_C.[102-107] However, several investigations do provide a scientific foundation for understanding the processing dependence of k_H and k_C.

Aelion's study of the influence of electrolyte concentration on the hydrolysis of TEOS in different solvents showed that k_H increases linearly with the concentration of H^+ or H_3O^+ in acidic media and with the concentration of OH^- in basic medium.[103] The reaction rate varies from 4.12×10^{-6} L mol^{-1} s^{-1} for a 0.063 mol L^{-1} HCl solution. This corresponds to a rate constant per unit concentration of electrolyte of 0.091 mol L^{-1} s^{-1} $[H^+]^{-1}$. Similar values are observed in basic media where the rate constant is about 0.040 L mol^{-1} s^{-1} $[OH]^{-1}$. There is a variation in the concentration of TEOS of 0.2 mol L^{-1} for the basic conditions versus 0.6 mol L^{-1} for the acid-catalyzed sol. The increase in [TEOS] can account for the increase in rate constant.

As discussed by Orcel[93] the nature of the solvent (dioxane, methanol, or ethanol) has a "secondary" effect on k_H, as well as the temperature dependence of the reaction (10-fold increase when the temperature varies from 20 to 45.5 °C). NMR experiments by Artaki, Zerda, and Jonas[100] show that k_H varies in the different solvents as follows: acetonitrile > methanol > dimethylformamide > dioxane > formamide, with k_H(acetonitrile) being about 20 times larger than k_H(formamide).

An increase of the R ratio (moles of water/moles of TEOS) from 1.86 to 3.72 induces k_H to increase from 0.042 to 0.059 L mol^{-1} s^{-1} [acid]$^{-1}$.[103] However, Schmidt et al.[104] found that the hydrolysis rate decreases when the R ratio increases from 0.5 to 2. Schmidt attributes this to the "special experimental conditions and the water acting as a proton acceptor which decreases the proton activity".[105]

The nature of the alkoxy groups on the silicon atom also influences the rate constant. As a general rule, the longer and the bulkier the alkoxide group, the slower the rate constant.[105,108,109] For example, in the case of

the hydrolysis of $Si(OR)_4$, $k_H = 51 \times 10^{-3}$ L mol^{-1} s^{-1} $[H^+]^{-1}$ for R = C_2H_5 and $k_H = 3 \times 10^{-3}$ L mol^{-1} s^{-1} $[H^+]^{-1}$ for R = $(CH_3)_2CH(CH_2)_3CH(CH_3)CH_2$.

From these results it is apparent that the dominant factor in controlling the hydrolysis rate is the electrolyte concentration.[93] However, the nature of the acid plays an important role. As outlined above, a minute addition of HCl induced a 1500-fold increase of k_H. However, Aleion reported "hydrolysis in glacial acetic acid as solvent is not particularly fast".[103]

Although these have been called "secondary" effects[103] and they are very small compared to those induced by addition of electrolyte, they are relatively important (e.g., the 10-fold increase of k_H with a variation of the processing temperature of 25.5 °C) and might be responsible for numerous observations in systems investigated in other works. For example, a systematic study of Mackenzie shows that the type of acid catalyst and nature of solvent have a large effect on TEOS gelation.[110]

Although the polycondensation of silicic acids has been studied extensively, as reviewed by Iler[15,76] there are little data on the rate constant of the condensation reaction.[93] A value of $k_C = 3.3 \times 10^{-6}$ L mol^{-1} s^{-1} has been reported by Artaki et al. for the dimerization of monosilicic acid.[102] However, no value of k_H is available for the same system. Artaki et al. showed that application of a pressure of 5 kbar to the system increased the polycondensation rate constant by a factor 10.[102]

There are many problems associated with the computation of reaction rate constants and especially the determination of the mechanisms of the reactions as well as the order of the reactions with respect to the constituents, as discussed by Schmidt et al.[105] When the order of the reaction varies with time, such as in Uhlmann et al.'s experiments, determining the rate constant becomes even more difficult.[106] For short periods of time, the order of the reaction can be considered constant. However, one must keep in mind that there are several hydrolysis and condensation reactions possible, each having its own rate constant.[107,111] Consequently, assumptions are necessary to allow the computation of k_H and k_C, which limits the characterization of the reactions to the early stages of the process.

Because of the above limitations, early studies of the influence of the experimental factors on the sol–gel process were primarily phenomenological, without specific values of the ratio k_H/k_C being determined for a single system. This situation has changed dramatically in the past few years. Many investigators have pursued the kinetics of silicon alkoxide hydrolysis using ^{29}Si NMR. It is one of the most useful techniques to follow the hydrolysis and first-stage polymerization of silicon alkoxide, because it allows the determination of the concentration of the different $Si(Or)_x(OH)_y$ and $(OH)_u(OR)_vSi–O–Si(OR)x(OH)_y$ species. Each of the monomer and dimer species has a specific chemical shift with respect to the metal alkoxide.[112]

Engelhardt et al.[113] employed ^{29}Si NMR as early as 1977 to investigate the condensation of aqueous silicates at high pH. Their results indicate that a typical sequence of condensation products is monomer, dimer, linear trimer, cyclic trimer, cyclic tetramer, and a higher order generation of discrete colloidal particles which are commonly observed in aqueous systems. This sequence

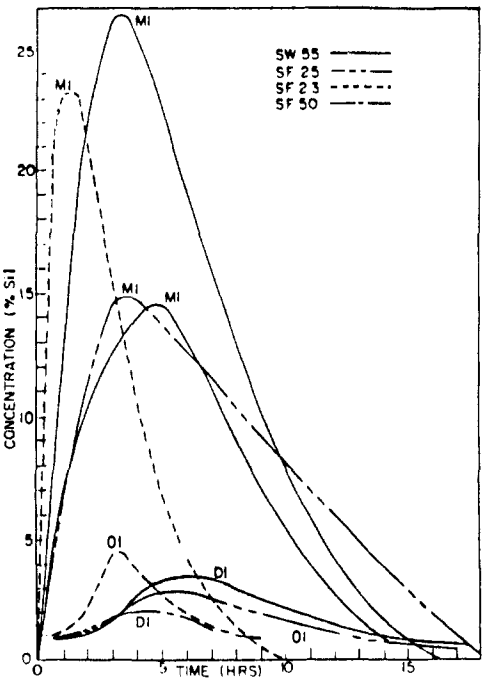

Figure 4. Variation of the concentration of M1 ($Si(OH)(OCH_3)_3$) and D1 ($(OCH_3)_3Si–O–Si(OCH_3)_3$) as a function of time for the different solutions.[96]

of condensation requires both depolymerization (ring opening) and availability of monomers (species that may be produced by depolymerization). However, in alcoholic solutions especially at low pH the depolymerization rate is very low. Iler[15] speculates that under conditions where depolymerization is least likely to occur, so that the condensation is irreversible and siloxane bonds cannot be hydrolyzed once they are formed, the condensation process may resemble classical polycondensation of polyfunctional organic monomers resulting in a three-dimensional molecular network. Owing to the insolubility of silica under these conditions, the condensation polymer of a siloxane chain cannot undergo rearrangement into particles. In sol–gel systems commonly employed for glass preparation, the water/alcohol ratio and pH are widely varied. Thus the importance of the reverse reactions depends on processing conditions, and it is anticipated that condensation may result in a spectrum of structures ranging from molecular networks to colloidal particles.

Yoldas[114] concluded that the hydrolysis reaction and the condensation reaction are not separated in time but take place simultaneously. It has been well established that the presence of H_3O^+ in the solution increases the rate of the hydrolysis reaction, whereas OH^- ions increase the condensation reaction.[115]

Orcel et al.[93–95,116] explored the effect of acid catalysis and formamide (a drying control chemical additive) on the hydrolysis and polycondensation rates of a TMOS silica system, using ^{29}Si NMR. By plotting the variation of the concentration of the species of interest from the NMR data as a function of time (Figure 4), one can obtain the rate constants for hydrolysis (k_H) and polycondensation (k_C) of the Si alkoxide, in this case TMOS.

Even though the assumptions involved in the computation of the rate constants are crude, such as first-order kinetics and no influence of the degree of substitution of Si atoms on the reaction rates, the order of magnitude of k_H and k_C, Table I, demonstrates im-

TABLE I. **Physicochemical Characteristics of the Different Gel Solutions**

sample	SW 55	SF 25	SF 50	SF 23
vol formamide/vol formamide + MeOH	0	25	50	25
H_2O	D1	D1	D1	pH = 3
10^3k_H, L mol^{-1} h^{-1}	12	7	2	25
k_C, L mol^{-1} h^{-1}	29	31	25	6
d, nm	2	2.2	2.5	

portant differences. These data show that acid catalysis increases the hydrolysis rate constant, k_H, by a factor of 2. The data also show that formamide decreases the hydrolysis rate and slightly increases the condensation rate. This can be attributed to the ability of $HCONH_2$ to form hydrogen bonds and to its high dielectric constant (ϵ = 110).[116] The presence of formamide also decreases the time of gelation (t_g). Additional details regarding the use of formamide and other drying control chemical agents (DCCAs) are discussed in refs 93 and 117.

The studies of Klemperer and colleagues[97,98] provide some of the most detailed evaluation of the extent of hydrolysis and condensation of silica prior to the onset of gelation. To identify the polysilicate intermediates formed during sol–gel processing, Klemperer et al.[97] used a protocol that combined quenching by diazomethane, fractionation using spinning band column distillation, identification by capillary gas chromatography, and structural characterization using $^{29}Si\{^1H\}$ NMR techniques (one-pulse, 1D-INADEQUATE, and 2D-INADEQUATE) to provide structural assignments and response factors for the components separated by gas chromatography. They[98] showed that under acidic conditions the polysilicate molecular size distributions, expressed in terms of mole percent of total silicon present as a function of degree of polymerization, exhibit maxima near the number-average degree of polymerization. There are mostly linear structures under acidic conditions. In contrast, under basic conditions the maximum of the distribution is at the monomer percent and extends to very high molecular weights. Thus, the distribution of polysilicate species is very much broader for basic conditions of hydrolysis and condensation, characteristic of branched polymers with a high degree of cross-linking, whereas for acidic conditions Klemperer et al.[98] conclude that there is a low degree of cross-linking due to steric crowding.

Raman spectroscopy is one means of assessing qualitatively the size of particles or scale of structure[118,119] when gelation occurs. Since the Raman intensity is proportional to the concentration of scatterers, sols and gels prepared with different experimental conditions can be compared by using a proper internal standard. In the study of the SiO_2–formamide system, methanol was used for calibration.[93-95] According to the NMR data, the concentration of CH_3OH is constant after $0.7t_g$ at 23 °C, and the solvent is significantly expelled from the gel after $\sim 6t_g$. Thus the calibrated Raman intensities are valid in the time frame $0.7t_g$–$6t_g$. Results for several gel solutions, with and without formamide, under basic and acidic conditions, are given in Figure 5.[96] These curves demonstrate that when formamide is present, i.e., samples SF 50 and SF 25, larger particles are formed at the gelation point. This is in good agreement with the NMR results.[93-95] Since formamide decreases the hydrolysis rate, fewer sites are available for condensation and larger particles are formed in the sol.[93,117]

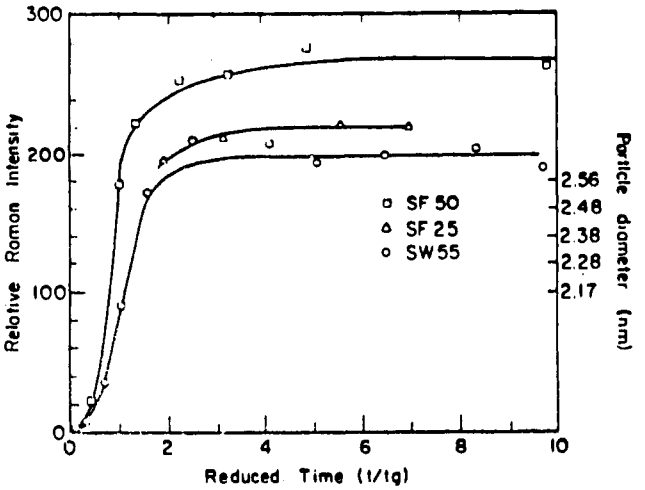

Figure 5. Variation with time of the relative Raman intensity of the 830-cm^{-1} band of the various gel solutions.[96]

The reaction of silica colloids with molybdic acid, a technique widely used for the characterization of soluble silicates,[120] can also be used to assess the size of particles developed in the sol. SiO_2 particles depolymerize in an acidic medium, and the monosilicic acid thus formed gives a yellow complex with Mo, which can be measured optically. A plot of the absorbance as a function of time allows the computation of the depolymerization rate constant, k_D, as a function of time.[93,96] For example, the values of k_D at $0.5t_g$ for several SiO_2–formamide solutions can be used to calculate the particle diameter.

Ultimately, k_D can be related to the particle diameter d through an empirical law:

$$\log d = a + b \log k_D \tag{5}$$

where a and b are constants (see Iler[120]) depending on experimental conditions, mainly solution pH. Since the solution pH of samples 55, 25, and 50 are nearly equivalent, it is possible to compare relative particle sizes by using eq 5 and assuming the values for a and b from Iler.[120] (Note: This is only an approximation since Iler's values are based on a pH = 2, SiO_2 solution.) The calculated values at the gelation point, shown in Table I, increase with increasing formamide concentration.

It has been shown[93,94] that the calibrated Raman intensity I_R is inversely proportional to k_D. Thus, I_R can be related to the sol particle size as

$$I_R = Ad^{1/b} \tag{6}$$

where A is a function independent of d. For the conditions described by Iler[120] $1/b = 3.48$. The theoretical basis for this value is developed in refs 93 and 94.

By use of $1/b$ and the values of d (eq 5) calculated from the Mo test, it is possible to compute an empirical value of 6.8 for A in eq 6. By use of eq 6 and the measured values of Raman intensity (Figure 5), the time-dependent change in sol particle size can be calculated. The results are shown in Figure 5 on the right-hand particle-size axis. By the time of gelation, the size of the sol particles grows to 2 nm without formamide, and with 50% formamide they grow to 2.5 nm.

These findings are similar to those of Klemperer et al.[97,98] in their studies of the effects of base vs acid

TABLE II. Chemical Characteristics of the TMOS Solutions (from Ref 94)

soln	$10^{-3}\,k_H$, mol h	$10^{-3}k_C$, mol h	vol fract CH_3OH in solv, %	gelation time, h
I	2	>32	50	6
II	12	29	100	40

catalysis on the size of polysilicate species prior to the onset of gelation.

Thus, Orcel et al.'s studies[94] show that the shape and size of polymeric structural units are determined by the relative values of the rate constants for hydrolysis and polycondensation reactions (k_H and k_C, respectively). Fast hydrolysis and slow condensation favor formation of linear polymers; on the other hand, slow hydrolysis and fast condensation result in larger, bulkier, and more ramified polymers.[150] As illustrated by the values of k_H and k_C reported in Table II, larger particles are anticipated for solution 1 (higher volume fraction CH_3OH in the solvent), which implies a lower value for the depolymerization rate constant: $k_I < k_{II}$.

By combination of these various analytical methods, the particle diameter (PD) of the silica particles in the sol at the different steps of the sol–gel process can be estimated. The results[94,156] are given in Table III, and it is possible to conclude that the particles are about 20 Å in diameter at the gelation point and larger particles are formed when formamide is present in the solution, as discussed in the next section on gelation.

IV. Gelation

The gelation point of any system, including sol–gel silica, is easy to observe qualitatively and easy to define in abstract terms but extremely difficult to measure analytically. As the sol particles grow and collide, condensation occurs and macroparticles form. The sol becomes a gel when it can support a stress elastically. This is typically defined as the gelation point or gelation time, t_{gel}. There is not an activation energy that can be measured, nor can one precisely define the point where the sol changes from a viscous fluid to an elastic gel. The change is gradual as more and more particles become interconnected. All subsequent stages of processing depend on the initial structure of the wet gel formed in the reaction bath during gelation.

Brinker and Scherer[121] point out that the sharp increase in viscosity that accompanies gelation essentially freezes in a particular polymer structure at the gel point. At this point gelation may be considered a rapid solidification process. This "frozen-in" structure may change appreciably with time, depending on the temperature, solvent, and pH conditions or upon removal of solvent.

A. Gelation Time

A number of investigators have shown that the time of gelation changes significantly with the sol–gel chemistry.[15,95,117,122,123] One of the most precise methods to measure t_{gel} was developed by Sacks and Sheu.[124] This method measures the viscoelastic response of the gel as a function of shear rate.

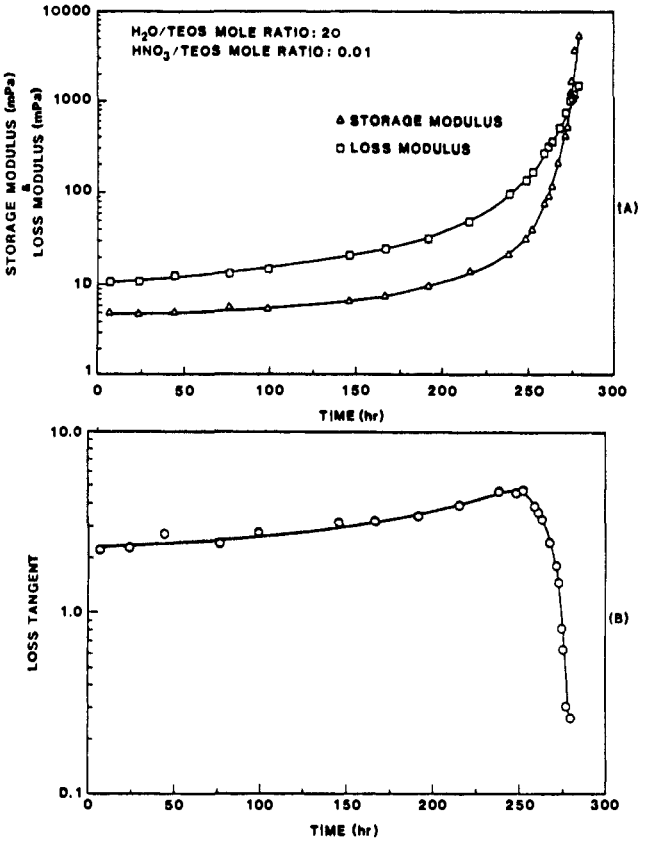

Figure 6. Loss tangent as a measure of gelation time (Sacks and Sheu, 1986). (A) Plots of storage modulus and loss modulus vs aging time for sol 1. (B) Plot of loss tangent vs aging time for sol 1.

They measured the complex shear modulus, G, by using a viscometer with a narrow gap. This ensures a well-defined shear rate as the cylinder in the sol oscillates at a frequency ω and a small amplitude γ. The complex shear modulus has the form

$$G = G'(\omega) + iG''(\omega) \tag{7}$$

where G' = storage modulus and G'' = loss modulus. The storage modulus arises from the elastic component of the sol–gel, while the loss modulus comes from the viscous component.

The relative measure of the viscous energy losses to the energy stored in the system is usually defined as the loss tangent:

$$\tan \delta = G''/G' \tag{8}$$

Figure 6 shows the large change in the loss tangent at the gelation time along with the changes in G' and G'' from Sacks and Sheu.[124] The rapid increase in the storage modulus near t_{gel} is consistent with the concept that the interconnection of the particles becomes suf-

TABLE III. Structural and Textural Properties of the Gels (from Orcel et al.[156])[a]

property	PD, Å	PR, Å	PV, cm^3/g	SA, m^2/g	D1, Å	D2, Å	d_f
soln I (with DCCA)	24	30	1.19	784	59	24	2.29
soln II (no DCCA)	20	12	0.356	607	58	20	2.25

[a] PD, particle diameter (Mo test); PR, pore radius; PV, pore volume; SA, specific surface area; D1, Guinier radius at gelation point; D2, Guinier radius on film heated at 200 °C; d_f, fractal dimension at gelation point.

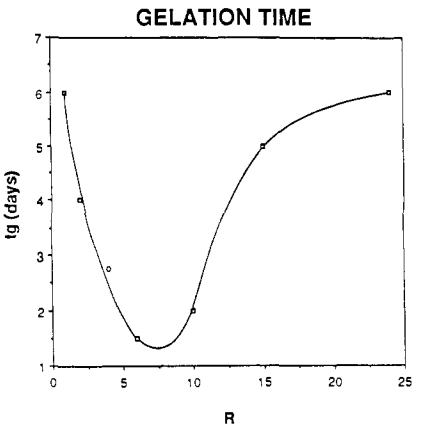

Figure 7. Variation of the gelation time with the R ratio.[128]

ficient to support a load elastically.

There is at least one indication that gelation time (t_g) is not an intrinsic property of the sol: t_g depends on the size of the container. Furthermore, gelation may occur at different extents of reaction completion. For example, in the case of the polymerization of TMOS, more silicon alkoxide must be hydrolyzed when the experimental conditions favor a ramified polymer rather than a linear one.

The dependence of t_g on solution pH has not been fully determined, but it appears from the work of Yamane et al. that the curve t_g vs pH has a bell shape.[125] In other words, gelation can be nearly instantaneous for very acidic or basic solutions of metal alkoxides. This behavior is very different from the gels prepared by destabilization of a silica sol where the curve has a S shape with the maximum around the isoelectric point of silica (pH $\sim$ 2) and a minimum near pH 5–6.[15] However, it should be noted that two solutions with the same pH may have different gelation times, depending on the nature of the counterion, all other parameters being equal. The anion and solvent also play a role in the kinetics of gelation,[110] and gelation can be either acid or base catalyzed.[72,126,127]

It is difficult to separate the effect of the alkoxy group from the effect of the solvent since gelation kinetics depends on the quantity of the solvent concentration. However, the trend is the longer and the larger the solvent molecule, the longer the gelation time. Similarly, Mackenzie has shown that the longer and the larger is the alkoxy group, the longer is t_g.[110]

The amount of water for hydrolysis has a dramatic influence on gelation time (Figure 7) from Colby et al.[128] For a R ratio (moles of water/moles of silicon alkoxide) of 2, t_g is about 7 h (gelation process at 70 °C with HF as catalyst) and decreases to 10 min for R = 8.[128] For low water contents, generally an increase of the amount of hydrolysis water decreases the gelation time, although there is a dilution effect. It can be predicted[93] that for higher water contents, the gelation time increases with the quantity of water. The location of the minimum in the curve t_g vs R, such as shown in Figure 7, depends on the experimental conditions, such as nature of the chemicals, catalyst, and temperature.

Polymerization reactions are usually thermally activated, and this is observed for the hydrolysis and polycondensation of solutions of silicon alkoxides. For example, Mackenzie has shown that a molar solution of TEOS in methanol gels in 49 h at 4 °C, in the presence of HF, and in about 0.3 h at 70 °C.[110]

Although it is important to know how t_g varies with various experimental parameters, the knowledge thus developed is empirical and qualitative, and a better description of the system is needed in order to optimize the process.

B. Viscosity of the Sol–Gel System

The sol–gel process has the unique advantage of allowing the preparation of the same composition, such as silica, in markedly different physical forms, fibers, coatings, monoliths, just by varying a few experimental conditions. As reviewed by Orcel,[93] the processing parameter that must be controlled is the viscosity of the sol–gel system. For example, the casting density of a sol was shown by Klein and Garvey to be the determinant in the manufacture of monoliths (between 1 and 1.2 g/cm^3 for acid-catalyzed TEOS).[129] Several investigators have shown that fibers can be drawn from a sol only for a range of viscosity that is greater than 1 Pa s.[73,75,130–133] Coatings can be applied with the most efficiency when the concentration of oxides is within certain limits (several tens of grams of oxide per liter) which fix the viscosity.[69,134–139] Controlling these processes requires understanding the rheological properties of the sol–gel system. However, there are few quantitative studies relating gelation to rheological variables.[124] Some attempts have been used to define the point of gelation by associating gel formation with a sudden increase of the viscosity or reaching a maximum of viscosity.[130,132,140,141]

The viscosity of a solution undergoing hydrolysis and polycondensation is time dependent and is related to the size of the particles. The larger the molecules, the higher the viscosity. Thus, any variation of the processing parameters that induces an increase of the apparent size of the particles increases the viscosity. For example, acid-catalyzed silica sol–gel samples have a higher viscosity than neutral or base-catalyzed solutions.[130,142]

The effect of the concentration of water on viscosity is more complex. Orcel[93] reviews the general behavior as follows: at low water content, an increase of the amount of H_2O increases viscosity, which reaches a maximum and then decreases for a further increase of the concentration of water.[142] A similar effect is obtained by varying the concentration of silicon alkoxide.[143,144]

Sacks and Sheu's rheological studies[124] show that a silica sol prepared with the alkoxide process goes from a Newtonian behavior to shear thinning and, finally, thixotropy, which is especially useful in describing the sol–gel transition. Furthermore, they demonstrated[124] that spinnability is possible only when the solution is shear thinning or slightly thixotropic.

C. Sol Structure

The rheological data summarized in the preceding section demonstrate that there is a major evolution of structure during the sol–gel transition. The system evolves from a sol, where there are individual particles more or less weakly interacting with each other, to a gel, which basically becomes a continuous molecule occupying the entire volume. Consequently, it is important to characterize the evolution of the structure of the sol

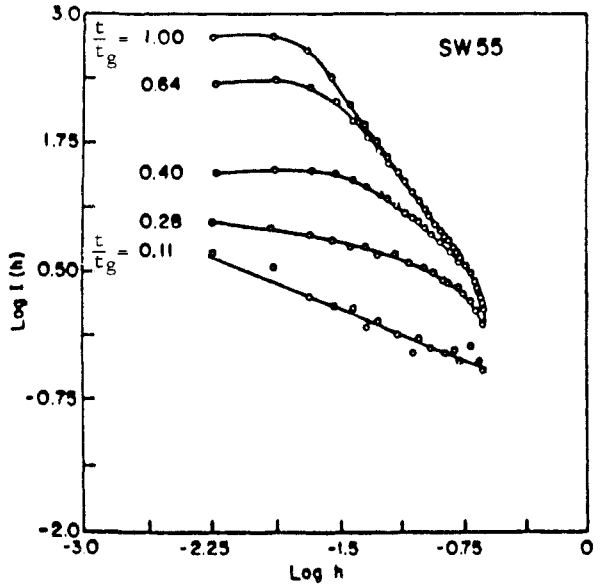

Figure 8. Variation with time of log $I(h)$ vs log h curves for a SW55 sample (no formamide).[156]

during the gelation process.

Only a few techniques are available to follow structural evolution at the nanometer scale of sol–gels. They include small-angle X-ray scattering (SAXS), neutron scattering, and light scattering, each of them giving complementary information, and transmission electron microscopy. Small-angle X-ray scattering allows the determination of a characteristic length of the particle (Guinier's radius of gyration, or electronic radius of gyration)[145-147] and a fractal dimension, which gives some information on the structure of the polymer (branched vs linear) and on the growth mechanism.[148] The application of SAXS to a number of gel systems has been reported by various authors.[59,80,148-156]

Small-angle neutron scattering (SANS) has also been applied to the study of silica sols.[157] Results similar to those from SAXS are obtained, but further developments of the SANS technique may produce additional insight to the sol–gel process.[158]

Light scattering has been used for a long time to characterize macromolecular solutions. Although this technique should be useful in following the sol–gel transition, it has received very little attention in the sol–gel literature. However, the characteristic dimension probed by visible light scattering is >10 nm, and therefore it cannot be used to characterize the early stages of the gelation process.[149] Recent development of short-wavelength UV lasers may make it possible to extend light-scattering studies to the range of 3 nm and thereby could follow most of the gelation process.

The major conclusion of the various scattering studies is that acid-catalyzed sols develop a linear structure with very little branching. In contrast, base-catalyzed systems are characterized by highly ramified structures.[150,151]

Figure 8 is a Porod plot showing SAXS scattering curves typical of a sol prepared by hydrolyzing TMOS.[93,156] The log of the scattering intensity, I, is plotted as a function of the scattering factor h. The scattering factor is defined as $h = (4\pi/\lambda) \sin(\theta/2)$. As time increases from the sol stage ($t/t_g = 0.11$) toward gelation ($t/t_g = 1.00$), there is an increase in the size of X-ray scatterers. However, after a critical time (t/t_g = 0.28) no new scattering centers are formed. When formamide is present, the critical reduced time for formation of scattering centers is longer.[93] The fractal nature of the network formed can be calculated from the slope of the Porod plot and is discussed in a later section, as are additional SAXS investigations.

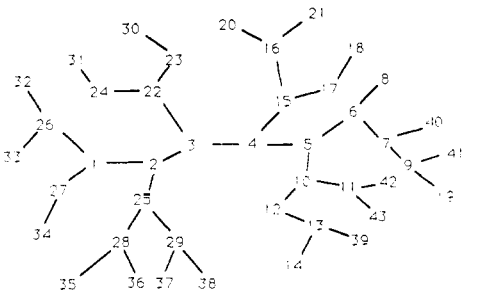

Figure 9. $Z = 3$; N = total number of bond sites = 43; n = total number of node bonds = 81; $P = 0.7$.

D. Classical or Mean-Field Theory of Gelation

The classical or mean-field theory of polymerization was developed by Flory.[79] The basis structure of this model looks like a tree and is called a Cayley tree or Bethe lattice. Figure 9 shows a Cayley tree model for a polymer that forms a connected, gel-forming cluster without forming rings. In this tree, the functionality or maximum number of bonds, z, that are allowed to form at each numbered bond site is

$$z = 3$$

Other polymers have different values for this parameter. For example, silicic acid has a functionality of $z = 4$. Four bonds may form at every site where silicon is present.

Returning to our model with $z = 3$, we can define the probability, P, of a bond forming at each site:

$$P \equiv \frac{\text{number of bonds}}{\text{total number of node bonds}} \tag{9}$$

$$P = n/(Nz) \tag{10}$$

where n = number of node bonds, N = number of sites, and z = dimensionality of the polymer. Thus, in our simple example, shown in Figure 9

$$N = 43; \quad z = 3; \quad n = 81 \tag{11}$$

This means that some bonds are counted twice. The number of connections for each numbered node is counted. For example (a) node 34 has one bond, (b) node 27 has two bonds, and (c) node 1 has three bonds. Therefore, the probability for a connection for each site in this example is

$$P = n/(Nz); \quad P = 81/[(43)(3)]; \quad P = 0.6 \tag{12}$$

This example forms a gel, as we have conceptually defined it, since the cluster is continuously connected from one side to the other. Thus, there must be at least two connections per node for the cluster to be a gel. This defines the critical probability, P_c, for gel formation to be

$$P_c = 1/2 \tag{13}$$

or in terms of the functionality of the polymer[324]

$$P_c = 1/(z - 1) \tag{14}$$

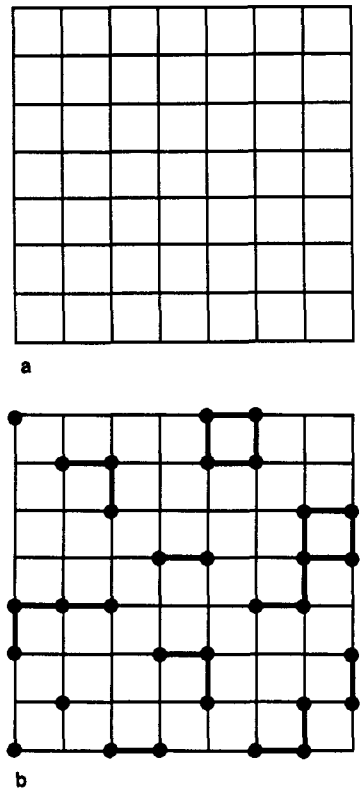

Figure 10. Site percolation model: (a) empty grid; (b) Raman filling of grid.

This defines then the degree of reaction at the gel point. The distribution of molecular weights can also be determined. However, there is a fatal flaw in this model. Because no rings are allowed, there is an increasing number of nodes as the radius of the cluster increases.

In fact, the mass of this type of cluster increases as the fourth power of the radius as shown by Zimm and Stockmayer[159] and de Gennes.[160] In real materials the mass must increase linearly with volume as the third power of the radius.

However, this model is still useful in visualizing the gelation of silica sol-gels. It yields a degree of reaction of one-third:

$$P_c = 1/(z - 1) = 1/3 \quad (15)$$

at the time of gelation. That means that two-thirds of the connections are still available and play a role in subsequent processing. This value is lower than the experimental evidence as we shall see in the next section. It does however represent the minimum degree of reaction before gelation can occur as presented by Flory.[324]

E. Percolation Theory

Percolation theory and its relationship to gelation has been reviewed by Zallen[161] and Stauffer et al.[162] Percolation allows for rings or closed loops to form, and thus the mass of percolation models increases with the cube of the radius.

Figure 10 shows a simple percolation model. Starting with an empty grid (Figure 10a), intersections are randomly filled with particles (filled circles). If two circles or particles are adjacent, then bonding will occur (Figure 10b). Loops of various sizes may form as the structure expands. This eliminates the fatal error of the classical model and is called a site percolation model.

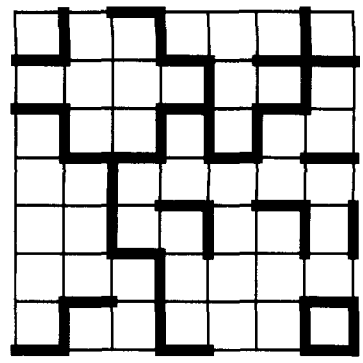

Figure 11. Bond percolation model.

In a manner similar to the classical model, the probability, P, that a site may be filled is defined as

$$P = n/N \quad (16)$$

where n = number of filled sites and N = total number of sites.

With the simple example in Figure 10

$$n = 32 \quad (17)$$

$$N = 64 \quad (18)$$

Thus

$$P = 1/2 \quad (19)$$

This simple model shows that for this value of site filling, complete connectivity or gelation is unlikely for the site model. Experimental results indicate that

$$0.6 < P_c \leq 0.84 \quad (20)$$

for silica sol-gel systems, as reviewed by Zarzycki.[81] Thus, this model must be modified to increase the connectivity.

By starting with all the sites filled and randomly adding bonds, the connectivity increases over the site model. Figure 11 shows a bond percolation model. Again we can define the probability of bonding as

$$P = n/N \quad (21)$$

where n = number of bonds and N = total number of bond sites.

In the case of the example in Figure 11 we have

$$n = 39 \quad (22)$$

$$N = 112 \quad (23)$$

$$P = 0.35 \quad (24)$$

where gelation appears likely.

The bond percolation model is dependent on the lattice. Table IV shows a summary of the percolation threshold for various lattices based on Brinker and Scherer.[70] The table also shows the volume fraction, ϕ_c, of the gel at gelation and the filling factor, v.

F. Fractal Theory

The fractal model of structures was designated as such by Mandelbrot[163] and gives order to the many seemingly random patterns generated by nature, such

TABLE IV. **Percolation Threshold for Various Lattices (from Brinker and Scherer[70])**

dimensionality d	lattice[a]	coordination z	$1/(z-1)$	p_c^{bond}	p_c^{site}	filling factor v	$\phi_c = v p_c^{site}$
1	chain	2	1	1	1	1	1
2	triangular	6	0.200	0.347	0.500	0.907	0.45
2	square	4	0.333	0.500	0.593	0.785	0.47
2	kagomē	4	0.333	0.45	0.653	0.680	0.44
2	honeycomb	3	0.500	0.653	0.698	0.605	0.42
3	fcc	12	0.091	0.119	0.198	0.741	0.147
3	bcc	8	0.143	0.179	0.245	0.680	0.167
3	sc	6	0.200	0.247	0.311	0.524	0.163
3	diamond	4	0.333	0.388	0.428	0.340	0.146
3	rep[b]	~8	~0.143		~0.27	~0.637	~0.16
4	sc	8	0.143	0.160	0.197	0.308	0.061
4	fcc	24	0.043		0.098	0.617	0.060
5	sc	10	0.111	0.118	0.141	0.165	0.023
5	fcc	40	0.026		0.054	0.465	0.025
6	sc	12	0.091	0.094	0.107	0.081	0.009

[a] fcc = face-centered cubic; bcc = body-centered cubic; sc = simple cubic; rep = random closed-packed. [b] Less precise values, determined experimentally.

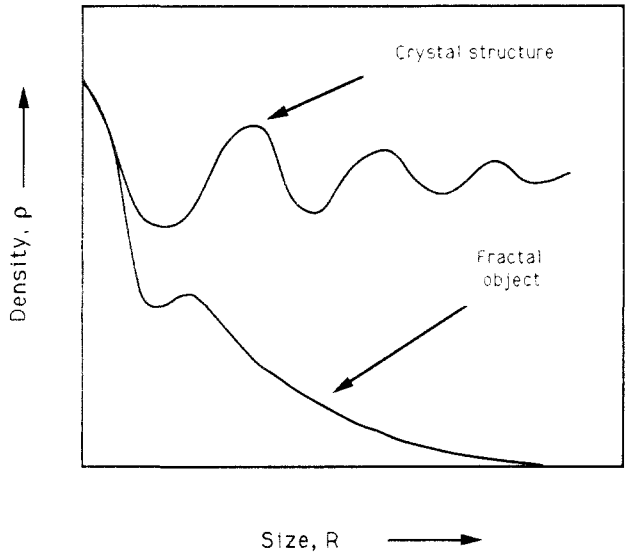

Figure 12. Density of fractal objects.

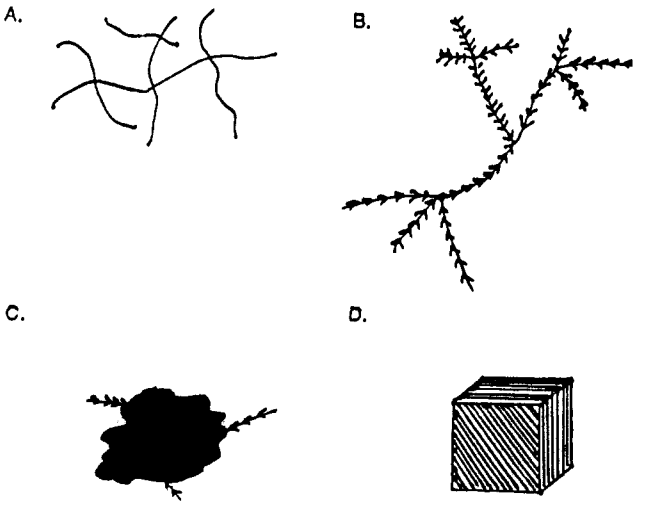

Figure 13. Fractal objects: (A) linear structures, $1 < d_f < 1.5$; (B) fernlike structures, $1.5 < d_f < 2$; (C) fractally rough structures, $2 < d_f < 3$; (D) solid structure, $d_f = 3$. Reprinted from ref 70; copyright 1989 Academic Press.

as trees,[163] galaxies,[164] or the surface of the sun.[165] Witten and Sander[166,167] and Witten and Cates[168] have demonstrated the fractal nature of diffusion-limited aggregation of particles. Growth processes that are apparently disordered also form fractal objects.[168] Sol–gel particle growth has also been modeled by using fractal concepts.[81,153,169]

The nature of fractals requires that they be invariant with scale. This is a symmetry that requires the fractal to look similar no matter what level of detail is chosen. For example, a tree as a whole has a very similar structure as a small branch within that tree.

The second requirement for mass fractals is that their density decreases with size (see Figure 12). Thus, the fractal model overcomes the problem of increasing density of the classical model yet retains many of its desirable features.

Fractal objects are quantified by their fractal dimension, d_f. Figure 13 shows objects with increasing fractal dimension.[70] For linear-like structures

$$1 < d_f < 2 \tag{25}$$

(as shown in Figure 13B). Fractally rough structures have a mass fractal dimension

$$2 < d_f < 3 \tag{26}$$

TABLE V

Keefer's model[153]	hydrolyzed monomer	fractal dimension d_f
nonfractal	100% triple	3
fractal	33% double	1.8
	33% triple	
	33% fully	
fractal	50% double	1.67
	50% fully	

(as shown in Figure 13C). Finally, uniform nonfractal objects have a fractal dimension

$$d_f = 3 \tag{27}$$

(as shown in Figure 13D). The mass of a fractal then is related to the fractal dimension and its size or radius, R, by

$$M \propto R^{d_f} \tag{28}$$

Therefore, computer models can be constructed to generate particle growth and measure the resulting fractal dimension.

One such fractal gelation model was developed by Keefer.[153] He postulated that sol particles grow from partially hydrolyzed TEOS ($Si(OC_2H_5)_4$). When fully hydrolyzed TEOS was used in the model, a fully dense particle was formed that had no fractal nature.

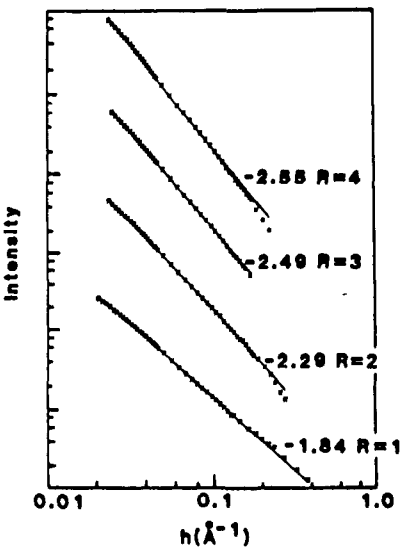

Figure 14. Small angle X-ray scattering curves (slit smeared) from 1 M solutions of $Si(OC_2H_5)_4$ hydrolyzed with varying amounts of H_2O; 0.01 NH_4OH was used as a catalyst. Reprinted from ref 153; copyright 1986 John Wiley & Sons, Inc.

Table V shows selected models with varying degrees of hydrolysis. This model yields values for d_f similar to those found experimentally through SAXS.

G. Small-Angle X-ray Scattering (SAXS)

Fractal particles with a radius of approximately 20 nm may be studied by SAXS. It can be shown (see ref 93 for a detailed review of this theory), that the scattered intensity (I) of X-rays for small angles is related to the fractal dimension of the particle, d_f:

$$I(h) \propto h^{-d_f} \tag{29}$$

$$h = 4\pi(\sin \sigma)/\gamma \tag{30}$$

where 2σ = scattering angle and λ = wavelength. Additionally the monomer involved in the fractal particle must be small:

$$R_g \gg h^{-1} \gg a \tag{31}$$

where R_g = radius of gyration and a = primary particle radius.

The radius of gyration is basically the radius of the scattering center derived from the number of scattering centers, N, per unit volume, v.

This leads to the equation for the scattering intensity known as Guinier's law:[145-147,169]

$$I(h) = N\rho_e^2 v^2 \exp[-\tfrac{1}{3}R_g^2 h^2] \tag{32}$$

where ρ_e = electronic density.

Figure 14 shows SAXS curves for various TEOS and H_2O sols with different R ratios, from Keefer's studies.[153] As the water content increases, (increasing R), the fractal dimension increases. That is, the particles become more dense.

The primary particle of radius, a, is between 1 and 2 nm as shown by Orcel et al.[94] and can be modeled by rings and chains of three to four silica tetrahedra. The secondary fractal particle has a radius, R_g, of 5–20 nm as seen from SAXS.[122]

For the TMOS-based sols investigated by SAXS, Figure 8 shown earlier, the fractal dimension, d_f, increases with time as does the Guinier radius (R_g). This behavior is shown in Figure 15 based on the data of Figure 8. The structure reaches a fractal dimension around 2.3 at the gelation point. Table V summarizes results of the structural and textural properties for two TMOS + H_2O solutions, with and without formamide as a DCCA.[156]

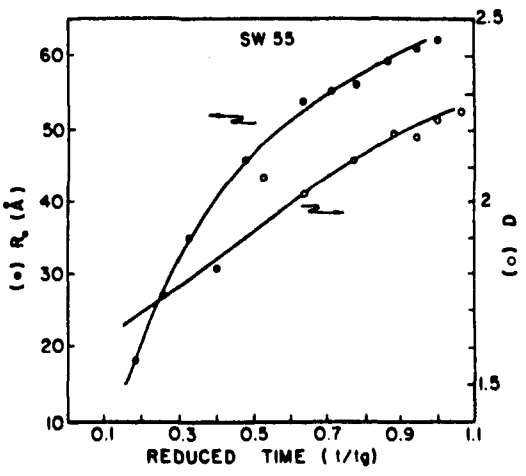

Figure 15. Time evolution of electronic radius of gyration (R_0) and fractal dimension (D) of a SW55 solution.[156]

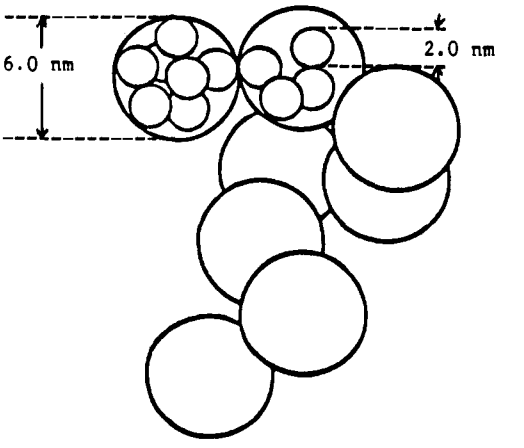

Figure 16. Schematic representation of primary and secondary particles in a TMOS-based alkoxide gel.

Near the gelation point the sols prepared from TMOS and H_2O are formed of particles of about 6.0-nm diameter compared to scattering units of about 2.0-nm diameter for the films.[156] Dilution experiments showed that the radius of gyration measured in the sols does not vary with the quantity of solvent.[93,156] This result indicates first that the Guinier approximation is valid for these systems and second that the polymer is relatively rigid.[152] These measurements are in very good agreement with the values obtained by the Mo acidic test.[93]

These results suggest that the gel structure is formed of different units, e.g., primary particles of about 2.0-nm diameter that agglomerate in secondary particles of about 6.0-nm diameter (Figure 16). On the basis of geometric considerations, these secondary particles contain at most 13 primary particles. Gelation occurs when the secondary particles are linked to each other, forming a three-dimensional network across the sample. Aggregation of particles carrying a surface charge can be modeled by the classical Derjaguin–Landau–Verwey–Overbeek (DLVO) theory.[171] This theory predicts

that the activation barrier to aggregation increases linearly with the size of two equal particles. Thus, the rate of aggregation would decrease exponentially with their size. Smaller particles however will aggregate with larger ones at a much higher rate. Thus, two distributions of particles are predicted, small newly formed particles and large aggregating particles.[325] This description of the structure of the sol and gel is confirmed by another X-ray diffraction study by Himmel et al.[170] They showed that gels manufactured from hydrolysis and polycondensation of TEOS by a small amount of acidic water are made of primary particles of about 1.0-nm diameter that associate in secondary chainlike clusters. The size of these clusters can be approximated as 6.0 nm in diameter, which is the average diameter of the pores. Also, TEM experiments on silica particles prepared by the Stober process[171] demonstrate that nucleation and growth occur by a coagulative mechanism, which supports the description of the gel structure given above.

The analysis of the diffraction curves in the Porod region leads to the computation of the fractal dimension (d_f). The quantity is dependent on the shape and geometry of the diffraction centers and also indicates a possible growth mechanism. Table III reports[156] the value of the fractal dimension of the sols near the gelation point. These values suggest a percolation cluster (PC) or a diffusion-limited aggregation (DLA) mechanism. Particles grow by addition of small polymeric units to randomly added sites on a nucleus (PC) or through a random walk to a seed cluster (DLA).[152] This description is in good agreement with the observation of a structure composed of agglomeration of units of different sizes: secondary particles made of several primary particles, which in turn agglomerate to form a gel.

In conclusion, the Keefer fractal model yields a range of fractal dimensions from 1.6 to 2.4 depending on the degree of hydrolysis. As the fractal dimension increases, the pore radius of the resulting gel should decrease. This relates well with the work of Orcel and others, where the degree of hydrolysis and condensation (or reaction rates) determine the pore-size distribution. The effects of adducts such as OH, HF, ammonia, or formamide control the rate of hydrolysis by raising the activation energy for the removal of water in order for condensation to occur.

V. Theoretical Studies

A. Hydrolysis and Condensation

Two models for the $Si(OR)_4$ hydrolysis reaction have been proposed, one in which a trivalent[172] and another in which a pentavalent[173] transition state is formed. Zerda and Hoang's work[174] using high-pressure Raman spectroscopy to study the hydrolysis of TMOS indicates that the model involving a pentavalent transition is correct. In the case of base catalysis, eq 33, the reaction

$$OH^- + \equiv Si\text{–}OCH_3 \rightarrow \equiv Si(OH)\text{–}OCH_3^- \rightarrow \equiv Si\text{–}OH + OCH_3^- \quad (33)$$

is caused by a hydroxyl ion. The OH^- ion has high nucleophilic power and is able to attack the silicon atom directly. These attacks are aimed toward the silicon atom since the Si atom carries the highest positive charge. At acidic conditions, the proton is attracted by the oxygen atom of the OCH_3 group, eq 34. This causes

$$H_3O^+ + \equiv Si\text{–}OCH_3 \rightarrow \equiv Si(H)(H_2O)\text{–}OCH_3^+ \rightarrow \equiv Si\text{–}OH + CH_3OH + H^+ \quad (34)$$

a shift of the electron cloud of the Si–O bond toward oxygen, and as a result the positive charge of the silicon atom increases. A water molecule can now attack the silicon atom, and a transition state is formed.[174]

The hydrolysis reaction is sufficiently slow that its dynamics can be studied by using high-pressure Raman spectroscopy, as shown by Zerda and Hoang.[174] For the first-order kinetics, the reaction rate constant is found from the slope of the logarithmic plot of the concentration of the reactant against time. Because the magnitude of Raman bands is proportional to the concentration of the molecules in the system, the reaction rate can be found from the time dependence of the band intensity. The pressure dependence of the reaction rate is related to the volume of activation.[175,176] At a pH varying from 4.9 to 7.5 and at a 1:10 molar ratio of TMOS to water, Zerda and Hoang determined the volume of activation, $\Delta V^{\ddagger}_0$, and its intrinsic, $\Delta V^{\ddagger}_i$, and solvent, $\Delta V^{\ddagger}_s$, components. $\Delta V^{\ddagger}_i$ represents the change in the volume due to changes in bond lengths and angles. It is negative when a new bond is formed. $\Delta V^{\ddagger}_s$ represents the change in volume due to changes in surrounding medium (electrostriction) during the activation step. Analysis of the results[174] ($\Delta V^{\ddagger}_0 = -52 \pm 10$, $\Delta V^{\ddagger}_i = -2$, $\Delta V^{\ddagger}_s = -50$ cm^3/mol) showed that in the transition state the silicon atom is in a pentavalent state. This was the first experimental proof for the pentavalent state of silicon in the transition stage of the hydrolysis reaction. These experimental results confirm a series of theoretical calculations.

Davis and Burggraf[177-180] have proposed mechanisms, based upon quantum mechanical calculations, for anionic silanol polymerization in which participation of hypervalent siliconates is important. As noted above hypervalent silicon is an important candidate as an intermediate in this chemistry. Strong anionic nucleophiles have been shown to form pentacoordinate complexes with silanes without activation in the gas phase.[181] Also, certain pentacoordinate siliconates are readily stabilized in solution.[182]

An important key to understanding silanol polymerization chemistry is identifying how water is eliminated as the polymerization proceeds. Davis and Burggraf's calculations[177-180] suggest that water is more readily eliminated from hypervalent siliconates than tetravalent silicates in hydroxide-catalyzed silanol polymerization. However, accurate prediction of the entire process of water elimination using an MNDO program is difficult because MNDO overpredicts dissociative activation energies and does not model hydrogen bonding interactions.[182] These faults are due to overestimation of core–core repulsions between atoms when they are separated by approximately van der Waals distances. The AM1 semiempirical program has largely overcome this drawback; see refs 183–186 for details. Consequently, Burggraf and Davis[182] have modeled silicic acid reactions using AM1 to predict siliconate elimination reactions as influenced by other nucleo-

philic species that can complex to form hypervalent intermediates. They applied semiempirical molecular orbital calculations to examine the formation of pentacoordinate silicic acid complexes with hydroxide ion and fluoride ion, as well as neutral adducts with hydrogen fluoride, ammonia, and formamide. They also have calculated reaction paths for water elimination from silicic acid complexes with hydroxide ion, fluoride ion, and hydrogen fluoride. The qualitative semiempirical picture of the reaction surface has been quantified by employing high-level ab initio calculations for selected intermediates and transition-state structures. The adducts studied were chosen because of their potential as catalysts or drying control agents in sol–gel processing chemistry. For example, as discussed earlier, formamide is used as a drying control additive for sol–gel chemistry to control the ratio of rates of siloxane hydrolysis and silanol polymerization.

The semiempirical methods used in Davis and Burggraf's research are part of the MOPAC program available from the Quantum Chemistry Program Exchange (QCPE) at the University of Indiana.[183] Semiempirical molecular orbital calculations were performed using MNDO6 and AM17 methods developed by Dewar and co-workers.[184,185] Revised silicon parameters were used for MNDO calculations.[186] All stationary points on the potential surfaces were fully optimized by using procedures of the MOPAC program. Force constant calculations and intrinsic reaction coordinate calculations were performed for each stationary point to determine the nature and connectivity of the potential surface.

Ab initio calculations were performed using the GAUSSIAN86 program and basis sets it contains.[187] All ab initio calculations in their work were single-point calculations at AM1 geometries. Estimates of energies at the MP1/6-31++G(d) level[188] were calculated by assuming correlation effects and polarization effects are additive.[189–191] Comparisons of ab initio results and semiempirical results are used to establish a quantitative benchmark for semiempirical energies in order to solve problems that are too large for high-level ab initio methods.[192]

For reaction of any nucleophile with silicic acid, two possible outcomes are (1) addition and (2) abstraction. By studying the possible reaction paths for the removal of water, the proton-abstracting pentacoordinated silicon has no activation energy for water removal. In contrast, the pentavalent silicon has a relatively large activation energy for removal of water if the proton is added and constrained to form its most stable structure before the water is removed.

Figure 17 shows both the proton abstraction and hydroxyl paths that include the addition of pentacoordinated silicon as an intermediate in the condensation reaction. The more favorable proton abstraction path is one where a proton from a silanol moves toward the hydrogen-bonded OH as the OH moves toward the silicon. This forms a pentacoordinated silicon intermediate where water easily escapes.

If, on the other hand, the OH is moved toward the silicon to form a stable pentacoordinated structure, the energy is much lower. From this structure, a significant activation energy is then required to eliminate the water.

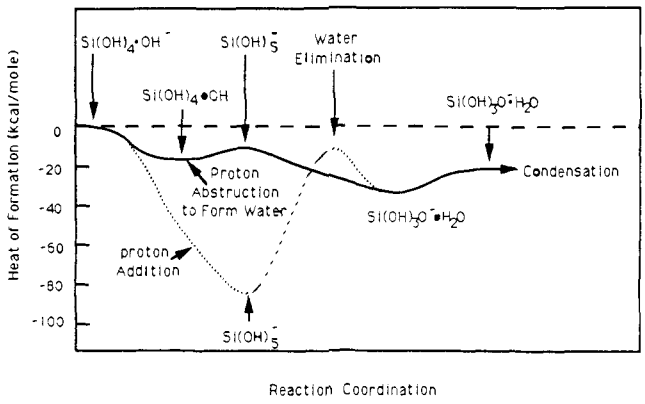

Figure 17. Formation of pentacoordinate silicon.

Burggraf and Davis[182] used MNDO, AM1, and ab initio molecular orbital models to predict the proton abstraction and resulting pentacoordinate silicon. They constructed similar models for HF ammonia and formamide adducts on silicic acid. For HF they also predict that the pentacoordinated silicon created by proton abstraction is the more favorable path to water elimination. The difference is that water elimination from HF adducts has a slight energy barrier. This indicates a shift to a slower condensation rate for the HF–silanol system over the OH–silanol system.

Ammonia and formamide adducts with silicic acid form by hydrogen bonding. Formamide is predicted to form a bistable bond in which one oxygen–silicon bond is shorter than the other. The long bond oxygens permit more favorable hydrogen-bonding interactions.

Burggraf and Davis[182] also calculated the energy of water adducts on silicic acid. They found that there were very small energy differences between the pentacoordinated water adducts and the corresponding hydrogen-bonded water adducts. This result is important when considering the effect of water adducts on rings of silica tetrahedra discussed in a later section.

B. Gelation

In the previous sections, we saw that experimental analyses of silica gelation using SAXS, Raman spectroscopy, and a Mo dissolution technique led to the conclusion that a gel network is preceded by the formation of very small clusters, or primary particles, of silica tetrahedra. The primary particles are apparently formed by polycondensation that favors nearly closed clusters of tetrahedra rather than linear chains.

This conclusion regarding the gelation and resulting ultrastructure of acid-catalyzed alkoxide-derived silica gels has been tested by West et al.[193] and Davis and Burggraf[194] using semiempirical quantum calculations.

The calculations done by West et al. used an intermediate neglect of differential overlap (INDO) molecular orbital model.[193] The INDO program was made available by the Quantum Theory Project at the University of Florida.[195] The calculations done by Davis and Burggraf used the AM1 model.[194]

The silica structures evaluated contain from one to six silica tetrahedra. In each model two bridging oxygens and two nonbridging oxygens are bonded to each silicon. One hydrogen is bonded to each of the nonbridging oxygens to terminate the structure and balance the charge. Both ring and chain models of silica tetrahedra were evaluated, and their energies compared.

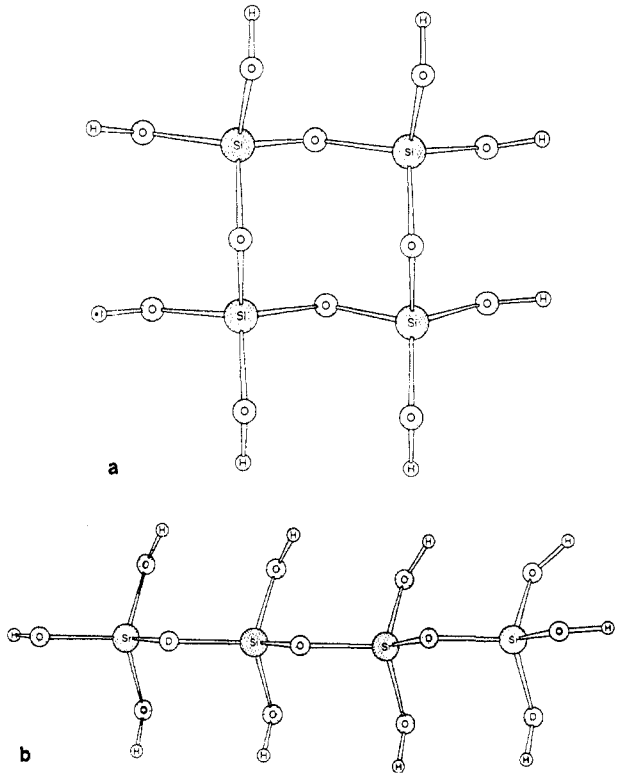

Figure 18.

TABLE VI. **INDO Calculations for Silica Structures**

no. of silica tetrahedra	struct	INDO energy per Tetrahedra, au	HOMO-LUMO UV cutoff wavelength, nm
1	tetrahedra	-73.82	87.1
2	chain	-64.72	130.7
2	ring	-55.82	112.8
3	chain	-61.74	132.7
3	ring	-55.86	106.2
4	chain	-60.25	139.6
4	ring	-55.80	114.3
5	chain	-59.35	134.2
5	ring	-55.76	144.3
6	chain	-58.55	135.8
6	ring	-55.79	114.1

Figure 18 shows the 2-D projections of chain and ring structures for four silica tetrahedra that have been geometrically optimized to minimize the molecular energy by using INDO calculations. These projections are typical of the hydroxylated silica structures modelled by West et al.[193] and Davis and Burggraf.[194] The clusters were each optimized for the minimum energy by using a molecular mechanics (MM2)[196] routine. The molecular orbitals were determined by using geometrically optimized INDO calculations. The molecular energies were evaluated and compared to establish the relative stability of each structure. The energy gap between the highest occupied molecular orbital (HOMO) and the lowest unoccupied molecular orbital (LUMO) for the single states and the corresponding UV cutoff wavelength were determined. The calculated optical properties are compared with experimental values in the properties section of this review.

Table VI, summarizing the INDO calculations, is shown to compare the relative stability of the INDO structures. The more negative the energy, the more stable the structure. These differences are exaggerated because each chain structure has an extra water molecule when compared to the ring structure.

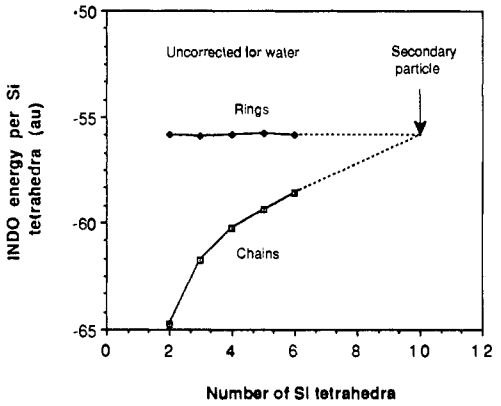

Figure 19.

TABLE VII. **Cluster Sizes for Rings and Chains of Tetrahedra**

no. of silica tetrahedra N	cluster size, Å		INDO (chain–ring), au
	rings	chains	
2	6.6	9.1	8.9
3	7.1	12.7	5.9
4	9.3	16.3	4.4
5	11.3	19.8	3.6
6	11.9	23.4	2.8

Figure 19 shows the INDO energy per silica tetrahedra for rings and chains as a function of the number of tetrahedra. It suggests that the chain structures are more stable than the rings for small number of silica tetrahedra. This has been observed experimentally by Klemperer and Ramamurthi[97] and Orcel and Hench[116] using NMR spectroscopy, where a linear, as opposed to a ring, growth model most consistently interprets the experimental structural evidence prior to gelation.

As mentioned earlier, investigators[94] have proposed models for the structure of acid-catalyzed silica gels containing two levels of structure formed before gelation. These models propose the formation of primary particles, of diameter 1–2 nm, which agglomerate to form secondary particles of about 4–6 nm before drying. The secondary particles give rise to the pore structure after drying.

Table VII shows the differences in the INDO structural energies between chains and rings (C–R). The relative stability of chains compared to rings decreases as the number of silica tetrahedra increases by the decrease in the difference between their calculated INDO energies. The difference is estimated to reach zero as the number of tetrahedra reaches about 10 or 12, when the driving force for rings becomes more favorable than for chains. This result is similar to the size range where secondary particle growth stops in acidic silica sols.[94] Acid catalysis ensures complete hydrolysis of the silica tetrahedra, as used in these calculations. The size of the INDO-calculated rings or clusters for 10–12 tetrahedra appears to fall within the range of the radius of gyration of the primary particles calculated from SAXS analysis of acid-catalyzed silica sols.[94,156]

As gelation occurs, the cross-linking of the structure becomes more dominant. A statistical analysis conducted by Zarzycki[81] indicates that chain growth is limited by this process and rings must be formed. The energy differences in the ring structures in the INDO model are very small. This indicates that a broad distribution of ring sizes may be possible in a gel as they

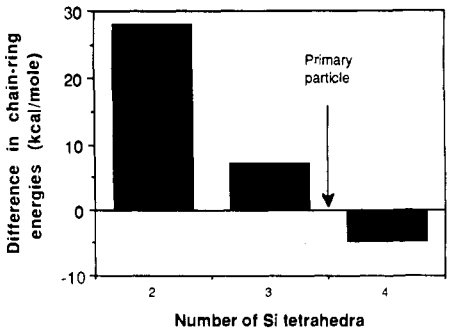

Figure 20. AM1 corrected energy difference.

TABLE VIII. **AM1 Enthalpies of Rings and Chains at 25 °C (kcal/mol)**

no. of silica tetrahedra N	ΔH_f			
	chain	ring	water	differences
1	-296.8			
2	-545.4	-458.2	-59.2	+28.0
3	-794.0	-727.6	-59.2	+7.2
4	-104.3	-991.7	-59.2	-4.6

become energetically more favorable.

Davis[194] recalculated the energetics of rings and chains using AM1. His calculations were corrected for the extra water molecule in the chains as compared to the rings. The AM1 energies were also corrected for zero-point energy and converted to enthalpies at 25 °C. These corrections moved the crossover energy from 10 to 12 tetrahedra to 3 or 4 tetrahedra (see Figure 20). Table VIII shows the enthalpies, ΔH_f, in kcal/mol for rings and chains and their differences.

Chains are still the most likely to occur in the early stages of hydrolysis and condensation. The important feature is that chains and rings are reversed in energy difference when three to four tetrahedra or more are formed. The driving force to produce chains is eliminated, and therefore 4-fold rings are very likely. This corresponds very closely to the 1–2-nm primary silica particles that form prior to agglomeration, as shown in Tables III and VII. Thus, results from quantum mechanical calculations compare quite favorably to experimental observations for the ultrastructure development in alkoxide-derived silicas.[197-204]

VI. Aging

When a gel is maintained in its pore liquid, its structure and properties continue to change long after the gel point. This process is called aging. Four processes can occur, singly or simultaneously, during aging, including polycondensation, synerisis, coarsening, and phase transformation. Although there is an extensive literature on aging by Iler,[15,76,120] and Scherer has made an effort to describe aging phenomena theoretically,[70,205] there is relatively little detailed knowledge of aging mechanisms and kinetics and even less quantitative analysis of the effects of aging on gel structure and properties.[206]

Polycondensation reactions, eqs 3 and 4, continue to occur within the gel network as long as neighboring silanols are close enough to react. This increases the connectivity of the network and its fractal dimension. Syneresis is the spontaneous shrinkage of the gel and resulting expulsion of liquid from the pores. Coarsening is the irreversible decrease in surface area through dissolution and reprecipitation processes.

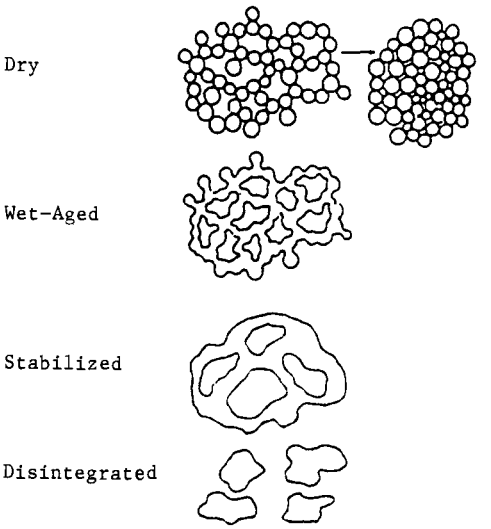

Figure 21. Stages in aging of gel: (A) Gel as formed and dried. Shrinks on drying, giving small pore volume and pore diameter. (B) Wet heat-aged—increased coalescence. Little shrinkage on drying. Pore diameter larger than the dried sample A. (C) Further heat aged or autoclaved. Structure-coarsened small area and large pores but same pore volume as sample B. (D) Disintegration to irregular round particles.

A. Polycondensation

Usually in alkoxide-based gels the chemical hydrolysis reaction is very rapid and is completed in the early stage of sol preparation, especially when the sol is acid catalyzed. For silica gels synthesized in alcoholic solutions, i.e., made by hydrolysis and condensation of alkoxides, nuclear magnetic resonance (NMR,[207,208] Figure 21) and Raman spectroscopies[209] show that the number of bridging bonds increases long after gelation. The condensation reaction continues to occur because of the large concentration of silanol (SiOH) groups in a newly formed gel. As the hydroxyls are lost during aging, new bonds are formed, creating more cross-linked structures. ^{29}Si NMR results of Kelts et al.[207] show substantial amounts of Q^2 species at the gel point, and the proportions of Q^3 and Q^4 species increase with time long after gelation. As discussed earlier, Q^n represents a Si atom bonded through a bridging oxygen to n other Si atoms.

Since the chemical reaction is faster at higher temperature, aging can be accelerated by hydrothermal treatment, which increases the rate of the condensation reaction.

B. Syneresis

The shrinkage of the gel and the resulting expulsion of liquid from the pores is called syneresis.[76,205,210] Syneresis in alcoholic gel systems is generally attributed to formation of new bonds through condensation reactions, which increases the bridging bonds and causes contraction of the gel network. In aqueous gel systems, or colloidal gels, the structure is controlled by the balance between electrostatic repulsion and attractive van der Waals forces. Therefore, the extent of shrinkage is controlled by additions of electrolyte. Vysotskii and colleagues[211,212] have shown that the rate of contraction of silica gel during syneresis has a minimum at the isoelectric point (IEP). For silica this point is at a pH of 2, at which the silicate species are un-

charged.[76] Since the condensation is the slowest at that point, this suggests that the shrinkage is driven by the condensation reaction in eq 3.

It has also been suggested by Scherer[70,205] that contraction is driven by the tendency to reduce the huge solid–liquid interfacial area of the gel. This might be accomplished by flexure of the solid phase, bringing surfaces into contact, in which case it would be indistinguishable from the reaction-driven mechanism. That means the chemical potential of the gel is reduced by both chemical reactions (since the condensation reaction is exothermic) and the reduction in the solid–liquid interfacial area. But Scherer also shows that the latter suggestion is not supported by experimental results.[83] The syneresis contraction rate increases with concentration of silica in the sol and with temperature. When organic solvents are present, they may form hydrogen bonds with the silanol groups, which inhibit condensation and slow syneresis. Vysotskii and Strazhesko show that the rate of syneresis decreases with time.[211] This could result from the increasing stiffness of the network as more bridging bonds are formed.

Ponomareva et al.[213] found that the total syneresis strain is greater at lower temperatures, although the contraction rate is slower. They argued that at higher temperature the condensation reaction is faster, so the gel becomes stiff faster and shrinkage is prevented. If this is so, it implies that the shrinkage is not proportional to the scale of reaction. They conclude each bond does not cause a certain amount of strain. Another factor that may affect the rate of contraction is the permeability of the gel to the flow of liquid in the pores.

C. Coarsening

Another process, called "coarsening" or "Ostwald ripening", is discussed at length by Iler[76] and co-workers.[214] Since convex surfaces are more soluble than concave surfaces, if a gel is immersed in a liquid in which it is soluble, dissolved material will tend to precipitate into regions of negative curvature. That means that necks between particles will grow and small pores may be filled in, resulting in an increase in the average pore size of the gel and decrease in the specific surface area.

Since the solubility of silica increases at high pH, so does the rate of coarsening of silicate gels. It is not surprising that the rate of coarsening of gels is similarly pH dependent. The pore-size distribution in a silica xerogel increases as a result of aging in a basic solution.

At a given normality, Sheinfain et al.[215] found the effect of solution on aging to decrease in the order HCl > H_2SO_4 > H_3PO_4; however, the rate of aging was independent of the type of acid if the activity of the proton was the same in each solution. They examined the coarsening of silica gels in concentrated mineral acid ($1 < pH < 2$) and showed that silica is even soluble at very low pH. Iler[76] provides a number of references concerning the change in the surface area and the pore size during aging. The reduction in surface area is produced by dissolution and reprecipitation. A high pore volume results because the stiffer gel produced by aging does not shrink as much under the influence of capillary pressure.

Okkerse[77] has shown that the texture of silica can be affected in every stage of its preparation, including gelation, after-treatment of the hydrogel by aging and washing with various liquids, and drying. These influences can be qualitatively understood and predicted on the basis of a condensation theory of aging. This theory attributes a major role to the rate of the condensation reaction of silicic acid in all stages during the development of the texture.

D. Processing Parameters That Affect Aging

Time, temperature, and pH are parameters tht can effectively alter the aging process. Iler[122] recognized that once the gel structure has been formed it can be further modified in the wet state by treatment to (1) strengthen the structure without greatly affecting the pore structure (sometimes referred to a gel reinforcement) or (2) enlarge the pore size and reduce the surface area by a process of dissolution and redeposition of silica, thereby coarsening the gel texture.

Sheinfain et al.[215] recognized the first two distinct stages in the thermal-aging process. The more extensive the wet aging, the subsequently dried gel shrinks less and the pore volume and diameter are greater, but there is very little change in surface area. Second, upon further aging the surface area begins to decrease while the pore size continues to increase. However, there is then little further change in pore volume. The explanation is clear from the stages of aging shown in Figure 21. The first stage involves only an increased coalescence or bonding between the ultimate particles which strengthens the gel so that it shrinks less upon drying.

Heating the gel in water until the specific surface area has been reduced by 10–50% can strengthen the weak gel structure. Heating gel in water at 80–100 °C generally brings about reinforcement but does not modify the pore structure. It is interesting that at 80 °C Liu showed[206] there was no effect unless the gel had a surface area greater than 200 m^2/g.

Prolonged aging of silica gel with an initial surface area of 920 m^2/g in water at pH 6.8 at room temperature was carried out by Sheinfain et al.[215] The surface area dropped from 725 to 420 m^2/g, while the pore radius increased from 9 to 43 Å. However, the porosity also increased from 0.31 to 0.90 cm^3/g. The structure was thus strengthened so that shrinkage upon drying was reduced. The reinforcement was striking when samples were first washed with acetic acid and then dried. Since the surface tension of acetic acid is only one-third that of water, the reinforced gel had a much higher pore volume of 2.36 cm^3/g, which is a low-density gel.

The rate of coarsening of silica increases with temperature and pressure, as discussed by Iler.[76] Aging in water above 100 °C under pressure in an autoclave brings about far greater structural changes than can be obtained at 100 °C. Van der Grift et al.[216] prepared silica gels by neutralization of alkaline silicate solutions and aged them in an autoclave in water at various temperatures. When the temperature was above the boiling point of water, the sample was exposed to steam at high pressure, resulting in hydrothermal aging.

Washing the pore liquor out of a gel is also an "aging" step, and the pH of the wash water is critical in the case of gels made from acid-catalyzed silicate precursors. The final properties of such gels depend on both the pH at which the gel was formed and the pH in which

it was washed (aged) before drying. For example, Okkerse et al.[217] heated a series of gels for 1–4 days at 80 °C in water, acid, and potassium chloride solutions and found that if the gel had a specific surface area greater than about 200 m^2/g, then it underwent a decrease in surface area. There was little effect at pH 2, but in neutral or alkaline solution, especially in the presence of salt, the gel texture was markedly coarsened. For example, the surface area decreased from 752 to 452 m^2/g while pore radius increased from 13 to 22 Å, but volume remained at 0.5 cm^3/g.

Soaking a silica gel in dilute ammonium hydroxide solution at 50–85 °C can result in drastic coarsening of the gel texture. Girgis[218] reported that even soaking a silica gel at pH 10–11 for 1 day at 20 °C caused the surface area to drop from 650 to 467 m^2/g with a corresponding increase in pore radius. It might be thought that since silica does not dissolve at low pH, acids would have little effect on wet aging other than to adjust pH. However, Sheinfain et al.[215] found that treating the gel with strong acids, HCl, HNO_3, or concentrated H_2SO_4 before drying increases the pore volume of the dried gel without lowering the surface area. This is because the acid promotes coalescence between particles without particle growth and coarsening of the texture. On the other hand, 8 N H_2SO_4 caused a drop in surface area from 700 to 300 m^2/g and at the same time increased the pore volume.[215] Thus, strong acids (pH < 2) promote the aging of silica gel but, unlike alkalis as an aging promoter, cannot dissolve the gel if added in excess.

It is seen that aging and thermal treatments result in a one-way process: loss of specific surface area and an increase in pore size. The pore size can be enlarged also by dissolution of some of the silica. Sheinfain et al.[215] reported that treating a gel with 0.5 N KOH or dilute HF can enlarge the pores from 0.7 to 3.7 nm. If silica were dissolved away evenly from all the surface, there should be an increase in specific surface. However, it is probable that regions of lower radius of curvature will dissolve more rapidly so that the specific area may actually decrease.

The fractal nature of a gel will also be a major influence on the gelation and aging process as discussed earlier.[219] Condensation reactions between gel network segments will be more important when the number of interconnections is large.[151]

E. Properties

During aging, there are changes in most physical properties of the gel. In the study of aging kinetics of silica gel, the textural properties (i.e., pore size, porosity, and surface area) are of great importance. With respect to drying behavior, it is the change in mechanical properties during aging that is most important.

Inorganic gels are viscoelastic materials responding to a load with an instantaneous elastic strain and a continuous viscous deformation. Since the condensation reaction creates additional bridging bonds, the stiffness of the gel network increases, as does the elastic modulus, the viscosity, and the modulus of rupture. This is illustrated in Figure 22, which shows the increase in modulus of rupture of silica gel during aging for a gel with a water/TMOS ratio of 16/1.[220] The modulus of rupture of a gel aged at 105 °C reaches 40 Pa by 40

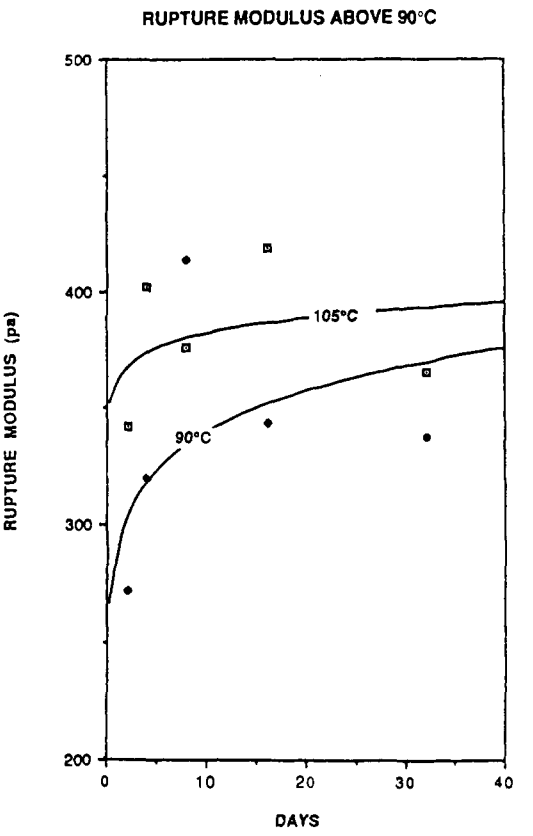

Figure 22. Rupture of modulus of wet gel (made from TMOS) versus aging time.[220]

days. West et al.[220] showed that gel strength increased logarithmically with times ranging between 1 and 32 days. The strength increased exponentially with temperature between 25 and 105 °C. The strongest gels produced had rupture moduli of approximately 400 Pa.

Similar data were obtained by Pardenek et al.[221] for polymer gels as well as for colloidal gels made from fused silica. Dumas et al.[222] followed the shear modulus for 9 months in gels made from TEOS and found that it continued to increase. The strength of the gel also increased with aging. For that reason, it is advisable to age large monolithic gels before drying to reduce the chance of cracking.[52,53] The greater stiffness of the aged gel reduces the shrinkage during drying as mentioned before, especially if the aging treatment is performed under hydrothermal conditions.

VII. Drying

The drying behavior of porous solids has been extensively studied by Sherwood,[223-225] Keey,[226] Mujumdar,[227,228] Moore,[229] Whitaker,[230] Cooper,[231] Ford,[232] and Scherer.[70,82-88,233] However, most of the data have been on powder systems with relatively large pores. Even the few quantitative studies conducted on gels by Kawaguchi et al.[234] and Dwivedi[235] have been on large pore gels. Consequently, theoretical analyses of gel drying such as by Scherer[70,80-88,233] or by Zarzycki[81] using Cooper's model for ceramic powders[231] have been based upon classical concepts of drying.

It has been generally accepted since the time of Sherwood[70,233-235] that there are three stages of drying:

Stage 1: During the first stage of drying the decrease in volume of the gel is equal to the volume of liquid lost by evaporation. The compliant gel network is deformed

by the large capillary forces, which causes shrinkage of the object. In classical large-pore systems, this first stage of drying is called "the constant rate period" because the evaporation rate per unit area of the drying surface is independent of time.[229-236] A detailed review of the drying phenomena associated with the constant rate period is presented in Brinker and Scherer.[70] This behavior is applicable to gels made by colloidal precipitation (method 1) or base-catalyzed alkoxide gels (method 3) that have pores >20-nm average diameter.

However, a recent quantitative analysis by Wilson[237] and Wilson and Hench[238,239] of the drying kinetics of acid-catalyzed alkoxide gels shows that for gels with pores <20 nm the rate of drying in stage 1 is *not* constant but in fact decreases substantially. As discussed below, this behavior is due to changes in pore radii during drying, which cause substantial reductions in vapor pressure of the liquid in the small pores. For large or small pore gels the greatest changes in volume, weight, density, and structure occur during stage 1 drying. Stage 1 ends when shrinkage ceases.

Stage 1 ends and stage 2 begins when the "critical point" is reached; classical drying theory calls this the "leatherhard point".[232-236,240] The critical point occurs when the strength of the network has increased, due to the greater packing density of the solid phase, sufficient to resist further shrinkage. As the network resistance increases, the radius of the meniscus is reduced. Eventually, at the critical point, the contact angle approaches zero and the radius of the meniscus equals the radius of the pore. This condition creates the highest capillary pressure, and unable to compress the gel any further, the pores begin to empty, which is the start of stage 2. In stage 2 liquid transport occurs by flow through the surface films that cover partially empty pores. The liquid flows to the surface where evaporation takes place. The flow is driven by the gradient in capillary stress, as described by Whitaker.[241] Because the rate of evaporation decreases in stage 2, classically this is termed "the first falling rate period".[242-244]

Stage 3: The third stage of drying is reached when the pores have substantially emptied and surface films along the pores cannot be sustained. The remaining liquid can escape only by evaporation from within the pores and diffusion of vapor to the surface. During this stage, called the "second falling rate period",[225] there are no further dimensional changes but just a slow progressive loss of weight until equilibrium is reached, determined by the ambient temperature and partial pressure of water. Whitaker[230,241] has developed a theoretical analysis of the second falling rate period. Brinker and Scherer[70] review the factors in this stage that are relevant to the drying of gels.

A comparison of Dwivedi's results[235] on the drying of an alumina gel with those of Wilson and Hench[238,239] for an acid-catalyzed alkoxide silica gel illustrates the importance of pore size in gel drying behavior. Dwivedi prepared the alumina gels using the Yoldas[57] method, which yields gels with pores ≫20 nm. Samples up to 3 mm thick were weighed at periodic intervals during drying at 80 °C. Figure 23, from Dwivedi,[235] shows that the rate of water loss was constant from his gels during stage 1 (within the range of the considerable experimental error caused by removing the sample from the oven for weighing). He showed that the rate was similar

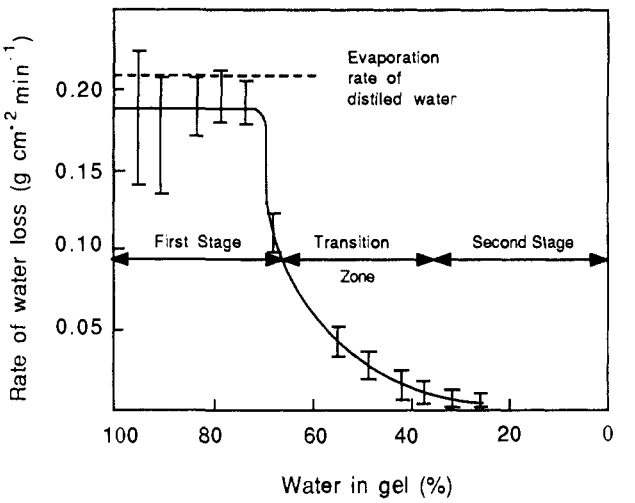

Figure 23. Plot of rate of water loss against water in the gel for various initial thickness gel sections.[235]

to that of evaporation from a free layer of distilled water. The gel lost pore liquid at a constant rate until the critical point was reached at about 35% water remaining in the gel, or onset of stage 2. Dwivedi reports that the constant-rate period was independent of gel thickness and was controlled by surface vaporization fed by capillary flow of pore liquid to the surface.

The drying rate of Dwivedi's gels decreases considerably from the critical point onward in stage 2, the first falling rate period (called the transition zone by Dwivedi),[235] until the onset of stage 3 (called the second stage by Dwivedi). He found that 87% of the initial liquid present in the gel was removed in stage 1, 10% in stage 2, and only 3% in stage 3. He concluded that water transport in stage 3 was by diffusion in the gas phase. He also found that cracking almost always occurred at some point in stage 2, where the water–air interface moves inward and was strongly dependent on the thickness of the gel. At dried thicknesses less than 80 μm the gel shrinkage was primarily perpendicular to the surface and cracks seldom occurred. At 40-μm thickness no cracks occurred. At thicknesses >80 μm shrinkage was both radial and perpendicular and cracking was prevalent. Dwivedi[235] explains the thickness sensitivity of cracking in terms of differences in the rate of diffusion of water in the transition between stages 2 and 3.

Brinker and Scherer[70] show quantitatively that it is indeed the difference in shrinkage rate between the inside and outside of a drying body that results in a tensile drying stress, σ_x. They show that the tensile stress (σ_x) as a function of thickness (L) is

$$\sigma_x(L) \approx L\eta_L V_E/3D \qquad (35)$$

where η_L = viscosity of the liquid, V_E is the evaporation rate, and D is the permeability of the network. This equation shows that as the thickness of a gel (L) increases or the evaporation rate, V_E, increases, the probability of cracking increases. For example, Brinker and Scherer[70] show that for a "typical gel" with strength after casting of ~0.1 MPa, η_L = 0.001 Pa s, L = 1 cm, and permeability $D = 10^{-14}$ cm^2 the strength will be exceeded for any drying rate, $V_E > 0.03$ μm/s. This corresponds to a minimum drying time of $L/V_E \approx 4$ days. This result is consistent with the observation that a gel will spontaneously fracture when exposed to the

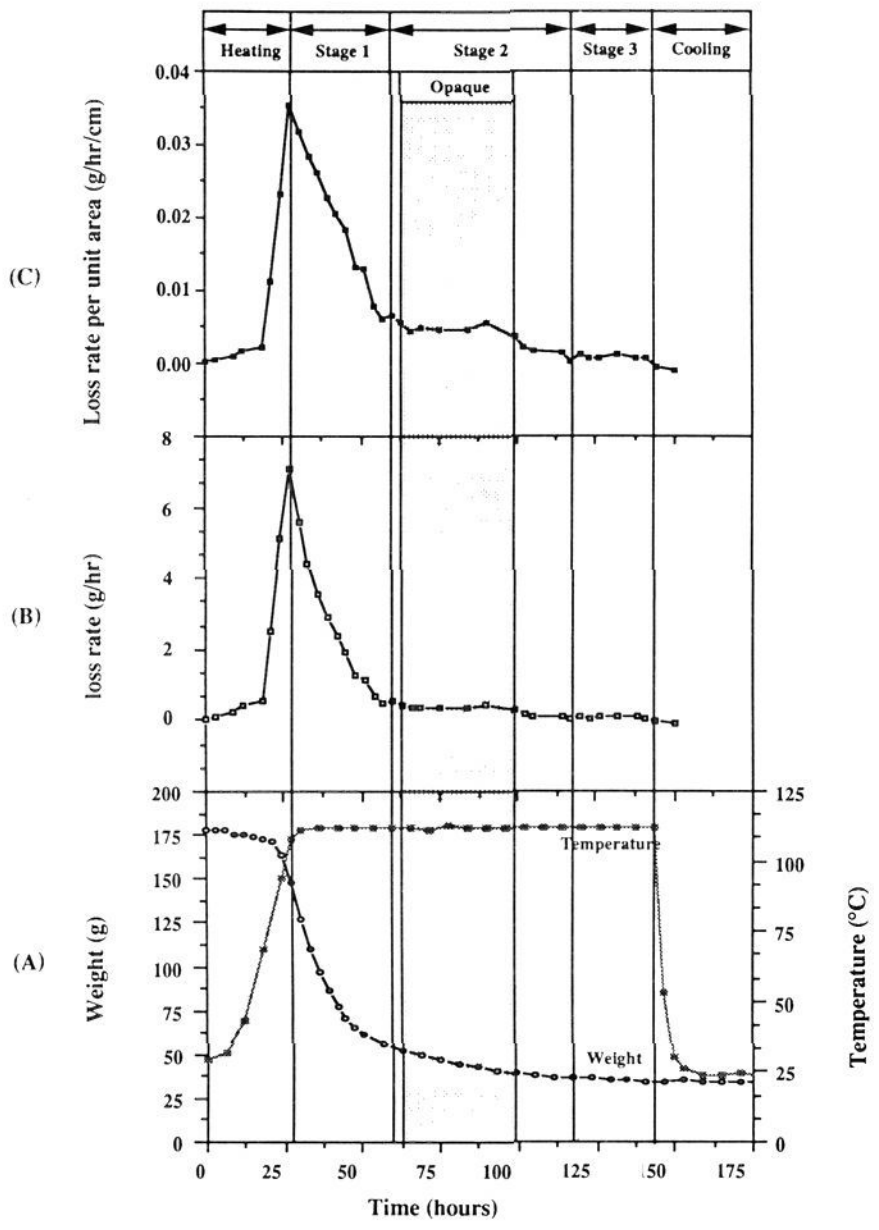

Figure 24. Time dependence of (A) temperature and weight; (B) absolute loss rate; (C) loss rate per unit area for gel A.[237]

atmosphere after casting. It also is consistent with the fact that traditional porous ceramic bodies are much more crack resistant during drying. Since the permeability of a 50% porous body with 1-μm pores has a value of $D \approx 10^{-10}$ cm^2, the stress will be 10^4 smaller than in a gel drying at the same rate.

When the pores in a gel are <5 nm, characteristic of acid-catalyzed alkoxide gels, the analysis of drying stresses is complicated by the fact that stage 1 is *not* a constant-rate period of drying. This is in dramatic contrast to all classical drying experiments. As shown in Figure 24, from Wilson and Hench,[239] the evaporation rate from the gel during stage 1 dropped from a maximum of 0.034 to 0.013 g/(h cm^2) at the critical point, even though the meniscus remained at the surface throughout this stage, as required by the definition of stage 1. These data were taken by use of a specially designed drying apparatus developed by Wilson[237] that permitted simultaneous monitoring of sample dimensions, weight, and optical properties at constant temperature and atmosphere without removing the samples from the drying chamber.[238] Consequently, high accuracy was obtained. Wilson and Hench[239] show the time dependence of weight and dimensions of a representative silica gel monolith in Figure 25. The relationship between relative weight (W/W_0) and relative volume (V/V_0) of the gel during the various stages of drying is shown in Figure 26. The change between stage 1 and stage 2 is very clear.

The reason for the decrease in drying rate in stage 1 for these gels is associated with the effect of pore

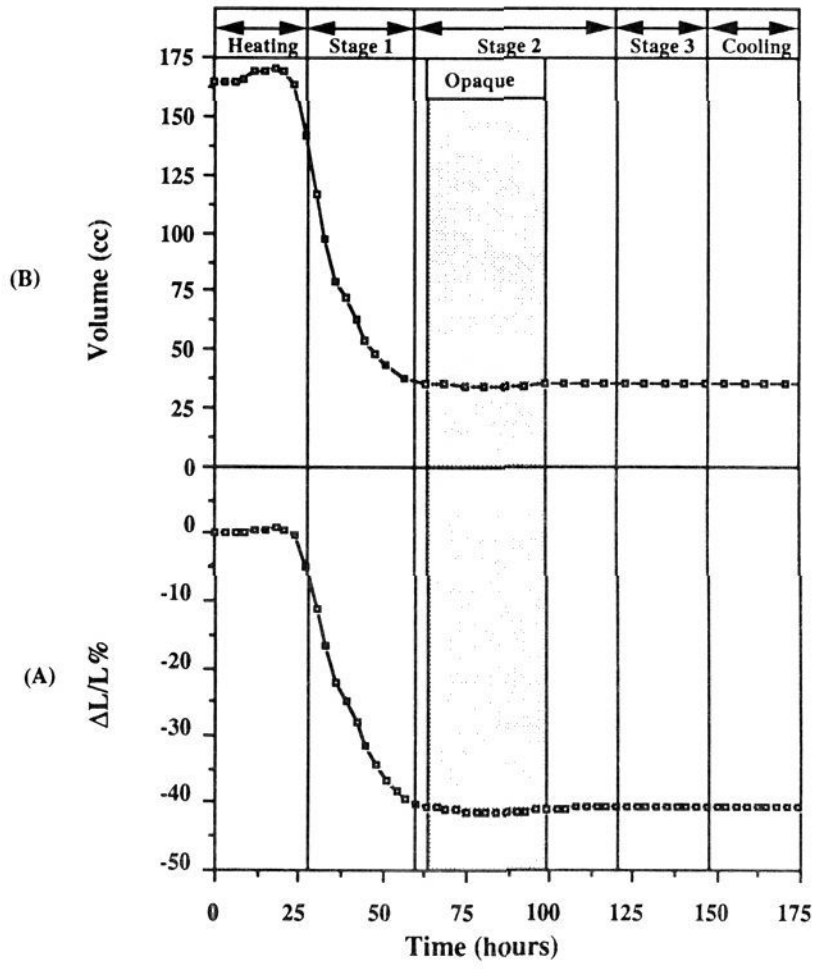

Figure 25. Time dependence of (A) linear reduction; (B) volume reduction $\Delta L/L$ percent for gel A.[237]

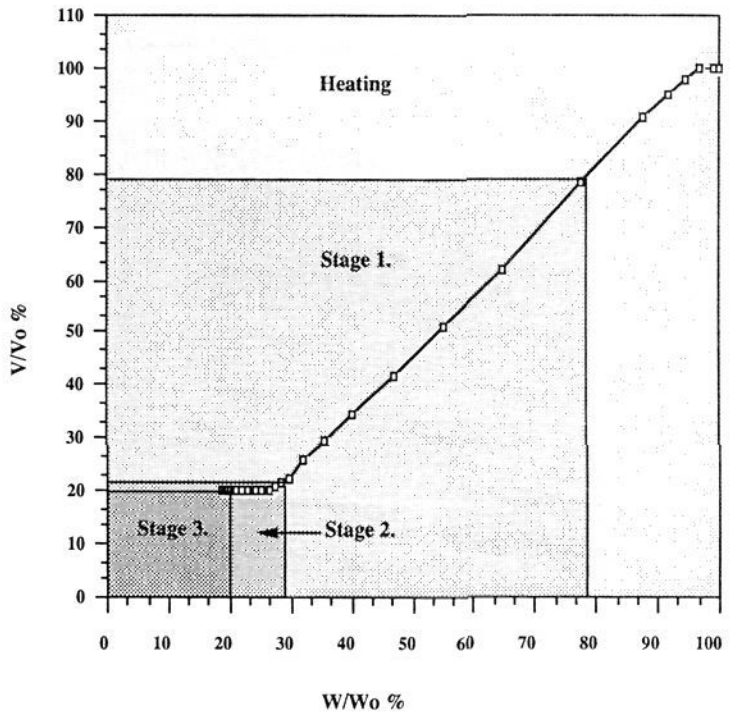

Figure 26. W/W_0 percent vs V/V_0 percent for gel B.[237]

radius on evaporation rate. Recall that acid-catalyzed alkoxide gels have very small pores, <5 nm. The evaporation rate from the gel is dictated by the difference between the vapor pressure at the evaporating surface, P_s, and the vapor pressure of the ambient atmosphere, P_a. Evaporation continues as long as $P_s > P_a$ with a rate (V_e):

$$V_e = K_e(P_s - P_a) \tag{36}$$

where K_e is a constant.

The vapor pressure of a surface comprised of a large number of very small pores, P_v, will be influenced by the radii of the pores, as described by the Gibbs–Kelvin equation

$$\ln \frac{P_s}{P_0} = \frac{B\gamma}{RT}\frac{2}{r_m} \tag{37}$$

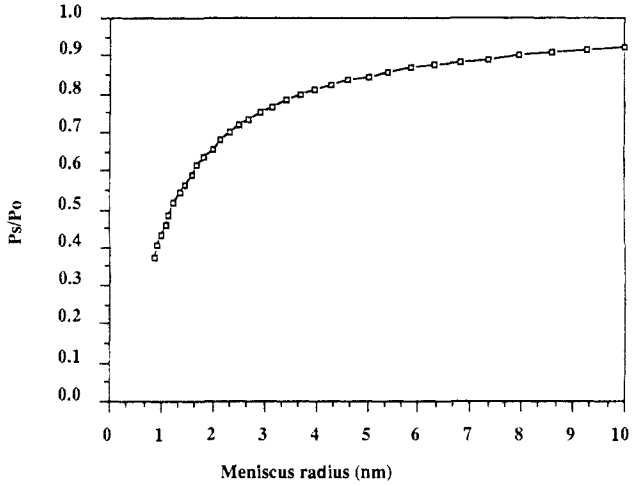

Figure 27. Reduction of vapor pressure with decreasing meniscus radius as predicted by the Gibbs–Kelvin equation.[237]

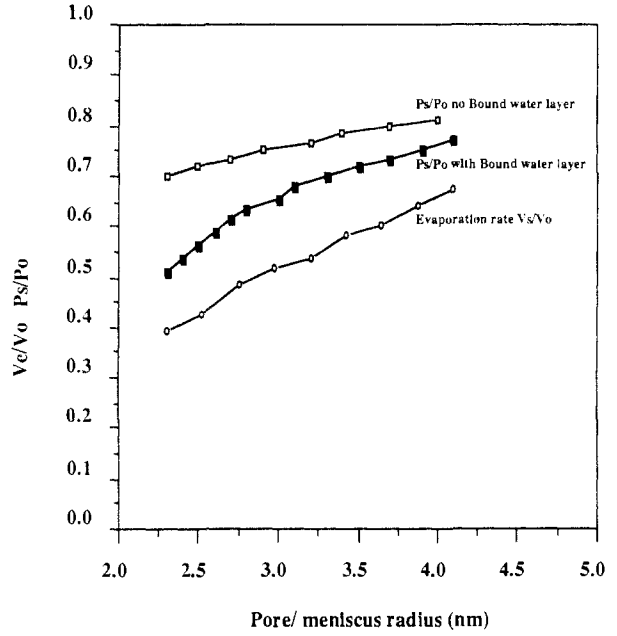

Figure 28. Comparison of observed evaporation rate (V_e/V_0) to that predicted by the Gibbs–Kelvin equation.

where P_s is the vapor pressure over the meniscus of the pore, P_0 is the vapor pressure over a flat surface (760 Torr), B is the molar volume of the liquid (0.18 g/cm^3), R is the gas constant (8.314×10^{-7}), T is temperature (kelvin), r_m the radius of curvature of the meniscus (meters), and γ the difference in the solid–vapor and liquid–vapor interfacial energies (γ = 0.072 J/m^2). Figure 27 plots the dependence of vapor pressure on the pore radius, using the values above in the Gibbs–Kelvin equation, from Wilson and Hench.[239]

The average pore radius of the acid-catalyzed alkoxide silica gels when dry is 2.3 nm. The structural density can be assumed to remain constant during drying. Therefore, the decrease in dimension during drying (Figure 25) should also be indicative of the decrease in pore radius during shrinkage of the gel. This assumption yields an average pore radius of the wet gel to be ~4.1 nm. Thus, the change in the ratio of evaporation rate between a free surface (V_0) and the gel surface (V_e/V_0) during stage 1 should be comparable to the drop in vapor pressure (P_s/P_0) predicted by the Gibbs–Kelvin equation as the gel shrinks.[239] Figure 28

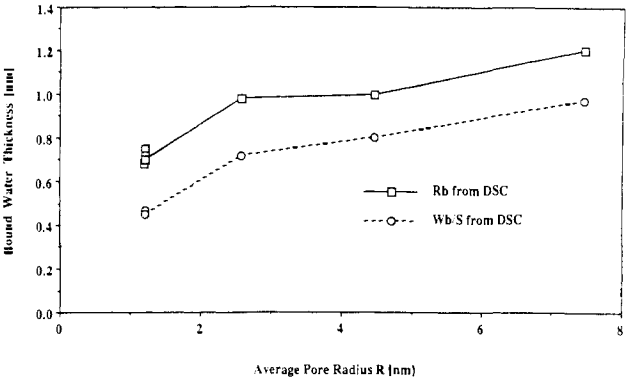

Figure 29. Dependence of the bound water thickness on the average pore radius.[247]

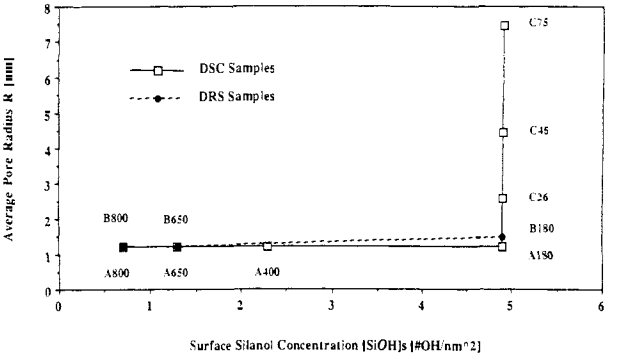

Figure 30. Dependence of the pore size on the silanol concentration.[247]

compares the measured ratio of evaporation rates (V_e/V_0) for the gel in stage 1 as a function of the pore radii in the gel. The ratio of evaporation rates predicted by the Gibbs–Kelvin equation is also plotted in Figure 28. The Gibbs–Kelvin equation predicts higher evaporation rates than are observed.

An important contribution to the depressed evaporation rate from the small pore gel is the presence of a bound layer of water on the pore surfaces. The bound water layer has a structure that is substantially more ordered than free water and possesses properties, such as melting point, that are markedly different than bulk water. Wallace and Hench[245–247] used dielectric relaxation spectroscopy (DRS) and differential scanning colorimetry (DSC) to analyze the properties and calculate the thickness of the bound water layer in acid-catalyzed alkoxide silica gel monoliths with porosity nearly identical with those used in the Wilson and Hench[237–239] drying experiments.

A fundamental assumption made in relating the DRS and DSC studies to drying kinetics is that the structure of water adsorbed into the pore network of a dried gel, the starting condition for the Wallace and Hench[247] study, is nearly equivalent to the structure in the gel during stage 1 drying. This appears to be a reasonable assumption since Wallace and Hench[247] show that bound water thickness appears to be dependent upon pore radius and temperature (Figure 29). This result is valid for two different models: a bound cylindrical layer and a bound statistical layer of water. The pore radius is also independent of surface silanol concentration (Figure 30).

When H_2O is adsorbed onto the surface of silica, the first H_2O molecules form H bonds with, on average, two

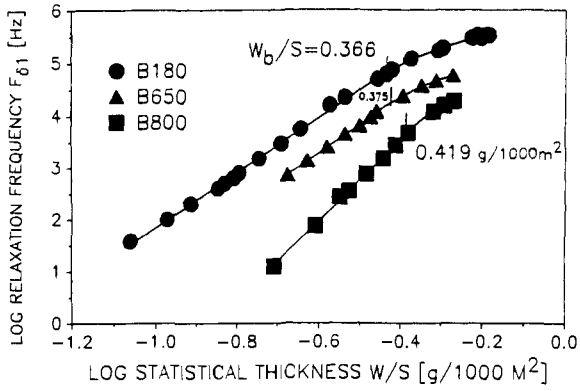

Figure 31. Logarithmic dependence of the relaxation frequency on W/S.[246]

surface silanols. Before a complete monolayer is formed, clusters of H-bonded H_2O molecules start forming around the silanols,[248] followed by multilayer condensation. A portion of the H_2O adsorbed directly adjacent to the surface, called the bound H_2O fraction, F_B, does not show a freezing or melting transition in a DSC, while remaining diffusionally mobile as shown by Guerin.[249] The exact state of this bound layer of H_2O is not well understood. The remaining free H_2O fraction, F_F, adsorbed in silica gel pores exhibits a suppressed melting point, T_M. The questions especially relevant to drying of gels are (1) Does the structure of the pore water change as the pores shrink? (2) What causes the changes? (3) What is the extent or thickness of the bound surface H_2O?

Differential scanning calorimetry (DSC) and dielectric relaxation spectroscopy (DRS) were used to determine the effect of pore texture and structure on the statistical thickness of the adsorbed H_2O.[246,247] Three sets of monolithic gels were investigated. Series A and B had a constant pore radii but were heat treated to decrease the surface silanol concentration, $[SiOH]_S$. Series C had a constant $[SiOH]_S$ = 4.9 OH/nm^2, based on Zhurvalev's analysis,[250] but increasing pore radii. These variables relate directly to the structure of H_2O in drying gels as both the average pore radius, R, and the surface silanol concentration change during drying.

The dependence of the frequency, $F_{\delta 1}$, of the maximum of the dielectric loss tangent spectra of the gel, tan δ, was measured by using DRS on series B gels as a function of the H_2O content, W[grams of H_2O/grams of SiO_2] by Wallace and Hench.[246,247] The dependence of $F_{\delta 1}$ on W changed from a logaithmic to a linear dependence at the bound H_2O content, W_B (Figure 31). This change in dependence at W_B is related to the change from bound to free H_2O, where W_B is a statistically averaged measurement due to the dynamic nature of the system on the time scale being measured. The DRS spectra were measured as a function of W, up to the saturated pore H_2O content, W_S, on three cylindrical SiO_2 gels (series B) heat treated at 180, 650, and 800 °C in order to decrease $[SiOH]_S$.

In addition, the latent heat of fusion, l_F (J/g), and latent heat of vaporization, l_V, of the H_2O adsorbed in powdered SiO_2 gel monoliths were measured by using DSC[247] with a heating rate of 10 °C/min. In sample series A, $[SiOH]_S$ was decreased by a factor of 7 (the same as for series B) while keeping R = 1.2 nm. In series C, R was increased from 1.2 (sample A180) to 7.45 nm (sample C75) while keeping $[SiOH]_S$ = 4.9 OH/nm^2.

The ratio of l_F/l_V for free H_2O is 0.148. If it is assumed that all the adsorbed H_2O vaporized, then l_V is a measure of the saturated H_2O content, W_S. Therefore the ratio of l_F/l_V for the adsorbed H_2O divided by 0.148 equals the fraction of free H_2O, F_F, in the pores. The flat and cylindrical thicknesses of the bound and free pore H_2O can then be calculated from fractions F_F and F_B as discussed below.

The pore volume, V (cm^3/g), and surface area, S (m^2/g), were measured by using N_2 adsorption isotherms, and R (nanometers) = $2000V/S$. The $[SiOH]_S$ values were assumed for the stabilization temperature of each sample by using data taken from Zhuravlev.[250]

The shape of the pores in gels is difficult to characterize, due to their size and complex fractal nature, as discussed earlier. For the same reason talking about the "true" thickness of a bound H_2O layer in micropores is meaningless due to these geometric considerations and the dynamic properties of H bonding. (See the following sections for a discussion of the quantum effects at the SiO_2–H_2O interface.) For this reason assumptions about the shape of the pores must be made before any conclusions about the "thickness" can be reached.

Considering the result of Vasconcelos topological model of gel texture[89,251] and Wallace's analysis of water adsorption,[247] the porosity can be considered as one long cylinder whose length decreases during sintering while R is constant. Consequently, a cylindrical "thickness" can be calculated for the bound and free H_2O fractions adsorbed on the cylindrical pores. This is done by calculating the radius, R_F (i.e., "thickness" for a cylindrical geometry), of the cylindrical core of free H_2O occupying the same fraction of area of the circular cross section (radius R_C) of a pore as F_F. Therefore the free H_2O cylindrical thickness $R_F = R_C F_F^{1/2}$. The bound cylindrical thickness $R_B = R_C - R_F$ for F_B (see Wallace and Hench).[247]

The dielectric relaxation that DRS is measuring is a space charge polarization at the measuring electrodes due to H^+ hopping, and the change from a logarithmic to a linear dependence of $F_{\delta 1}$ on W at W_B is related to the completion of the bound H_2O layer. Consequently, the fraction of free ($F_F = W_F/W_S$) and bound ($F_B = W_B/W_S$) H_2O can then be calculated from the DRS results. The logarithmic dependence of $F_{\delta 1}$ on the statistical H_2O thickness W/S, which makes no assumptions about the pore geometry, is presented in Figure 31 for sample series B. It shows that the bound H_2O statistical thickness W_B/S increases slightly as the processing temperature of the gel, T_S, increases. It also shows that for a given value of W/S, $F_{\delta 1}$ decreases as the bulk density, D_B, increases. All the structural results are listed in Wallace.[252]

Figure 32 shows some of the experimental DSC curves for the same Wallace and Hench samples.[247] The increase in the relative ratios of freezing point, l_F, to boiling point, l_V, is clearly visible as R increases. Both freezing point suppression and boiling point rise occur for increased pore radius. The dependency of the bound H_2O thickness on $[SiOH]_S$, calculated for flat and cylindrical geometries from the DRS and DSC data, is shown in Figure 33. The bound H_2O thickness does not change significantly with $[SiOH]_S$ (if anything it

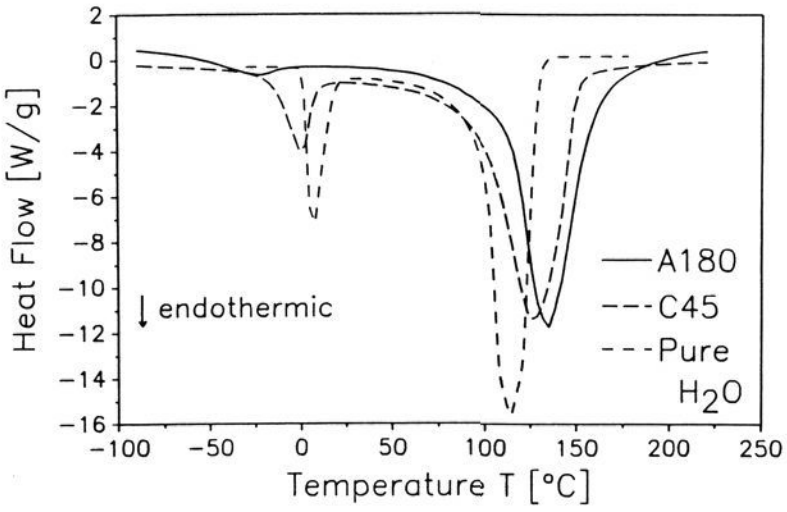

Figure 32. Experimental DSC spectra.[247]

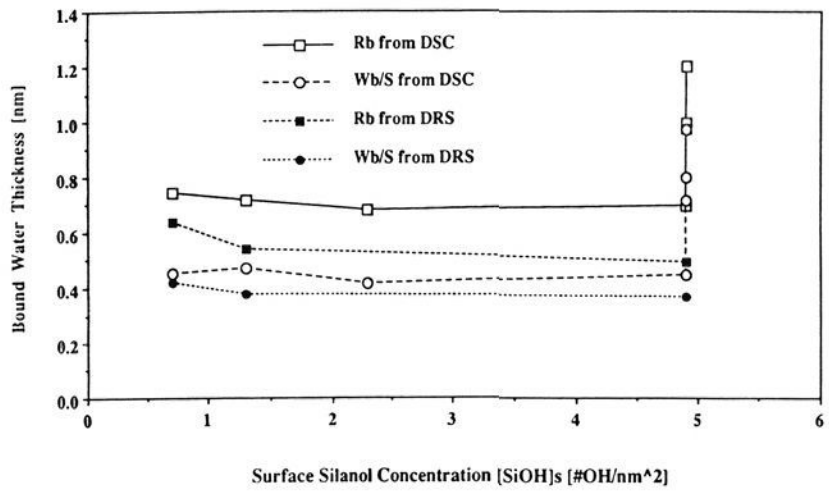

Figure 33. Dependence of the bound water thickness on the silanol concentration.[247]

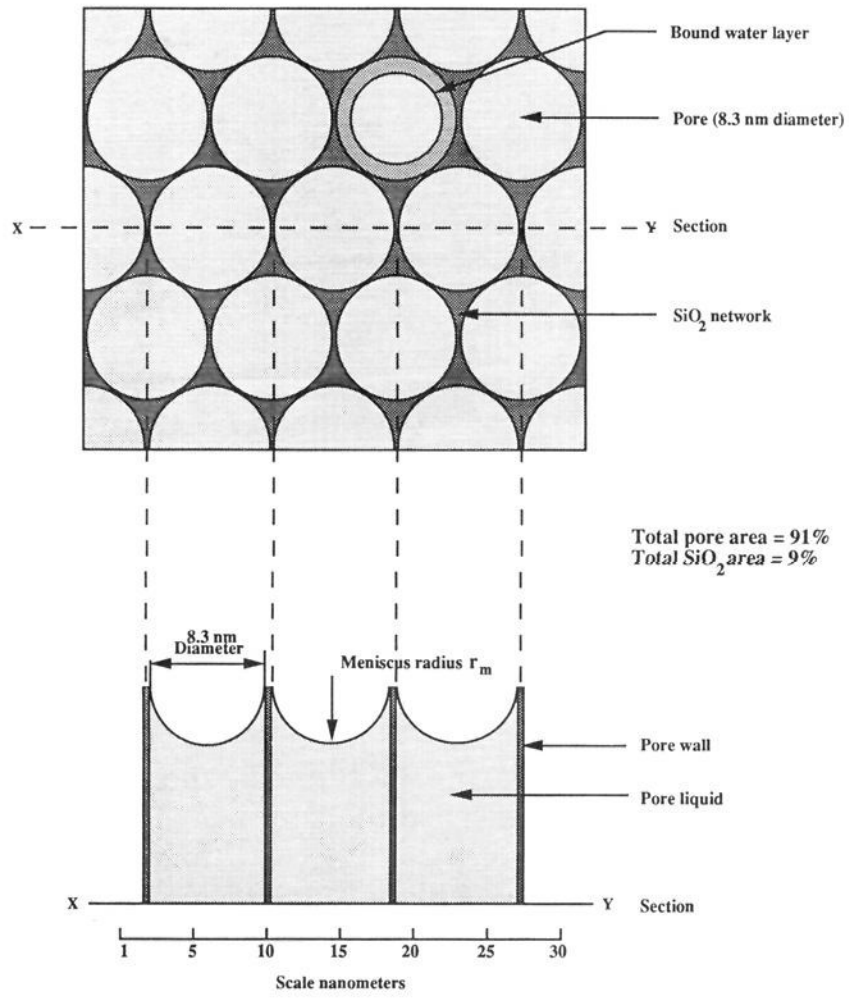

Figure 34. Schematic representation of gel surface at the beginning of stage 1.[237]

increases as $[SiOH]_S$ decreases) but increases with R. The bound water thickness is plotted as a function of R in Figure 29, showing that thickness approximately doubles. For constant R, the fraction of bound H_2O, F_B, the associated bound statistical thickness, W_B/S, and the bound cylindrical thickness, R_B, values appear to increase slightly with bulk density, when the associated $[SiOH]_S$ decreases by a factor of 7. The DSC data therefore imply that the "thickness" of the adsorbed H_2O layer depends not on $[SiOH]_S$ but rather on R. The DRS data appear to confirm the DSC conclusions, with the "thickness" of the bound H_2O layer decreasing slightly with increasing $[SiOH]_S$, but the influence of the measurement temperature on the bound H_2O layer thickness must also be considered.[249]

Guerin[249] used H^+ NMR to investigate the temperature dependence of the statistical thickness W_B/S of bound H_2O on two amorphous silica powders, Spherosil XOR 75 and Aerosil 200. Spherosil XOR 75 is a porous silica gel powder, $S = 200\ m^2/g$, with S due to the internal concave pores, as in the Wallace and Hench study. Aerosil 200 is a nonporous submicrometer silica powder, $S = 85\ m^2/g$, with all S due to the external convex surface. Guerin showed that for the assumed flat geometry, W_B/S is thicker in the concave pores of Spherosil than on the convex Aerosil particles at a specific temperature, T. She also showed that for either sample W_B/S approximately doubled when T increased from 220 to 260 K. This means that both pore geometry and temperature influence W_B/S. In the Wallace and Hench study[247] T_M increased from 221 to 266 K in silica gel series C as R increased from 1.2 to 7.45 nm. F_B and therefore W_B/S and R_B are calculated at T_M for each sample. The doubling in W_B/S and R_B seen in series C could therefore be due to the increase in the measuring temperature, i.e., T_M, and/or the increase in R.

These studies show that adsorption behavior of H_2O on SiO_2 gels is largely governed by pore geometry rather than surface chemistry, as well as temperature. This is in agreement with the fractal dependence of S, of a mesoporous SiO_2 gel, on the size of the molecular yardstick used in sorption isotherms.[253,254] S depends entirely on the size of the adsorption molecule and not on its adsorbent–adsorbate physisorption interactions.[254] The increases in F_B observed, for constant R, with the increase in bulk density are probably related to the associated increases in helium pycnometry structural density from 2.11 to 2.30 g/cm^3 for these acid-catalyzed gels. This is also discussed in detail by Wallace[252] and summarized in section VIII on stabilization in this review.

The inference with regard to drying gels is that as pores shrink the "thickness" of the bound surface H_2O layer decreases slightly, while increasing drying temperature tends to increase the "thickness". This implies that the ratio of the free to bound H_2O fractions decreases during drying and is not influenced by $[SiOH]_S$.

A. Stage 1: Drying

Combining the drying analysis of Wilson[237] and the pore analysis of Wallace[252] yields a schematic of the gel surface at the beginning of stage 1 drying (Figure 34). The surface area is initially largely free water, separated by a relatively small areal fraction of gel network with a transition zone of bound water. As the free water evaporates, the solid network is drawn together by the capillary stresses which decreases the areal fraction of free water and increases the areal fraction of solid. At the critical point, the end of stage 1, the structural schematic is as depicted in Figure 35. The decreasing rate of evaporation throughout stage 1 is a consequence

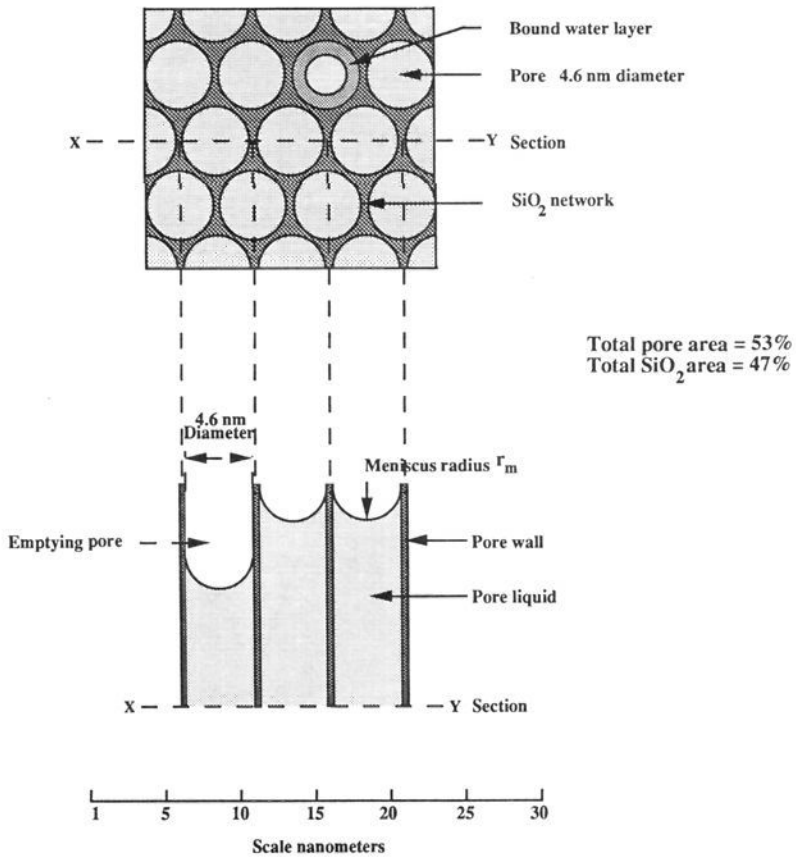

Figure 35. Schematic representation of gel surface at the end of stage 1 (critical point). Drawn to the same relative scale as Figure 34.[237]

of the effective pore radius decreasing from 3.2 to 1.3 nm. The bound water is apparently not removed until much higher temperatures in the stabilization regime.

This analysis of effects of pore radius on stage 1 evaporation also explains why Dwivedi[235] and Kawaguchi[234] observed a classical constant rate period during the drying of their gels. The magnitude of vapor pressure reduction required to produce a noticeable decrease in evaporation rate during stage 1 does not occur until menisci of $r_m < 10$ nm are formed. Menisci of this radius cannot form in pores of the dimensions reported for their gels, and no significant change in the evaporation rate was seen.

B. Stage 2: The Opaque Stage

The second stage starts at the critical (or leatherhard) point. At this point the meniscus radius is equal to the pore radius and is able to penetrate the bulk. The loss rate of the acid-catalyzed alkoxide silica gels[239] steadies at a constant, low value of $\sim$0.008 g/(h cm^2). This stage is consistent with the stage Scherer[70] terms the "first falling rate period". Liquid is driven to the surface by gradients in capillary pressure, where it evaporates due to the ambient vapor pressure being lower than inside the pores.

Shortly after entering the second stage, the gel is seen to turn opaque, starting at the edges and progressing linearly toward the center. There are several possible causes of this phenomena, including phase separation of the pore liquid or exsolution of gas from the liquid. The most plausible explanation is that put forward by Shaw,[255] who suggests that this phenomenon is caused by light scattering from isolated pores (or groups of pores) in the process of emptying, of such a dimension that they are able to scatter light. The data obtained during stage 2 indicate an increase in open porosity from $\sim$0.012 to $\sim$0.364 cm^3/g during the opaque transition, which started at $\sim$16% ($\pm$1.5%) moisture and ended at 6% ($\pm$1.5%) for both samples in Wilson and Hench's experiment;[239] see Figure 24.

C. Stage 3

After transparency is regained, Figure 2j shows that the loss rate of the acid-catalyzed alkoxide silica gel monolith gradually falls to a value of $\sim$0.001 g/(h cm^2) until no further weight changes occur. The transition to stage 3 is the hardest to identify, and its start is probably best defined as the end of the opaque stage. Scherer[70] describes stage 3 as the "second falling rate period", where the temperature of the body is not as strongly suppressed as when evaporation rates were higher. The remaining liquid evaporates within the pores and is removed by diffusion of its vapor to the surface. It is unaffected by local changes in temperature, ambient vapor pressure, flow rate, etc., as demonstrated for gel B in Wilson and Hench's study.[239] By the start of stage 3 the gel is to all intents and purposes dry. It can be removed from the drying chamber and dehydrated under much more severe conditions (180 °C at 0.1 Torr) without risk of cracking. Stress birefrigence measurements during drying indicate a gradual reduction in residual stress during stage 3 and the end of stage 2, because of the reduction in number of birefrigent lines and eventual elimination of the isogyres caused by biaxial strain.[237]

D. Cooling

During the cooling period (which can be rapid) the samples gained weight as shown in Figure 24. On cooling, gel B gained almost all of the weight lost during stage 3. As the chamber cools, the vapor pressure in the chamber rises until $P_a > P_s$ and condensation occurs within the pores.

E. Drying Failure

The drying times reported in Wilson and Hench's study[238,239] are the experimentally determined minimum for gels of 2–4-cm diameter without cracking. When samples fail, they do so at distinct points within the drying sequence. Cracking during stage 1 is rare but can occur when the gel has had insufficient aging and strength (see Scherer[70,83-88]) and therefore does not possess the dimensional stability to withstand the increasing compressive stress. If the loss rate is increased (by lowering the vapor pressure of the ambient atmosphere or increasing the draft rate), there comes a point where it exceeds the maximum rate of shrinkage. If this occurs, localized pore emptying results and surface cracks develop.

Most failure occurs during the early part of stage 2, the point at which the gel stops shrinking. This is the point at which the meniscus falls below the surface. A distribution of pore sizes exists in these materials, and some pores must empty before others. At the start of stage 2 the modulus of the gel is very high and the compressive stress is in the order of $\sim$100 MPa. The pores that empty first (at the larger end of the distribution) stop shrinking at the point of emptying and can only passively shrink under the influence of nearby saturated pores. The possibility of cracking at this point is great due to the high stresses and low strain tolerance of the material. Cracking during stage 3 does not occur, in the experience of Wilson.[237] The moisture

level and thus the stress is considerably diminished by this point, and cracking generally will not occur even under fairly extreme dehydration conditions unless very large defects are present. Hench et al. have discussed the types of defects that can be introduced during gel processing and their effects on strain concentration.[53] Successful drying of large gel monoliths requires control of the drying rate through the opaque stage and elimination of processing defects during mixing, casting, and gelation.

VIII. Stabilization

A. Introduction

Optically transparent dried silica gel monoliths have been made by Hench et al.[52,53] of over 80-mm diameter. This new type of optical material is termed type VI gelsil,[52] and its physical characteristics are described in the properties section of this review. A critical step in preparing type VI gel–silica is stabilization of the porous structure as indicated in Figure 3. Both thermal and chemical stabilization is required for the material to be used in an ambient environment. The reason for the stabilization treatment is the very large concentration of silanols on the surface of the pores of these large surface area (>400 m^2/g) materials.

Chemical stabilization involves removing the concentration of surface silanols below a critical level so that the surface does not rehydroxylate in use. Thermal stabilization involves reducing the surface area sufficient to enable the material to be used at a given temperature without reversible structural changes. The mechanisms of thermal and chemical stabilization are interrelated because of the extreme effects that surface silanols and chemisorbed water have on structural changes. In fact, full densification of the silica gels, transforming them to a glass, is nearly impossible without dehydration of the surface prior to pore closure. Dehydration, dilation, and contraction of the silica network with adsorption and desorption of water are equally important in forming a stable porous gel monolith (type VI) or a fully dense gel–glass monolith (type V).[52,53,256]

B. Dehydration

A major problem in producing gel–silica optics is removal of gel surface hydroxyl groups and hydrogen-bonded pore water, which give rise to atomic vibrational energy absorption in almost the entire range of ultraviolet to infrared wavelengths (160–4500 nm) and decreases the optical applications of silica–gel monoliths. Consequently, to achieve the theoretical optical performance of silica, complete dehydration is imperative.

Many chlorine compounds—some of these include methylated chlorosilanes, such as $ClSi(CH_3)_3$, $Cl_2Si(CH_3)_2$, $Cl_3Si(CH_3)$, silica tetrachloride ($SiCl_4$), chlorine (Cl_2), and carbon tetrachloride (CCl_4)—can completely react with surface hydroxyl groups to form hydrochloric acid,[256–259] which then desorbs from the gel body at a temperature range (400–800 °C) where the pores are still interconnected. In a study by Wang and Hench,[52,54,260] carbon tetrachloride was used successfully to achieve complete dehydration of ultrapure gel–silica monoliths.

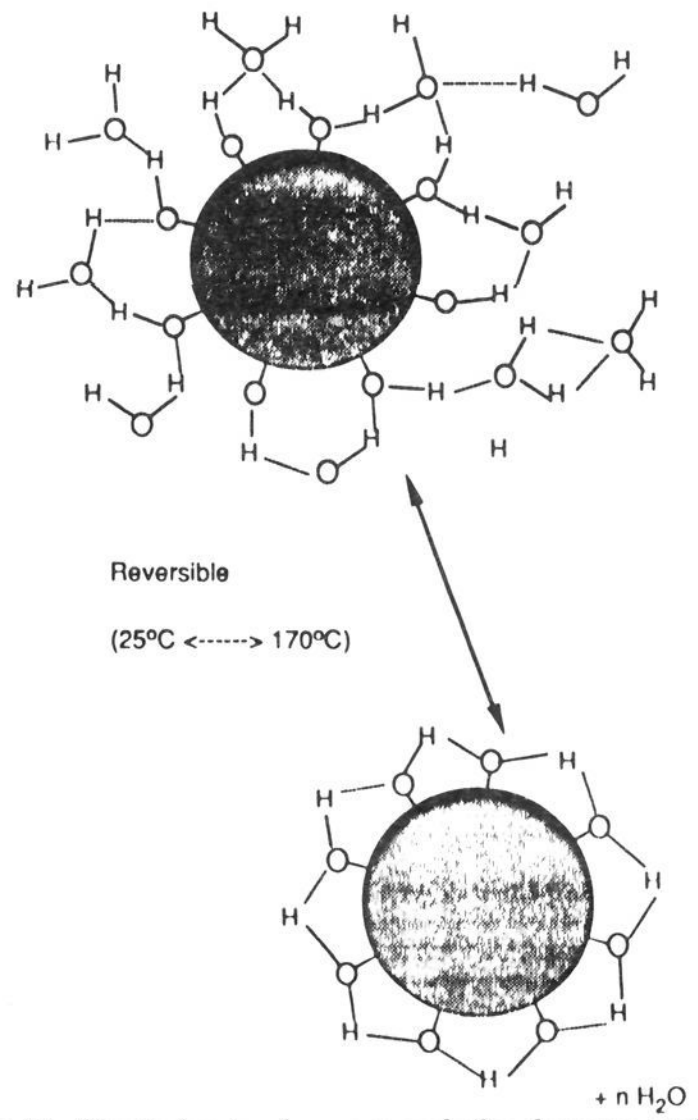

Figure 36. *Physical water decreases and silanol groups condense* in the range of room temperature and 170 °C.[260]

To achieve dehydration it is necessary to recognize that "water" is present in two forms: free water within the ultraporous gel structure (i.e., physisorbed water) and hydroxyl groups associated with the gel surface (i.e., chemisorbed water). The amount of physisorbed water adsorbed to the silica particles is directly related to the number of hydroxyl groups existing on the surface of silica. During the 1950s and 1960s, researchers Young,[261] Benesi and Jones,[262] Hockey and Pethica,[263] Kiselev,[264] and McDonald[265] contributed much information regarding the hydration/dehydration characteristics of the silica gel/water system, as summarized below: (1) The physisorbed water can be eliminated, and surface silanol (Si–O–H) groups condensed starting at about 170 °C, as shown in Figure 36.[260]

(2) The dehydration is completely reversible, up to about 400 °C, as shown in Figure 37.[260] Decomposition of organic residuals, up to 400 °C, was also confirmed by using DSC and TGA for TMOS-derived silica gels, as discussed by Wang.[266]

(3) Above 400 °C, the dehydration process is irreversible as a result of shrinkage and sintering across pores, as shown in Figure 38.[260] Thus, the amount of existing hydroxyl groups on the gel surface is an inverse function of the temperature of densification. UV–vis–NIR absorption data also show that the reduction of surface hydroxyl groups occurs above 400 °C.

(4) Viscous flow occurs above 850 °C with the exact temperature depending on the pore size of a specific gel. The isolated hydroxyl groups on the gel surface react with each other, bringing particles together, thereby eliminating voids within the gel. If surface water is unable to be desorbed prior to pore closure, it is trapped inside the densified gel.

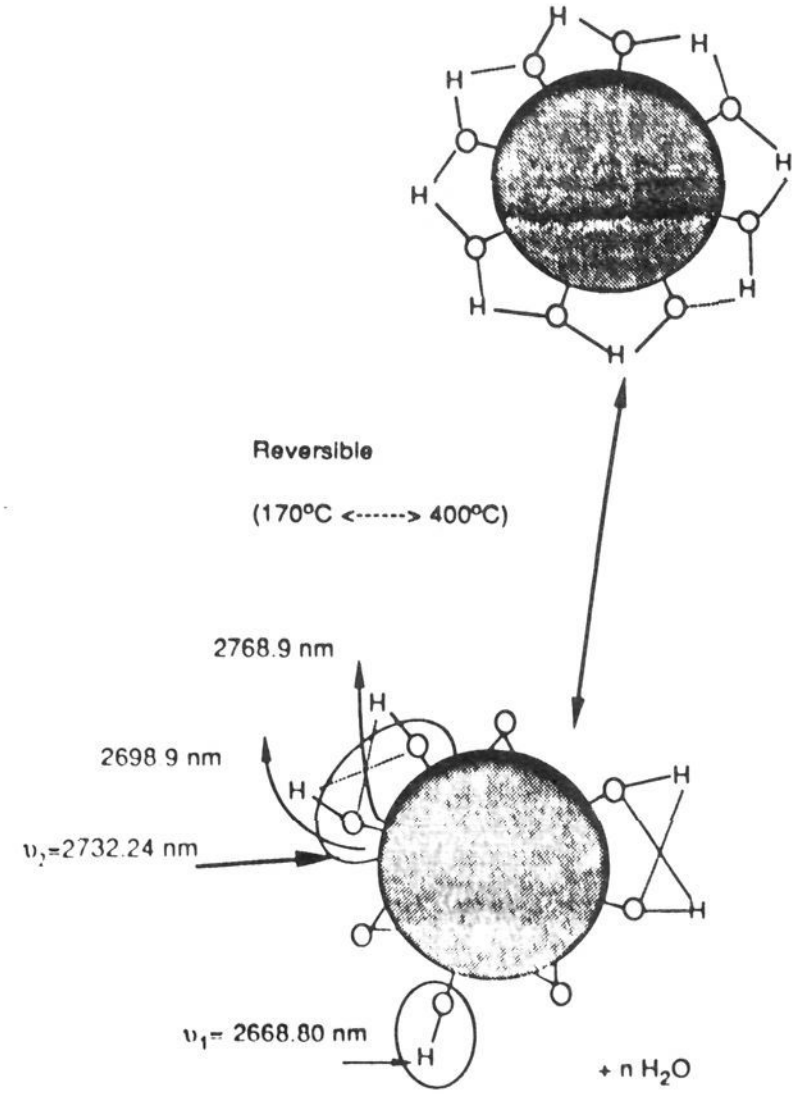

Figure 37. Surface silanol groups are reversible in the range 170–400 °C.[260]

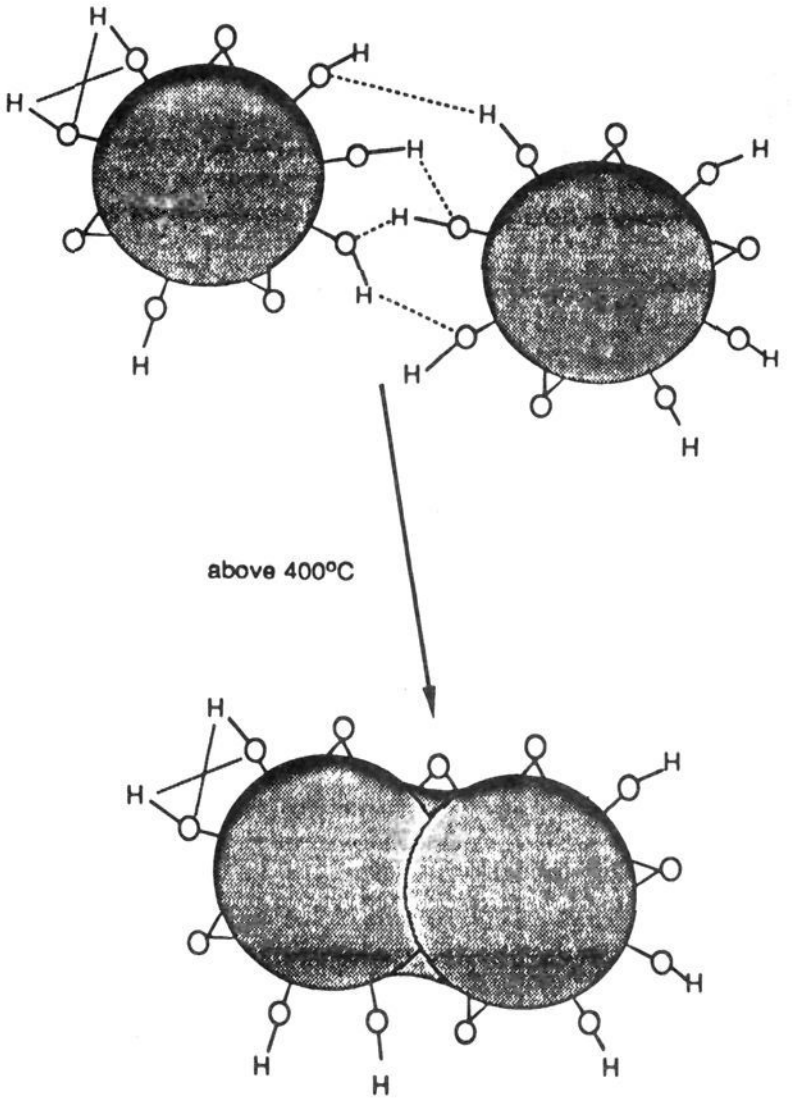

Figure 38. Irreversible elimination of adjacent hydroxyl groups.[260]

Young, in his early work,[261] found that the decrease in surface area of silica gel at high temperatures is a function of the time and temperature of the heat treatment. This supports the concept that the sintering mechanism is essentially the result of viscous flow, rather than surface diffusion. Impurities (i.e., surface water) effectively lower surface energy and thereby decrease the sintering temperature, presumably by facilitating viscous flow; Phalippou et al.[267] confirmed this point.

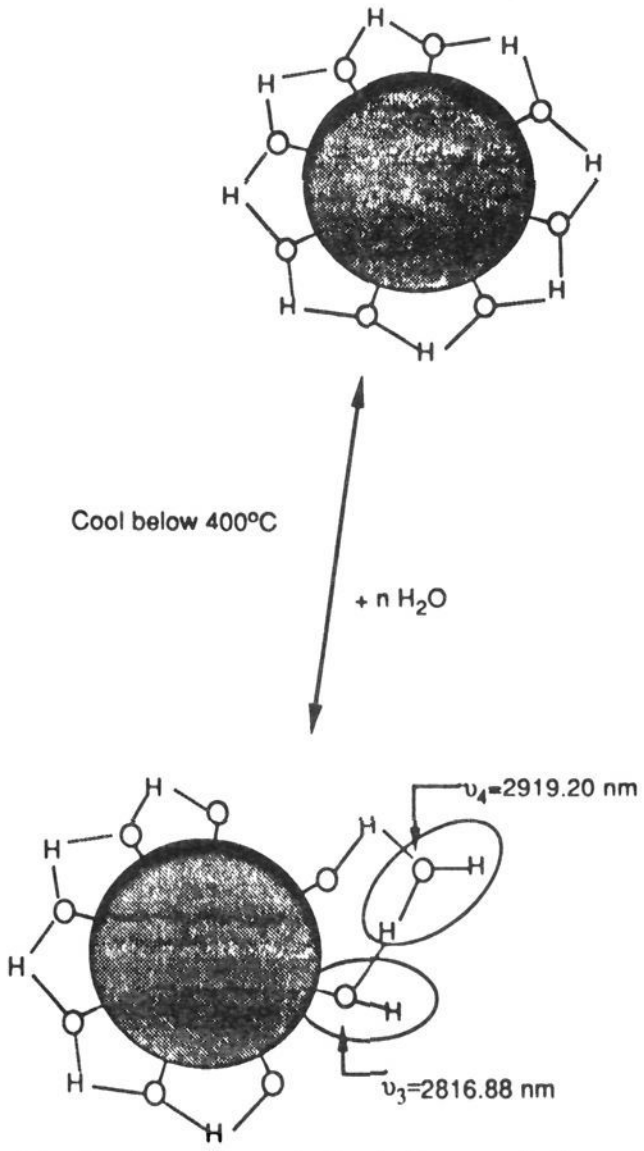

Figure 39. Reabsorption of physical water below 400 °C.[260]

Hair (see p 87 in ref 268) also proved that heating silica gel in the 170–400 °C range causes reversible dehydration via elimination of surface water and the formation of both single and adjacent surface hydroxyl groups, as illustrated in Figure 37. Hair found that at 400 °C, no more than half of the surface hydroxyl groups had been desorbed and that most of the remaining surface hydroxyl groups were adjacent to each other and therefore situated for preferential water adsorption (Figure 39). He stated that heating the gel above 400 °C causes a drastic, irreversible elimination of adjacent hydroxyl groups, as shown in Figure 38, until at about 800 °C, only single hydroxyl groups remain (Figure 40). As the temperature increases, single hydroxyl groups depart from the gel surface until the gel is densified; this occurs in the 850–1000 °C range. However, some single hydroxyl groups are still unable to escape from the gel surface and therefore can contribute to foaming of the gel as the temperature increases.

More importantly, Hair describes[268] that when the silica gel has been completely dehydrated, there are no surface hydroxyl groups to adsorb the free water; in other words, the surface is essentially hydrophobic. Clearly, it is the realization of this critical point that is the focus for making stable monolithic gels.

The vibrational overtones and combinations of hydroxyl groups and their associated molecular water, occurring in the 1250–3000-nm range, have been studied

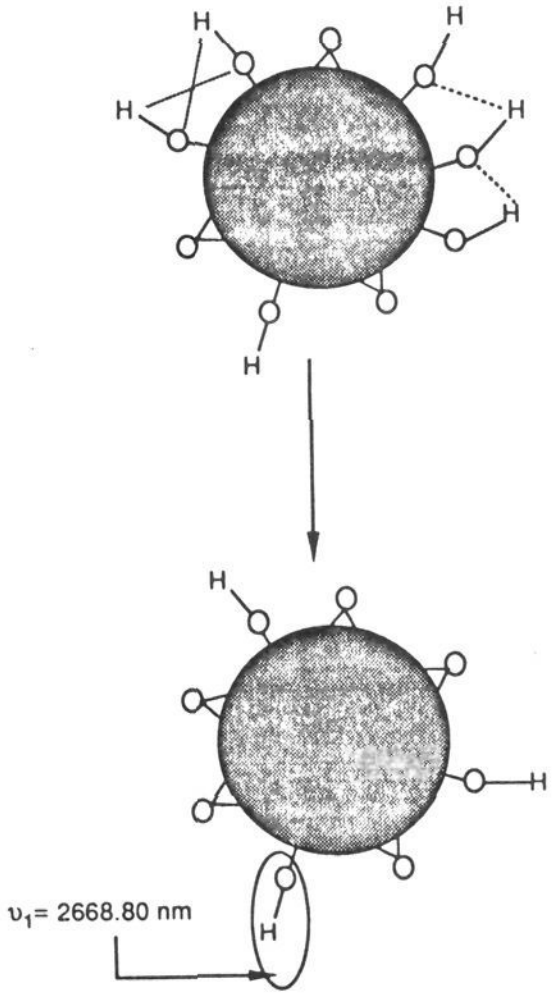

Figure 40. Only single hydroxyl groups remain at temperatures above 800 °C.[260]

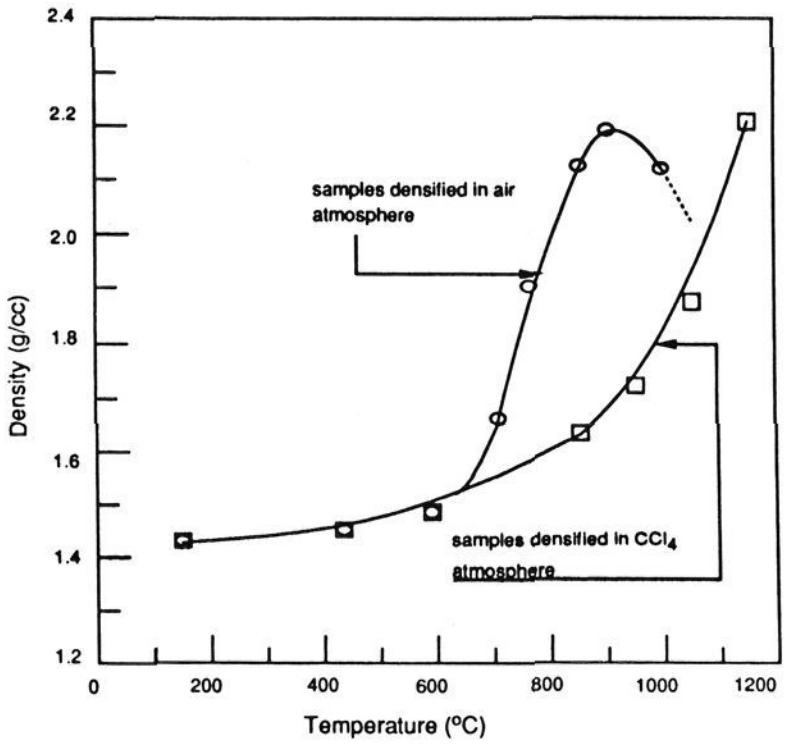

Figure 41. Density measurements at various temperatures for samples with or without CCl_4 treatment.[260]

by Anderson and Wickersheim.[269] Evaluation of a partially dehydrated (800 °C) silica gel shows an absorption peak at ν_1 = 2668.80 nm (see Figure 40), surely due to the fundamental stretching vibration of hydroxyl groups on the gel surface. These singular, or free, hydroxyl groups are also referred to as "isolated silanol groups". The symmetry of this peak indicates that these singular hydroxyl groups have no interaction with water molecules. The band at 1366.12 nm ($2\nu_2$) is the first overtone of the adjacent silanol group vibration ν_2 = 2732.24 nm (see Figure 37). The 1366.12-nm peak becomes less intense as the gel is heated and disappears with complete dehydration. The combination peak at 2207.51 nm ($\nu_2 + \nu_{OH}$(bend)) is the result of the hydroxyl ion's stretching and bending vibrations. Peri[270] suggests that this combination band is due to the Si–O–H stretching vibration and an out-of-plane O–H displacement (bending) vibration. This type of hydroxyl group is labeled an OH(2) group.

The adjacent hydroxyl groups also interact with free water (ν_3, Figure 39) to form hydrogen bonds; this effect causes a change in both the fundamental stretching vibration and its associated overtones and combinations. Therefore, the hydroxyl groups associated with water show a new combination peak at 2262.44 nm ($\nu_3 + \nu_{OH}$(bend)); this kind of hydroxyl group is called OH(3). The energy calculations by Benesi and Jones[262] predict that the fundamental stretching vibration of OH(3) at ν_3 = 2816.88 nm is a value shifted about 148.08 nm from the vibration of the free hydroxyl group at ν_1 = 2668.80 nm (OH(1)). From actual absorption data, McDonald[265] observed a peak at 2816.88 nm, indicating a strong interaction between free pore water and surface hydroxyl groups.

When a dehydrated silica gel is exposed to a slightly humid air atmosphere, sharp peaks appear at 2816.88 (ν_3), 2732.24 (ν_2), 1890.35 ($\nu_3 + 2\nu_{OH}$(bend)), 1459.85 ($2\nu_4$), and 1408.44 nm ($2\nu_3$). Hair (see p 89 in ref 268) believes that the intensity changes associated with adsorption of water indicate that all these bands are connected with the hydroxyl group which is associated with physical pore water. Further hydration results in a broadened band at about ν_4 = 2919.70 nm (Figure 39), characteristic of bulk water.

Cant and Little[271,272] and Hair and Chapman[273] tend to agree that for silica gel a sharp and slightly asymmetrical peak on the high-wavelength side, at 2668.80 nm (ν_1), together with a distinct band at 2732.24 nm (ν_2), can be attributed to freely vibrating surface silanol groups and to hydrogen-bonded adjacent silanol groups, respectively. In addition, a broad band at 2919.70 nm (ν_4) is due to the stretching of molecular water. Elmer et al.[274] in their study of rehydrated porous silica showed that the intensity of the peak at 2668.80 nm increases during rehydration. They also indicated that physical water prefers to adsorb on adjacent hydroxyl groups rather than on the singular hydroxyl groups. Studies of optical fibers by Keck, Maurer, and Schultz[275] found that the extrinsic hydroxyl groups also give rise to some noticeable overtones and combinations occurring roughly at 725, 880, 950, 1125, 1230, and 1370 nm. These absorptions strongly degrade the performance of optical fibers.

Most of the silica glasses manufactured by melt or synthetic methods result in impurities (e.g., water and/or metallic elements).[52] Three significant absorption peaks at 2732.24 (ν_2), 2207.51 ($\nu_2 + \nu_{OH}$(bend)), and 1366.12 nm ($2\nu_2$) are found to be the unique stretching vibration of adjacent silanol groups and their overtones and combinations in alkoxide-derived silica gel monoliths, discussed by Wang[266] and Hench and Wang.[260] No singular silanol group (ν_1) was found by using a high-resolution UV–vis–NIR spectrophotometer.

The bulk density measurements at various sintering temperatures for alkoxide-derived silica gel monoliths with and without chlorination treatment for dehydration are shown in Figure 41. The density of the water-rich (without chlorination) gel sample reaches a maximum (≈2.2 g/cm^3) at a temperature of about 860 °C, and the density of the water-free (with chlorination) gel sample has its maximum (≈2.2 g/cm^3) at a relatively

TABLE IX. Absorption Peaks of the Pore Water and the Surface Hydroxyl Groups of Gel-Silica Monoliths[266]

wavelength, nm	identification[a]	observation
2919.70	$*****\nu_4$	broad peak on a broad band
2816.88	$****\nu_3$	tiny peak on a broad band
2732.24	$***\nu_2$	joint of two small peaks at 2768.90 and 2698.90 nm
2668.80	$**\nu$	very sharp sym peak
2262.48	$\nu_3 + *\nu_{OH}$	broad band, no peak
2207.51	$\nu_2 + \nu_{OH}$	high broad asym peak
1890.35	$\nu_3 + 2\nu_{OH}$	high broad asym peak
1459.85	$2\nu_4$	tiny peak on a broad band
1408.44	$2\nu_3$	small peak on a broad band
1366.12	$2\nu_2$	very sharp sym peak
1237.85	$\{[2\nu_3 + \nu_{OH}] + [2\nu_2 + \nu_{OH}]\}/2$	small peak
1131.21	$2\nu_3 + 2\nu_{OH}$	tiny peak
938.95	$3\nu_3 + 2\nu_{OH}$	small peak
843.88	$3\nu_3 + \nu_{OH}$	no peak obsd
704.22	$4\nu_3$	tiny peak

[a] $*\nu_{OH}$: an out of plane bending vibration of Si-O-H bond. $**\nu_1$: stretching vibration of an isolated Si-O-H bond. $***\nu_2$: stretching vibration of an adjacent Si-O bond. $****\nu_3$: stretching vibration of a Si-O-H bond which is hydrogen bonded to water. $*****\nu_4$: stretching vibration of adsorbed water.

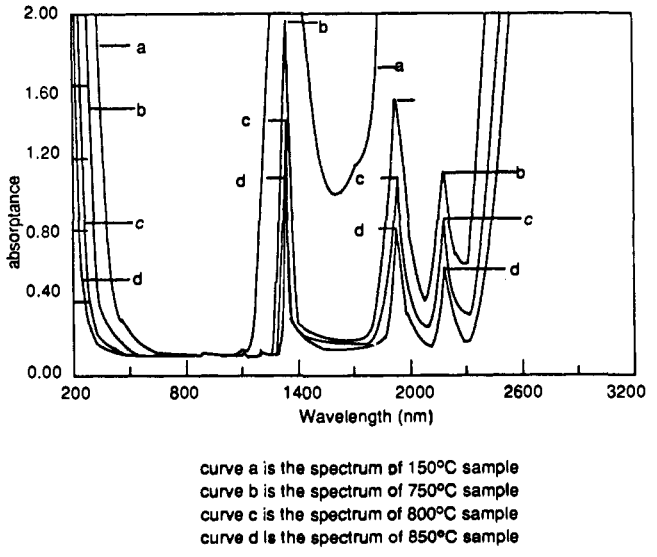

Figure 42. Absorption curves of partially densified gels in air.[260]

higher temperature of about 1100 °C. This indicates that the hydroxyl groups significantly decrease the sintering temperature by lowering the surface energy of silica.

The important absorption peaks and bands found in Wang's dehydration study[266] are summarized in Table IX. These peaks and bands found in the preparation of alkoxide-derived silica gel monoliths are identical with those discovered by previous researchers reviewed above on studies of silica gel powders.

Curves a–d in Figure 42 show the UV–vis–NIR spectra of silica gel monoliths heated in ambient air at various temperatures up to about 850 °C.[260] Overtone and combination vibrational peaks are observed at 704.22, 938.95, 1131.21, 1237.85, 1366.12, 1408.44, 1459.85, 1890.35, and 2207.51 nm. A very strong, broad absorption band occurs between 2400 and 3200 nm. None of these peaks have been eliminated by heating; instead they have only decreased in intensity with increasing temperatures. Clearly, the gel is not completely dehydrated, even when heated to the point of full densification; further heating results in a foaming problem.

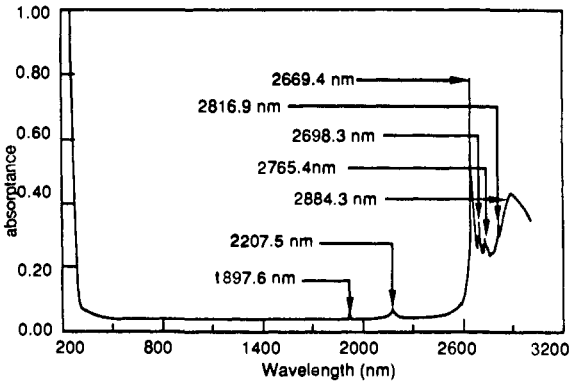

Figure 43. Absorption curve of gel partially densified in controlled CCl_4 atmosphere for a 950 °C sample of 3.8-mm thickness.[260]

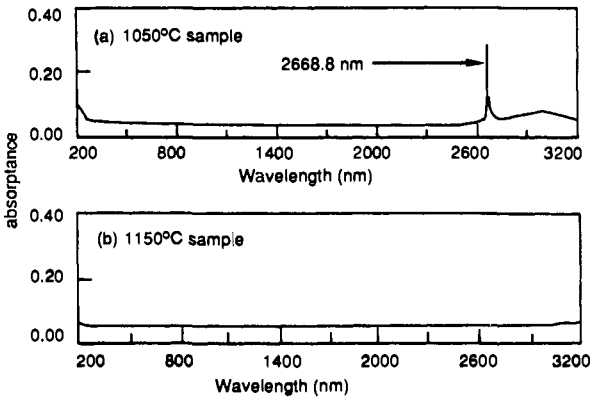

Figure 44. Absorption curves of gels partially densified in controlled CCl_4 atmosphere for a 1050 °C sample of 3.6-mm thickness and a 1150 °C sample of 3.4-mm thickness.[260]

Data obtained in Wang's work[260,266] show that a combination vibrational mode is identified at 2207.5 nm, resulting from the adjacent silanol stretching vibration at 2732.24 nm (ν_2) and the out-of-plane hydroxyl ion deformation vibration at 11494.25 nm (ν_{OH}(bend)). The peak at 1890.35 nm is a combination vibration of 2816.88 nm (ν_3) plus 2 times the bending frequency ($2\nu_{OH}$(bend)). The peak at 1459.85 nm ($2\nu_4$) seems to be the first overtone of the 2919.70-nm (ν_4) peak. The peak at 1408.44 nm ($2\nu_3$) observed is the first overtone at 2816.88 nm (ν_3), whereas the 1366.12-nm ($2\nu_2$) peak is from the first overtone of the fundamental hydroxyl stretching vibration observed at 2732.24 nm (ν_2).

The peak observed at 1237.85 nm is presumed to be an overlap from the contribution of two types of modes, which are 1221.00 ($2\nu_2 + \nu_{OH}$(bend)) and 1254.70 nm ($2\nu_3 + \nu_{OH}$(bend)). A tiny peak at 1131.21 nm is believed to be $2\nu_3 + 2\nu_{OH}$(bend), and a small peak at 938.95 nm is presumed to be a second overtone of 2816.88 nm ($3\nu_3$). There is a very tiny peak at 704.22 nm, which is a third overtone of 2816.88 nm ($4\nu_3$) as shown in Figure 42, curve d.

These results show that for critical optical applications where complete transmission over a broad range of wavelength is important, densification in an air atmosphere is obviously a failure. The resulting quality of this gel cannot compete with that of fused silica,[52] and it will never reach the point of complete dehydration.

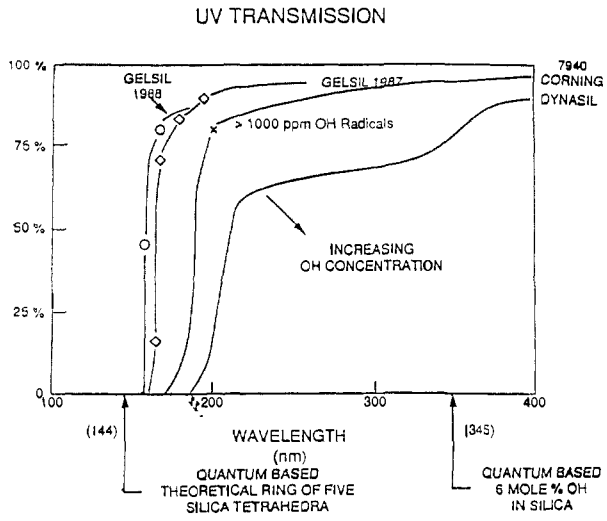

Figure 45. Improvements in UV transmission of alkoxide gel-silicas with time compared with quantum mechanics predictions of UV cutoff wavelength.[53]

Carbon tetrachloride treated samples were prepared at 850, 950, 1050, and 1150 °C, and their characteristic UV–vis–NIR absorption spectra compared, as shown in Figures 43 and 44 (from refs 260 and 266). Absorption peaks were visible at 2890.1, 2768.9, 2698.9, 2668.8, 2207.5, and 1897.6 nm for the 850 °C sample and at 2884.3, 2765.4, 2698.3, 2669.4, 2207.5, and 1897.6 nm for the 950 °C sample.

Stretching vibrations of the adsorbed physical water gives rise to typical broad absorption peaks at 2890.1 and 2884.3 nm, which are shifted from 2919.70 nm (ν_4) within a broad range from 2700 to 3200 nm. Absorption peaks at 2698.3 and 2698.9 nm are suggested[260,266] to be the result of the stretching vibrations of hydrogen–oxygen bonds of adjacent silanol groups. The 2768.9 and 2765.4-nm peaks are proposed[260,266] to be the result of stretching of the hydrogen bonds to the neighboring silanol oxygens, as shown in Figure 37. These two kinds of absorption peaks in general cannot be distinguished and thus form the combined broad peak at 2732.24 nm, which is observed by many researchers.[265,270,276,277] The sharp peaks at 2668.8 and 2669.4 nm are identified to be caused by vibrating surface isolated silanol groups (i.e., free hydroxyl groups).

The intensity of all absorption peaks decreases as the temperature increases. The spectrum from the 1050 °C sample shows only one peak, as shown in Figure 44,[260] occurring at 2668.8 nm (ν_1), which is caused by isolated hydroxyl groups. The sample heated to 1150 °C has a spectrum in which the water peaks have been eliminated, as shown in Figures 44 and 45 (from ref 260 and 53). The absorption loss due to water approaches zero as no water or hydroxyl absorption peaks are present at any wavelength. The quality of optical transmittance of this sample is significantly higher than that of traditional fused silica glass and equivalent to that of optical fibers used in communication systems.

One of the complications associated with use of chlorine compounds in the dehydration of silica gels is the incorporation of chlorine ions in the densified gel–glass structure. Susa et al.[256] describe a dechlorination treatment using an oxygen atmosphere at 1000–1100 °C after chlorination at 800 °C to remove the hydroxyl ions. The dechlorination reaction seems to be rate-determined by a diffusion process that is probably governed by the adsorption and desorption of chlorine atoms. Susa et al.[256] indicate that reducing the surface area by a presintering process is useful for reducing both the hydroxyl and chlorine content in the densified silica glass.

C. Structural Characterization

The structure of alkoxide-derived silica gels has been examined in some detail, by using Raman spectroscopy, from the dry gel through to the fully dense amorphous SiO_2.[326-330] Gottardi et al.[326] report the Raman spectra of a silica gel heated from 140 to 800 °C, showing the interrelated changes in intensity of the SiOH peaks at 980 and 3750 cm^{-1}, the cyclotrisiloxane D_2 and cyclotetrasiloxane D_1 "defect" peaks, at 495 and 605 cm^{-1}, respectively, and the main SiO_2 structural vibrations at 440, 800, 1060, and 1195 cm^{-1}. These results were reproduced by Krol et al.,[327,328] confirming the D_1 and D_2 peak assignments to be four- and three-membered siloxane rings respectively, and the formation of large concentrations of cyclotrisiloxane D_2 rings on the internal pore surface as the hydroxyl concentration and the internal pore surface area decrease with increasing temperature. The three-membered D_2 rings are strained in comparison to the four-membered D_1 rings and consequently can form only above 250 °C on the surface of the gels via the condensation of adjacent isolated surface silanols. In contrast the four-membered D_1 rings form initially in the sol stage and are retained until the gel is dense.[282]

The existence of another peak has been postulated by Mulder et al.[329] to explain the behavior of the peak at 490 cm^{-1} between 100 and 800 °C. He proposes that the symmetric stretch vibration of network oxygen atoms coupled to a network-terminating SiOH group gives rise to a strongly polarized Raman peak at 490 cm^{-1}, which he called the D_0 peak and which is transformed to the D_1 peak as the condensation reaction goes to completion. However, Brinker et al.[282] dispute this interpretation of the 495-cm^{-1} peak behavior with temperature.

Recent analysis of the structure of silica gels using low-frequency (0–200 cm^{-1}) Raman scattering has been interpreted by assuming that the gels are fractal. This infers that the scattering was characteristic of the scattering from fractons,[330,331] where fractons are defined as phonons with vibrational modes localized by the fractal nature of the structure. Most of this work has been done on hypercritically dried aerogels. Raman scattering from gels involves a large contribution due to the tail of the Rayleigh scattering peak. The intensity of this peak is proportional to the heterogeneous density fluctuations, and therefore in porous gels it can be up to 8 orders of magnitude more intense than the Raman peaks. Consequently, this tail is removed by thermal reduction using Bose–Einstein statistics, and the reduced Raman spectra is then analyzed.[330] Consequently, the reduced data must be interpreted cautiously due to the magnitude of the thermal correction.

D. Strained Defects

Brinker et al.[279-283] have used solid-state ^{29}Si magic-angle spinning NMR, XPS, ^1H cross-polarization MASS NMR, and Raman spectroscopy to investigate the local

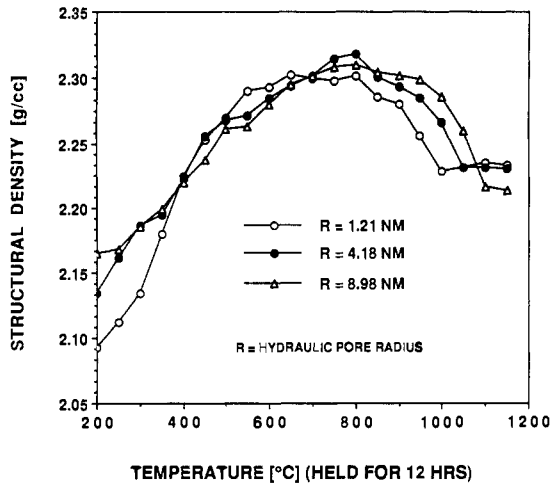

Figure 46. Dependence of the structural density ρ_s (g/cm^3) of alkoxide-derived porous silica gels, as a function of sintering temperature, for three different average hydraulic pore radii, R (nanometers).

silicon environment and siloxane ring vibrations in amorphous alkoxide (TEOS) derived silica gels. Their results relate the 608-cm^{-1} Raman "defect" mode in amorphous SiO_2 with reduced Si–O–Si bond angles indicative of strained three-membered rings of silicate tetrahedra.[282,283] They show[283] that dehydroxylation of the silica surface results in cyclotrisiloxane species that have altered acid–base characteristics due to the strained bonds. Their XPS experiments[283] indicate that the expected 0.35-eV shifts in silicon and 2p oxygen 1s binding energies which are due to the reduced bond angles are hidden within broad peaks due to the remaining hydroxyls. Brinker et al. also observe additional silicon 2p oxygen 1s and carbon peaks which are postulated to result from preferential absorption of extrinsic 1s carbon-containing species on sites with enhanced acid–base properties. Molecular orbital calculations by O'Keefe and Gibbs[284] have established that the optimized geometry of the cyclic trisiloxane molecule, $H_6Si_3O_3$, is planar with D_{3h} symmetry with a bond angle ϕ = 136.7°, which is 10° less than the 147° angle characteristic of traditional vitreous silica. Spectroscopic investigations of isolated model molecules by Galeener[285] show that the symmetric oxygen ring breathing vibration occurs at 586 cm^{-1}, which is close to the D_2 Raman bond observed for gels and glasses.[286]

The change in structural density of alkoxide-derived silica gels during thermal processing is apparently caused by at least four interrelated mechanisms. These mechanisms include the elimination of metastable three-membered rings (see above), the loss of hydroxyls, the loss of organic groups, and the relaxation of the SiO_2 structure. Figure 46, from Wallace and Hench,[287] shows the structural density ρ_s (g/cm^3) of a series of silica gel powders, held for 12 h at each temperature with average hydraulic pore radii R of 1.21, 4.18, and 8.98 nm. The true or structural density was measured by using He pycnometry. The structural density ρ_s starts out below that for amorphous silica (ρ_s = 2.20 g/cm^3) and goes through a maximum of about 2.30 g/cm^3 before equilibrating at full densification at about 2.22 g/cm^3. The average standard deviation of the measurements is about 0.004 g/cm^3. The observed variation of ρ_s with temperature is potentially due to a number of effects, including reducing the surface alkoxide and hydroxyl concentration, formation and elimination the metastable three- and four-membered siloxane ring surface defects (D_2 and D_1, respectively, in the Raman spectroscopy nomenclature), structural relaxation, completion of condensation reactions, and viscous flow. Considerable additional research is required to isolate each of these contributions to the observed changes in structural density of the gels.

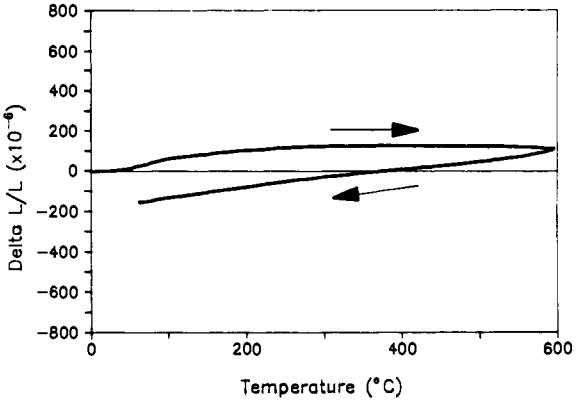

Figure 47. Expansion and contraction of 950 °C stabilized gel–silica cycled to 600 °C.[278]

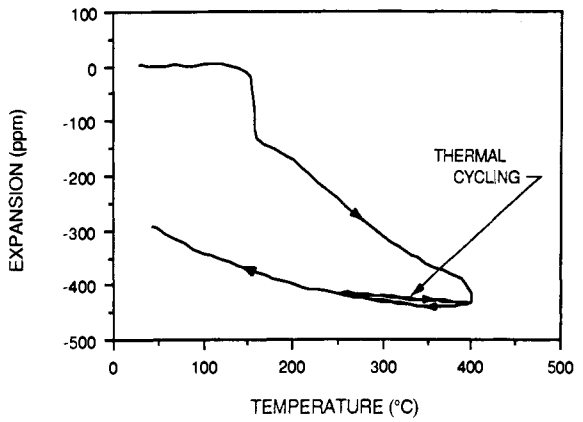

Figure 48. Repeated cycling of gel–silica above 250 °C.[278]

E. Dilation of Sol–Gel Silica Monoliths with Adsorbed Water

The expansion of porous gel–silica monoliths has been studied by using a dual pushrod Theta dilatometer.[278] The expansion and contraction showed a hysteresis with heating and cooling. Figure 47 shows this hysteresis for a sample stabilized to 950 °C. As long as the sample was cycled below approximately 500 °C, there was no hysteresis and the monolith appeared to be thermally stable.[278]

If thermal cycling is performed on the gel monolith, the hysteresis is reduced significantly. Figure 48 shows the thermal cycles performed on a porous gel monolith between 250 and 400 °C before cooling to room temperature. The material shrinks a lot initially, but during thermal cycling the expansion behavior is totally reversible. It is postulated that the expansion of porous gel–silica upon cooling below 250 °C was due to absorption of water onto the pore walls of the material. This was tested by running diatometry and thermogravimetric analysis (TGA) under an ambient atmosphere.[278] Figure 49 shows expansion in the dilatometer over 23 h at 23 °C due to water absorption onto the pore surfaces of the gel. Thus, adsorption of water into the

TABLE X. Silica Dilation

4 fold ring	INDO energy, au	diagonals Si-Si dist, Å (1)-(14)	diagonals Si-Si dist, Å (6)-(7)	av neighbor Si-Si dist, Å	water content, wt %	av expansion $\Delta L/L$, ppm
without H_2O	-223.4	4.6	4.5	3.2	0	0
with H_2O	-241.4	5.2	4.0	3.3	5.8	836

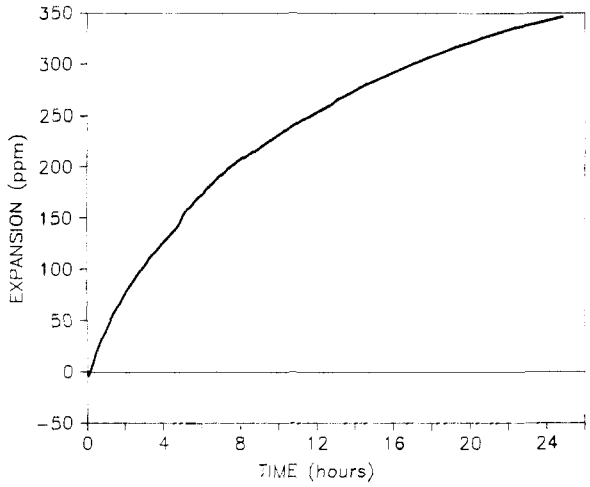

Figure 49. Expansion of porous gel-silica at room temperature over 24-h in ambient air.

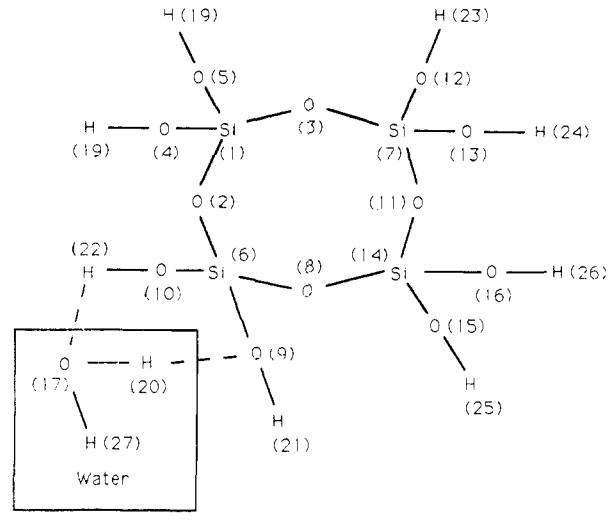

Figure 50. The 4-fold silica structure with one absorbed water molecule.[251]

porous sol–gel silica appears to dilate the gel structure.

F. Quantum Calculations of Water Adsorption onto Sol–Gel Silica

The INDO models presented earlier[193,194] attempted to show the energetics of rings and chains of silica tetrahedra during the sol to gel transition. After condensation is complete and thermal processing has occurred, the sol–gel silica monoliths should be primarily made up of rings. There is roughly an equal distribution of 4-fold, 5-fold, 6-fold, and 7-fold rings of silica tetrahedra in vitreous silica and equivalent structures are believed to be present in silica gels (Klemperer et al.[97]). The 4-fold ring shown in Figure 50 shows the structure selected by West et al.[288] to study the theoretical effect of water on silica rings. The water was hydrogen bonded to the silica cluster as predicted by Takahashi.[289] Intermediate neglect of differential overlap (INDO) molecular orbital theory developed by Zerner et al.[290] was used to optimize the structure in Figure 50. The 4-fold ring was geometrically optimized with and without the adsorbed water molecule.

Table X shows the results of the calculations for the dilation of the 4-fold silica ring. The distances between the diagonal silicon atoms are shown. The ring without water is uniform. However, the ring with the water adsorbed is elongated along the axis with the water. Also, the average silicon–silicon distance for neighboring atoms increases.

In an amorphous structure there should generally be a random orientation of the structural elongation. Some orientation can be imposed on an amorphous material through fiber drawing or spin casting. In gel monoliths with random structures some of the water-induced expansion will occur in regions of the glass where contraction of the rings can compensate, thereby inducing strain. However, on the average there is predicted to be a small expansion when the water is bonded to the structure.

TABLE XI

water content, wt %	$\Delta L/L$, ppm	water content, wt %	$\Delta L/L$, ppm
5.8	836	0.725	104
2.9	418	0.36	52
1.45	209		

The average bond length between neighboring silicon atoms increases with the bonding of water. This increase can be used to estimate the expansion and contraction ($\Delta L/L$) of porous sol–gel silica associated with adsorption and desorption of water. When the porous material is heated, there are two competing contributions to the observed thermal dilation: (1) the uniform increase in dimension due to thermal expansion of the silica structure; (2) a decrease in dimension due to contraction resulting from desorption of water from the surface of the pores. Upon cooling, the reverse occurs, i.e., there is an intrinsic contraction of the structural network and an extrinsic expansion as water is adsorbed (Figure 49). If the effect is linear, then the calculated expansion is shown in Table XI.

For the observed expansion, we have

$$(\Delta L/L)_{obs} = (\Delta L/L)_{H_2O} + (\Delta L/L)_{intrinsic} \quad (38)$$

then, solving for the extrinsic effect of water on heating the sample:

$$(\Delta L/L)_{H_2O} = (\Delta L/L)_{obs} - (\Delta L/L)_{intrinsic} \quad (39)$$

where the thermal expansion of the material can be calculated from Figure 47, shown earlier. Thus

$$(\Delta L/L)_{intrinsic} = 60 \text{ ppm} \quad (40)$$

with

$$(\Delta L/L)_{obs} = 200 \text{ ppm} \quad (41)$$

Then

$$(\Delta L/L)_{H_2O} = 140 \text{ ppm} \quad (42)$$

with approximately 1.0% water loss. This compares remarkably well with the calculated extrinsic expansion or contraction shown in Table XI, e.g.

$$(\Delta L/L)_{calc} = 150 \text{ ppm} \quad (43)$$

for a dilation or contraction caused by ~1.0% water absorption or desorption.

IX. Densification

Densification is the last treatment process of gels. As illustrated in Figure 3, densification of a gel network occurs between 1000 and 1700 °C depending upon the radii of the pores and the surface area. Controlling the gel–glass transition is a difficult problem if one wants to retain the initial shape of the starting material. It is essential to eliminate volatile species prior to pore closure and to eliminate density gradients due to nonuniform thermal or atmosphere gradients.

Initially gel-derived glasses were made by melting.[261] The interesting feature of the sol–gel process that was exploited in this early work was the molecular scale homogeneity of the gels, which helped prepare glasses that ordinarily devitrify at low temperatures. The use of hot pressing of gels by a number of investigators resulted in densification at lower temperature and produced a number of glasses that otherwise would have crystallized.[172-176] With successful stabilization treatments it is possible to manufacture monolithic dense gel-derived glasses by using furnaces, and sometimes vacuum, without applying pressure or heating to temperatures above the melting point.[52,53,140,256,297-302]

The amount of water in the gel has a major importance in the sintering behavior. The viscosity is strongly affected by the concentration of water,[303] which in turn determines the temperature of the beginning of densification. For example, a gel prepared in acidic conditions has a higher surface area and water content than a gel prepared in basic conditions and starts to densify about 200 °C sooner than the base-catalyzed gel, as shown by Nogami and Moriya.[140] Simultaneously with the removal of water, the structure and texture of the gel evolves. Gels have higher free energy than glasses mainly because of their very high specific surface area. During sintering the driving force is a reduction in surface area.[184] Most authors report a diminution of the specific surface area when the densification temperature increases.[110,142,304-306] However, it was shown that certain samples display first an increase of surface area until a temperature between 300 and 400 °C, and then the specific surface area decreases with a further increase of temperature.[297,307] The increase in surface area was attributed to the removal of water and organics.

The structural evolution during the gel to glass conversion is difficult to quantify in absolute terms because there is no definitive structure of a gel. However, it is possible to compare physical properties at different stages between gels and between gel and glass. Some work shows that the small pores close first for some gels[308,309] because they have a higher "solubility" in the gel or glass matrix due to their small radii of curvature. The major conclusion of several studies is that despite the complex manner in which the gel evolves toward a glass, once the gel has been densified and heated above the glass transition temperature, its structure and properties become indistinguishable from those of a melt-derived glass.[49,119,310-313]

There are at least four mechanisms responsible for the shrinkage and densification of gels (see Brinker and Scherer[70] for details): (1) capillary contraction; (2) condensation; (3) structural relaxation; (4) viscous sintering. It is possible that several mechanisms operate at the same time (e.g., condensation and viscous sintering). Using three different models, one can describe the sintering behavior of a gel. Frenkel's theory,[314] which is derived for spheres, is valid for the early stages of sintering, because of the geometrical assumptions. It is based on the fact that the energy dissipated during viscous flow is provided by the reduction in surface area. Scherer[315] developed a model for describing the early stage as well as the intermediate stage of sintering. It is assumed that the microstructure consists of cylinders intersecting in a cubic array. To reduce their surface area, the cylinders become shorter and thicker.[315] The last stage of densification is represented by the Mackenzie–Shuttleworth model, which is applicable only to systems with a closed porosity.[316] This set of models predicts reasonably well the behavior of gels upon heating, although more work needs to be done to recognize the contribution of each mechanism to the sintering process.[317]

Vasconcelos[251] and Vasconcelos et al.[89] have attempted to understand the structural evolution of the gel–glass transition using topological concepts. As indicated above, densification is the increase in bulk density that occurs in a material as a result of the decrease in volume fraction of pores. Consequently the parameter volume fraction (V_v) has been traditionally used to characterize a structure during sintering. Rhines[318] added to the metric parameters the topological concepts that provide complementary information about the sintering process.[230,319,321,322] In topological terms the densification process can be divided into three stages, according to the genus[318] (which is defined as the maximum number of non-self-reentrant closed curves that may be constructed on the surface without dividing it into two separate parts):[321]

First stage: growth of weld necks while the genus remains constant.

Second stage: the genus decreases to zero as the pores become isolated.

Third stage: the genus remains constant at zero while the number of pores goes to zero.

The introduction of topological parameters to the structural characterization of a material yields information that is not visible by considering metric parameters only. One important application of topological characterization is the characterization of interconnected pore structures suitable for diffusion, doping, catalysis, and impregnation procedures. In those cases, knowledge about the volume or surface area of pores is not enough to characterize the structure, because one has to know the extent of interconnection of the structure. The first topological model developed by Vasconcelos et al.[89] assumes a prismatic geometry in which the pores are tetrahedra connected by triangular prisms (Figure 51). The second model uses a cylindrical geometry (Figure 52). Correlating the volume of pores (V_v), the surface area of pores (S_v), the average branch size (L), and the average pore diameter (D) to

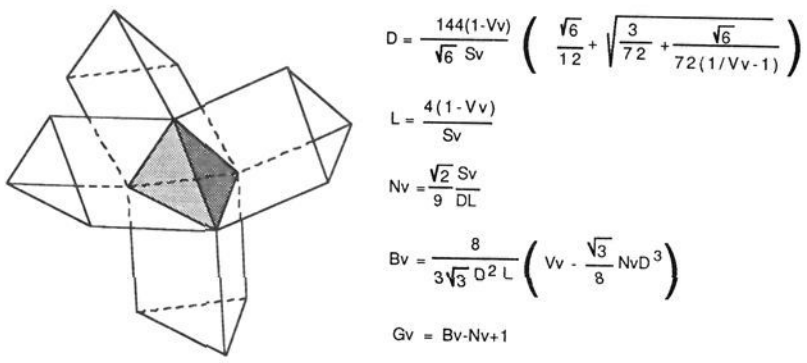

Figure 51. Tetragonal geometric model.

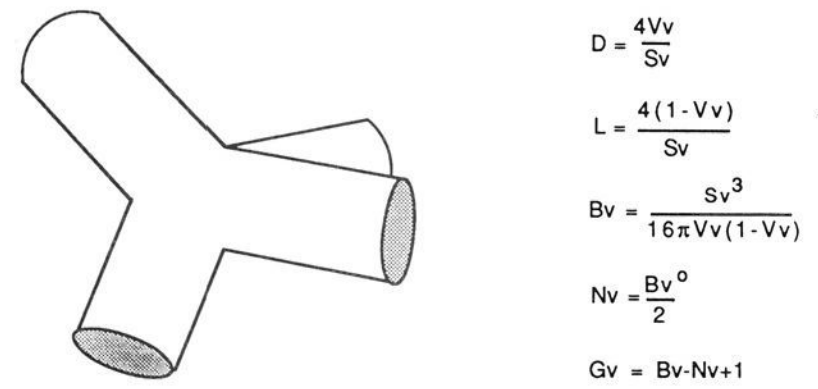

Figure 52. Cylindrical geometric model.[251]

a particular geometry, one obtains a unique set of solutions that yield the number of branches (B_v), number of nodes (N_v), the genus (G_v), and the coordination number of pores (CN), as shown in Figures 51 and 52.[89] The average pore size (D) reported for the cylindrical model is the mean lineal intercept of the pore phase.[322]

$$D = 4V_v/S_v \tag{44}$$

The prismatic model associates a volume to both the nodes and the branches of the pores, while the cylindrical model considers that all the volume is associated with the branches that form the porosity.[251]

As shown in Figure 53,[89] the models assume 4 as the average coordination number of pores (CN) in the dried stage. That initial stage usually corresponds to a maximum number of branches, nodes, and genus. In a sol–gel processed material the interconnected structure is developed during gelation, aging, and drying, as discussed in previous sections. In topological terms these processes correspond to the first stage of densification. During the second stage of densification, the genus decreases, but the number of nodes remains constant and the number of branches decreases. The pyramidal model (Figure 53a) assumes that when CN reaches 2, further elimination of branches leads to disappearance of nodes, and therefore both B_v and N_v decrease, keeping CN constant at 2 during the third stage of densification. At this stage of densification G_v is equal to 1 and it is kept constant during the third stage. The cylindrical model assumes a constant number of nodes for the entire process, and the coordination number varies from 4 to 0, as shown in Figure 53b. Both models can be incorporated in a generalized model[251] considering the zeroth Betti number (number of separate parts, P_v) in the expression $G_v = B_v - N_v + P_v$. During the third stage of densification, as the number of nodes and branches decrease, CN actually goes to zero. The temperatures indicated in Figure 53a correspond to the processing temperatures of the silica–gel monoliths.

The temperature dependence of the structural evolution of alkoxide silica gel monoliths as described by

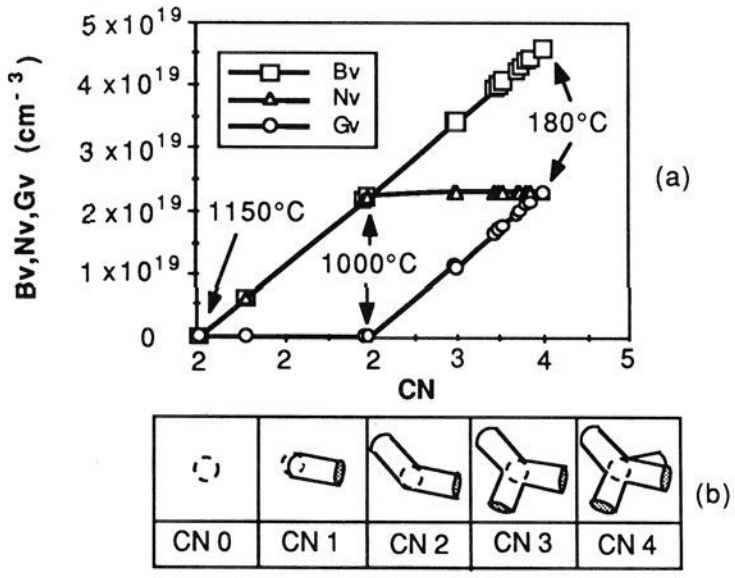

Figure 53. (a) Variation of the number of branches (B_v), number of nodes (N_v), and genus (G_v), as a function of the coordination number (CN). (b) Schematic of the evolution of the pore coordination number.[251]

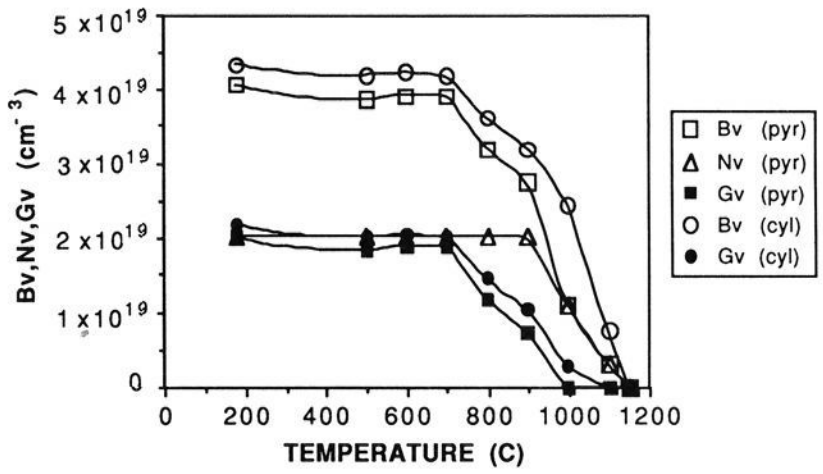

Figure 54. Variation of the number of branches (B_v), number of nodes (N_v), and genus (G_v) as a function of temperature of an organometallic silica–gel monolith.[251]

both models is shown in Figure 54. The genus decreases along with the number of pores at increasingly higher sintering temperatures. The models indicate the temperature for the beginning of the third stage of densification to be in the range 1000–1150 °C for these acid-catalyzed alkoxide silica gels. Despite differences in the numerical values of N_v, G_v, and B_v associated with the pyramidal and cylindrical models, they describe the structure in a very similar way, which is consistent with a topological description.

Because the number of nodes is constant during the second stage of densification and the genus is constant during the third stage of densification, the number of branches is a useful parameter to follow the evoluation of the structure. To make it numerically easier to compare the different topological states, a topological index (fraction of removed branches) has been defined by Vasconcelos[251] as follows:

$$\beta = 1 - (B_v/B_v^\circ) \tag{45}$$

where B_v° corresponds to the number of branches of an arbitrary reference state. If the dried state is chosen as reference, β for the dried sample is zero and β for the fully dense material is equal to 1. Thus the topological index β can be associated with the densification process changing from 0 to 1 with time. The rate of topological change will therefore be $d\beta/dt$.

The choice of the initial coordination number (CN°) does not affect the evaluation of B_v, but it influences the numerical values of N_v and G_v. For the beginning

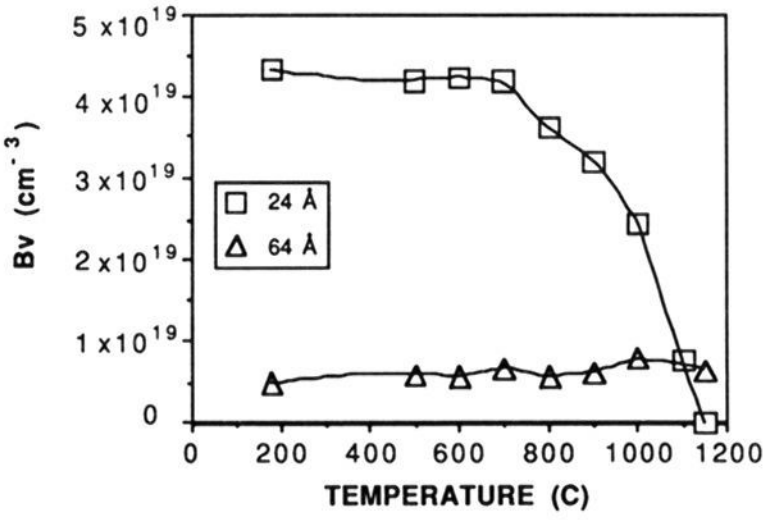

Figure 55. Variation of the number of branches (B_v) as a function of temperature for structures of 24- and 64-Å pore diameter.[251]

of the third stage of densification Vasconcelos shows that β is given by

$$\beta(G_v=0) = 1 - (2/CN°) \quad (46)$$

Application of the cylindrical topological model to structures of different pore sizes (24- and 64-Å average diameter) is shown in Figure 55. While B_v for the 24-Å structures decreases sharply after about 800 °C, B_v for the 64-Å structure remains roughly the same (in fact it increases slightly) over a much broader temperature range. An explanation for the apparently larger thermal stability of the large pore size structure is the smaller driving force for sintering associated with the smaller pore–solid surface area present in the large-pore structure.

Much larger structures ($G_v = 10^6$ cm^{-3}), such as those studied by Rhines and DeHoff,[319-322] show similar paths of topological evolution during densification (particularly a decrease in G_v as V_v decreases), indicating the broad spectrum of applications of the topological concepts. The path of microstructural evolution described for silica gel monoliths is similar to the path associated with the sintering of larger structures.[251]

Thus, application of topological modeling to the densification of sol–gel-derived nanometer-scale structures reveals the same principles as determined for the sintering of micrometer to millimeter scale powder structures. As shown in the next section, the topological evolution of the gel structure can be related to physical properties and presents potentially useful information that is complementary to traditional metric parameters.

X. Physical Properties

There are relatively few papers describing the thermal, mechanical, and optical properties of gel-derived monoliths. This is because of the difficulty of producing large stable structures, as reviewed in the previous sections. During 1988–89, processing optimization has been achieved for the production of gel-derived silica optical components. Hench et al.[52,53] described the processing and properties of these new materials, termed type V (fully dense) gel–silica and type VI (optically transparent porous gel–silica). The properties of types V and VI are compared with commercial fused quartz optics (types I and II) and synthetic fused silica optics (types III and IV).[52]

Type V gel–silica has excellent transmission from 160 to 4200 nm with no OH absorption peaks. As shown in Figure 45, the UV cutoff is shifted to lower wavenumbers by removal of OH from the gel glass. Also,

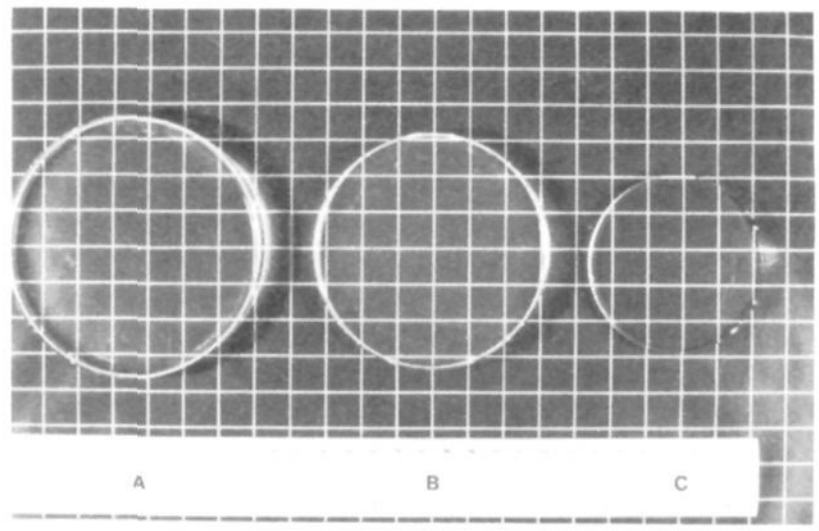

Figure 56. Sol–gel silica monoliths in the (A) dry state, (B) stabilized state (porous type VI), and (C) fully dense state (type V).[53]

quantum calculations, discussed earlier, predict this effect.[193]

Other physical properties and structural characteristics of type V gel–silica are similar to high-grade fused silica but offer the advantages of near net-shape casting, including internal cavities, and a lower coefficient of thermal expansion of 0.2×10^{-6} cm/cm compared with 0.55×10^{-6} cm/cm.[52,53] Optically transparent porous gel silica (type VI) has a UV cutoff ranging from 250 to 300 nm. Type VI gel–silica optics has a density as low as 60% of types I–V silica and can be impregnated with up to 30–40% by volume of a second-phase optically active organic or inorganic compound. Photographs of a dried alkoxide silica gel monolith, a type VI porous Gelsil sample and a fully dense type V Gelsil sample are shown in Figure 56.

Shoup and Hagy has shown that the colloidal method of making reflective silica optics[90] (method 1) yields a different thermal expansion behavior than types I–III vitreous silica, presumably due to the rapid quenching of the gel–glasses from 1720 °C.[332]

Bachman et al.[333] describe the use of centrifugal deposition of 12–40-nm colloidal silica powders to produce synthetic silica tubes used in the manufacture of optical telecommunication fibers. They report optical losses of $\alpha^{1300} = 0.97$ dB/km and $\alpha^{1550} = 0.77$ dB/km for optical fibers made by using the tubes. A Rayleigh scattering coefficient of $\alpha_R = 1.1$ dB/(km μm^4) was measured for the bulk sintered tubes, equivalent to that of the single-mode fibers. One of the main advantages of the sol–gel technique was very high accuracies (±0.05%) for the diameter, cross-sectional area, and wall thickness of the tubes.

Mechanical properties of the type VI porous gel–silica monoliths have been determined by Vasconcelos et al.[89,251] and related to the topological and metric features. The variation of flexural strength as a function of V_v shows relatively scattered data (Figure 57a). The flexural strength correlates better with β, as shown in Figure 57b, for the topological cylindrical model discussed in the Densification section. The points in Figure 57 represent an average; the total number of mechanical tests performed is 27. The true density data are incorporated into the topological modeling. The true density of some selected samples (of 24-Å pore diameter) is as follows: dried, 2.10 g/cm^3; 800 °C, 2.31 g/cm^3; 1150 °C, 2.20 g/cm^3.

Additional details of ultrastructure–poroperty correlations of various gel–silica monoliths are to be pub-

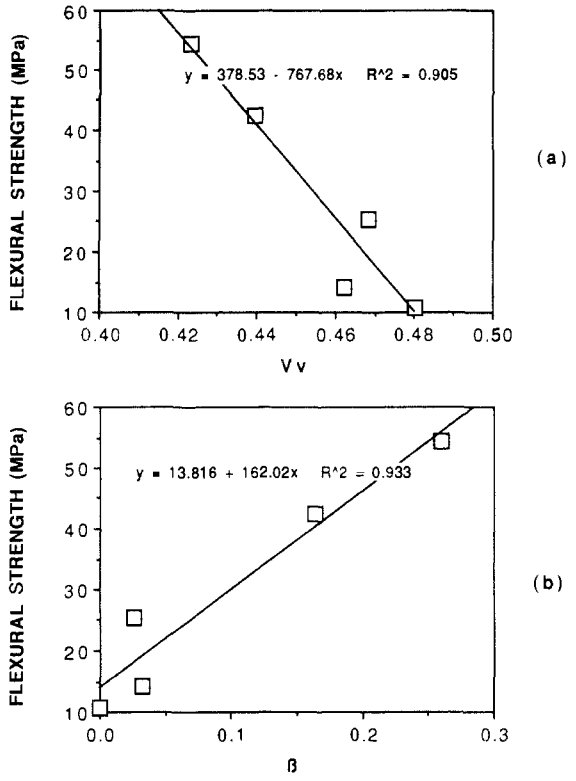

Figure 57. Variation of the flexural strength (a) as a function of the volume fraction of pores (V_v) and (b) as a function of the topological index β.[251]

lished later by Hench and Vasconcelos.[323]

XI. Conclusions

The goal of sol–gel processing is to control the structure of a material on a nanometer scale from the earliest stages of processing. For pure silica powders, fibers, and even monoliths this goal has been achieved. The potential of improved properties due to ultrastructural processing, control of higher purity, and greater homogeneity has been realized. Other engineering advantages of the lower temperature chemically based sol–gel processing such as net-shape casting, fiber pulling, and film coating have also reached economic potential.

Advances in understanding the science of sol–gel processing are less conclusive. General aspects of the chemistry of each of the seven sol–gel process steps are established. However, understanding of the molecular reaction mechanisms and the thermodynamics and kinetics of sol–gel systems is meager. Many studies involve model systems that yield self-consistent data but may not necessarily apply to processing formulas that yield useful materials. Only a few studies use multiple experimental methods to confirm reaction mechanisms or determine kinetics. Likewise, there are few investigations of the interrelationships between the seven processing steps. For example, many investigators have shown that base catalysis yields gels with a coarser texture than acid catalysis. However, there is little understanding as to how the differences in gel texture influences aging, drying, stabilization, or densification of the gels. Systematic studies on multicomponent gel systems are especially rare.

A major difficulty in developing molecular level understanding of the sol–gel processing is the extremely small scale of the structures involved. After gelation occurs, and often even at $t > 0.3$–$0.5t_g$, the substance usually must be treated analytically as a solid. Since the solid phase at t_g can be as little as 1–10% of the mass of the object, a cross section of the solid web is only a few molecules wide, but the length of the molecular chains extend throughout the object with an enormous number and complexity of interconnections. The molecular structure of the liquid phase in these gels is as important as the structure of the solid phase. However, the liquid characteristics deviate from classical liquids in many ways. The concept of phase boundary is stretched to the quantum mechanical limit. Consequently, it is quite likely that quantum mechanical based models are much more likely to yield the next level of understanding of sol–gel processes rather than a macroscopic fractal approach.

In some ways it may be useful to think of sol–gel science in terms of a few fundamental questions, i.e., How does the gel structure form? How does the structure evolve? How does it interact with its environment? How does it collapse? These questions parallel the fundamental questions in the biological sciences. It is fitting that they do, for silicon is the fifth most abundant element in the biosphere, and life forms with hydrated silicon exoskeletons, diatoms, are responsible for more than half of the carbon and nitrogen biochemical fixation that occurs annually on the earth.[334] The biological silicon-based structures of both plants and animals form at low temperatures and with elegant highly repetitive ultrastructures. The various theories regarding formation of biological silicon-based structures,[335] the metabolic pathways for silicon,[335] the role of silicon in osteogenesis,[336] atherosclerosis,[334] and even biogenesis[337] are of considerable current interest and debate. Thus, our quest for the answers to the fundamental questions of sol–gel science may also offer advances in the understanding of biological science and perhaps even of the origins of life and preservation of health. In our opinion, these answers are most likely to come from the exploration of molecular order and disorder at the interface of nanometer-scale structures.

Acknowledgments. We gratefully acknowledge the support of the Air Force Office of Scientific Research under Contract No. F49620-88-C-0073 during the course of this work.

References

(1) Ebelmen, M. *Ann. Chimie Phys.* **1846**, *16*, 129.
(2) Ebelmen, M. *C. R. Acad. Sci.* **1847**, *25*, 854.
(3) Graham, T. *J. Chem. Soc.* **1864**, *17*, 318.
(4) Liesegang, R. E. *Photogr. Archiv.* **1896**, 221.
(5) Heinisch, H. K. *Crystal Growth in Gels*; Pennsylvania State University Press: State College, PA, 1970.
(6) Ostwald, W. Z. *Phys. Chem.* **1897**, *27*, 365.
(7) Rayleigh, L. *Philos. Mag.* **1919**, *38*, 738.
(8) Lloyd, D. J. In *Colloid Chemistry*; Alexander, J., Ed.; Chemical Catalog Co.: New York, 1926; p 767.
(9) Holmes, H. N. In *Colloid Chemistry*; Alexander, J., Ed.; Chemical Catalog Co.: New York, 1926; p 796.
(10) Stern, K. H. *Bibliography of Liesegang Rings*; National Bureau of Standards Miscellaneous Publication No. 292, 1967.
(11) Roy, D. M.; Roy, R. *Am. Mineral.* **1954**, *39*, 957.
(12) Roy, R. *J. Am. Ceram. Soc.* **1956**, *39*, 145.
(13) Roy, R. *J. Am. Ceram. Soc.* **1969**, *52*, 344.
(14) McCarthy, G. J.; Roy, R.; McKay, J. M. *J. Am. Ceram. Soc.* **1971**, *54*, 637.
(15) Iler, R. K. *The Chemistry of Silica*; Wiley: New York, 1955.
(16) Stober, W.; Fink, A.; Bohn, E. *J. Colloid Interface Sci.* **1968**, *26*, 62.

(17) Tan, C. G.; Bowen, B. D.; Epstein, N. *J. Colloid Interface Sci.* **1987**, *118*, 290.
(18) Khadikar, C. The Effect of Adsorbed Poly(vinyl Alcohol) on the Properties of Model Silica Suspensions. Ph.D. Dissertation; University of Florida: Gainesville, FL, 1988.
(19) Overbeek, J. Th. G. *Adv. Colloid Interface Sci.* **1982**, *16*, 17.
(20) Overbeek, J. Th. G. *Adv. Colloid Interface Sci.* **1982**, *15*, 251.
(21) Sugimoto, T. *Adv. Colloid Interface Sci.* **1987**, *28*, 65.
(22) Matijevic, E.; Bundnick, M.; Meites, L. *J. Colloid Interface Sci.* **1977**, *61*, 302.
(23) Matijevic, E. In *Ultrastructure Processing of Ceramics Glasses and Composites*; Hench, L. L., Ulrich, D. R., Eds.; Wiley: New York, 1984; p 334.
(24) Matijevic, E. In *Science of Ceramic Chemical Processing*; Hench, L. L., Ulrich, D. R., Eds.; Wiley: New York, 1986; p 463.
(25) Matijevic, E. In *Ultrastructure Processing of Advanced Ceramics*; Mackenzie, J. D., Ulrich, D. R., Eds.; Wiley: New York, 1988; p 429.
(26) Barringer, E. A.; Bowen, H. K. *J. Am. Ceram. Soc.* **1982**, *65*, C199.
(27) Fegley, B., Jr.; Barringer, E. A. In *Better Ceramics Through Chemistry*; Brinker, C. J., Clark, D. E., Ulrich, D. R., Eds.; Elsevier: New York, 1984; Vol. 32, p 187.
(28) Fegley, B., Jr.; White, P.; Bowen, H. K. *Am. Ceram. Soc. Bull.* **1985**, *64*, 1115.
(29) Fegley, B., Jr.; Barringer, E. A.; Bowen, H. K. *J. Am. Ceram. Soc.* **1984**, *67*, C113.
(30) Hardy, A.; Gowda, G.; McMahan, T. J.; Riman, R. E.; Rhine, W. E.; Bowen, H. K. In *Ultrastructure Processing of Advanced Ceramics*; Mackenzie, J. D., Ulrich, D. R., Eds.; Wiley: New York, 1988; p 407.
(31) Hermans, M. E. A. *Sci. Ceram.* **1970**, *5*, 523.
(32) Kamiya, K.; Sakka, S.; Tatemichi, Y. *J. Mater. Sci.* **1980**, *15*, 1765.
(33) Susa, K.; et al. *Electron. Lett.* **1982**, *18*, 499.
(34) Rabinovich, E. M.; Johnson, Jr., D. W.; Mac Chesney, J. B.; Vogel, E. M. *J. Non-Cryst. Solids* **1982**, *47*, 435.
(35) Rabinovich, E. M.; Johnson, Jr., D. W.; Mac Chesney, J. B.; Vogel, E. M. *J. Am. Ceram. Soc.* **1983**, *66*, 683.
(36) Johnson, Jr., D. W.; Rabinovich, E. M.; Mac Chesney, J. B.; Vogel, E. M. *J. Am. Ceram. Soc.* **1983**, *66*, 688.
(37) Rabinovich, E. M.; Mac Chesney, J. B.; Johnson, Jr., D. W.; Simpson, J. R.; Meagher, B. W.; Mimarcello, F. V.; Wood, D. L.; Sigety, E. A. *J. Non-Cryst. Solids* **1984**, *63*, 155.
(38) Rabinovich, E. M. In *Ultrastructure Processing of Ceramics, Glasses and Composites*; Hench, L. L., Ulrich, D. R., Eds.; Wiley: New York, 1984.
(39) Carroll-Porczynski, C. Z. *Advanced Materials*; Chemical Publishing Co.: New York, 1962.
(40) McCreight, L. R.; Rauch, H. W., Sr.; Sutton, w. H. *Ceramic Fibers and Fibrous Composite Materials*; Academic Press: New York, 1965.
(41) Rauch, H. W., Sr.; Sutton, W. H.; McCreight, L. R. *Ceramic Fibers and Fibrous Composite Materials*; Academic Press, New York, 1968.
(42) Seufert, L. E. U.S. Patent No. 3,808,015, Apr 30, 1974.
(43) Miyahara, K.; Nakayama, N. Process for Producing Polycrystalline Oxide Fibers. U.S. Patent 4,159,205, 1979.
(44) Leitheiser, M.; Snowman, H. G. Non-Fused Alumina Based Abrasive Material. U.S. Patent Appl. 145,383, 1980.
(45) Dislich, H.; Hinz, P. *J. Non-Cryst. Solids* **1982**, *48*, 11.
(46) Dislich, H. In *Ultrastructure Processing of Ceramics, Glasses and Composites*; Hench, L. L., Ulrich, D. R., Eds.; Wiley: New York, 1984; p 100.
(47) Dislich, H. *J. Non-Cryst. Solids* **1985**, *72*, 599.
(48) Schroeder, H. *Opt. Acta* **1962**, *9*, 249.
(49) Mackenzie, J. D. *J. Non-Cryst. Solids* **1982**, *41*, 1.
(50) Mackenzie, J. D. In *Ultrasonic Processing of Ceramics, Glasses and Composites*; Hench, L. L., Ulrich, D. R., Eds.; Wiley: New York, 1984; p 15.
(51) Wenzel, J. In *Glass. Current Issues*; Wright, A. F., Dupuy, A. F., Eds.; Martinus Nijhojj: Dordrecht, Netherlands, 1985; p 224.
(52) Hench, L. L.; Wang, S. H.; Nogues, J. L. In *Multifunctional Materials*; Gunshor, R. L., Ed.; SPIE: Bellingham, WA, 1988; Vol. 878, p 76.
(53) Hench, L. L.; Wilson, M. J. R.; Balaban, C.; Nogues, J. L. Sol-Gel Processing of Large Silica Optics. Proceedings of 4th International Conference on Ultrastructure Processing of Ceramics, Glasses and Composites, Tucson, AZ, 1989.
(54) Wang, S. H.; Campbell, C.; Hench, L. L. In *Ultrastructure Processing of Advanced Ceramics*; Mackenzie, J. D., Ulrich, D. R., Eds.; Wiley: New York, 1988; p 145.
(55) Kistler, S. S. *Nature* **1931**, *127*, 742.
(56) Fricke, J., Ed. *Aerogels*; Springer Proceedings in Physics; Springer-Verlag: Heidelberg, 1986; Vol. 6.
(57) Phalippou, J.; Prassas, M.; Zarzycki, J. *J. Non-Cryst. Solids* **1982**, *48*, 17.
(58) Prassas, M.; Phalippou, J.; Zarzycki, J. *Int. Conf. Glasses, 13th*, Hamburg, Germany, 1985.
(59) Yoldas, B. E. *Bull. Am. Ceram. Soc.* **1975**, *54*, 286.
(60) Onoda, G., Hench, L. L., Eds. *Science of Ceramic Processing Before Firing*; Wiley: New York, 1978.
(61) Hench, L. L., Ulrich, D. R., Eds. *Ultrastructure Processing of Ceramics Glasses and Composites*; Wiley: New York, 1984.
(62) Hench, L. L., Ulrich, D. R., Eds. *Science of Ceramic Chemical Processing*; Wiley: New York, 1986.
(63) Mackenzie, J. D., Ulrich, D. R., Eds. *Ultrastructure Processing of Advanced Ceramics*; Wiley: New York, 1988.
(64) Uhlmann, D. R.; Weinberg, M.; Ulrich, D. R. *Ultrastructure Processing IV*; Wiley: New York, 1989.
(65) Brinker, C. J., Clark, D. E., Ulrich, D. R., Eds. *Better Ceramics Through Chemistry*; Elsevier: New York, 1984; Vol. 32.
(66) Brinker, C. J., Clark, D. E., Ulrich, D. R., Eds. *Better Ceramics Through Chemistry II*; Materials Research Society: Pittsburgh, PA, 1986; Vol. 73.
(67) Brinker, C. J., Clark, D. E., Ulrich, D. R., Eds. *Better Ceramics Through Chemistry III*; Materials Research Society: Pittsburgh, PA, 1988; Vol. 121.
(68) Zarzycki, J., Ed. Glasses and Ceramics from Gels. *J. Non-Cryst. Solids* **1986**, *1-3*, 1-436.
(69) Klein, L. C. *Sol-Gel Technology for Thin Films, Fibers, Preforms, Electronics and Specialty Shapes*; Noyes Publications: Park Ridge, NJ, 1988.
(70) Brinker, C. J.; Scherer, G. W. *Sol-Gel Science*; Academic Press: New York, 1989.
(71) Klein, L. C. *Glass Ind.* **1981**, 14.
(72) Sakka, S.; Kamiya, K. *J. Non-Cryst. Solids* **1980**, *42*, 403.
(73) Mukherjee, S. P. *J. Non-Cryst. Solids* **1980**, *42*, 477.
(74) Sakka, S. In *Treatise on Materials Science and Technology*; Tomozawa, M., Doremus, R., Eds.; Academic Press: New York, 1982; Vol. 22, p 129.
(75) Sakka, S. *Am. Ceram. Soc. Bull.* **1985**, *64*, 1463.
(76) Iler, R. K. *The Chemistry of Silica*; Wiley: New York, 1979.
(77) Okkerse, C. In *Physical and Chemical Aspects of Adsorbents and Catalysts*; Linsen, B. G., Ed.; Academic Press: New York, 1970; p 213.
(78) Davis, J. T.; Rideal, E. K. In *Interfacial Phenomena*; Academic Press: New York, 1963.
(79) Flory, P. J. *Principles of Polymer Chemistry*; Cornell University Press: Ithaca, NY, 1953; Chapter IX.
(80) Fricke, J.; Capo, In *Ultrastructure Processing of Advanced Ceramics*; Mackenzie, J. D., Ulrich, D. R., Eds.; Wiley: New York, 1988.
(81) Zarzycki, J. In *Science of Ceramic Chemical Processing*; Hench, L. L., Ulrich, D. R., Eds.; Wiley: New York, 1986; p 21.
(82) Scherer, G. W. In *Ultrastructure Processing of Advanced Ceramics*; MacKenzie, J. D., Ulrich, D. R., Eds.; Wiley: New York, 1988.
(83) Scherer, G. W. *J. Non-Cryst. Solids* **1986**, *87*, 199.
(84) Scherer, G. W. *J. Non-Cryst. Solids* **1987**, *91*, 83.
(85) Scherer, G. W. *J. Non-Cryst. Solids* **1987**, *91*, 101.
(86) Scherer, G. W. *J. Non-Cryst. Solids* **1987**, *92*, 122.
(87) Scherer, G. W. *J. Non-Cryst. Solids* **1987**, *89*, 217.
(88) Scherer, G. W. *J. Non-Cryst. Solids* **1988**, *100*, 77.
(89) Vasconcelos, W.; DeHoff, R. T.; Hench, L. L. In Proceedings of the 4th International Conference on Ultrastructure Processing of Ceramics, Glasses, and Composites; Tucson, AZ, 1989.
(90) Shoup, R. D. In *Ultrasonic Processing of Advanced Ceramics*; Mackenzie, J. D., Ulrich, D. R., Eds.; Wiley: New York, 1988; p 347.
(91) Sacks, M. D.; Tseng, T. Y. *J. Am. Ceram. Soc.* **1984**, *67*, 526.
(92) Sacks, M. D.; Tseng, T. Y. *J. Am. Ceram. Soc.* **1984**, *67*, 532.
(93) Orcel, G. The Chemistry of Silica Sol-Gel; Ph.D. Dissertation; University of Florida: Gainesville, FL, 1987.
(94) Orcel, G.; Hench, L. L.; Artaki, I.; Jones, J.; Zerda, T. W. *J. Non-Cryst. Solids* **1988**, *105*, 223.
(95) Orcel, G.; Hench, L. L. In *Science of Ceramic Chemical Processing*; Hench, L. L., Ulrich, D. R., Eds.; Wiley: New York, 1986; p 224.
(96) Hench, L. L.; Orcel, G. *J. Non-Cryst. Solids* **1986**, *82*, 1.
(97) Klemperer, W. G.; Ramamurthi, S. D. In *Better Ceramics Through Chemistry III*; Brinker, C. J., Clark, D. E., Ulrich, D. R., Eds.; Materials Research Society: Pittsburgh, PA, 1988; Vol. 121, p 1.
(98) Klemperer, W. G.; Mainz, V. V.; Ramamurthi, S. D.; Rosenberg, F. S. In *Better Ceramics Through Chemistry III*; Brinker, C. J., Clark, D. E., Ulrich, D. R., Eds.; Materials Research Society: Pittsburgh, PA, 1988; Vol. 121, p 15.
(99) Artaki, I.; Bradley, M.; Zerda, T. W.; Jonas, J.; Orcel, G.; Hench, L. L. In *Science of Ceramic Chemical Processing*; Hench, L. L., Ulrich, D. R., Eds.; Wiley: New York, 1986; p 73.
(100) Artaki, I.; Zerda, T.; Jonas, J. *J. Mater. Sci. Lett.* **1985**, *3*, 493.

(101) Artaki, I.; Sinha, S.; Jones, J. *J. Mater. Sci. Lett.* **1984**, *2*, 448.
(102) Artaki, I.; Sinha, S.; Irwin, A. D.; Jones, J. *J. Non-Cryst. Solids* **1985**, *72*, 391.
(103) Aelion, A.; Loebel, A.; Eirich, F. *J. Am. Chem. Soc.* **1950**, *72*, 5702.
(104) Schmidt, H.; Scholze, H.; Kaiser, A. *J. Non-Cryst. Solids* **1984**, *63*, 1.
(105) Schmidt, H.; Kaiser, A.; Rudolph, M.; Lentz, A. In *Science of Ceramic Chemical Processing*; Hench, L. L., Ulrich, D. R., Eds.; Wiley: New York, 1986; p 87.
(106) Uhlmann, D. R.; Zelinski, B. J.; Silverman, L.; Warner, S. B.; Fabes, B. D.; Doyle, W. F. In *Science of Ceramic Chemical Processing*; Hench, L. L., Ulrich, D. R., Eds.; Wiley: New York, 1986; p 173.
(107) Assink, R. A.; Kay, B. D. In *Better Ceramics Through Chemistry*; Brinker, C. J., Clark, D. E., Ulrich, D. R., Eds.; Elsevier: New York, 1984; Vol. 32, p 301.
(108) Schmidt, H.; Scholze, H. In *Glass. Current Issues*; Wright, A. F., Dupuy, A. F., Eds.; Martinus Nijhojj: Dordrecht, Netherlands, 1985; p 253.
(109) Schmidt, H.; Kaiser, A. *Glastechn Ber* **1981**, *54*, 338.
(110) Mackenzie, J. D. In *Science of Ceramic Chemical Processing*; Hench, L. L., Ulrich, D. R., Eds.; Wiley: New York, 1986; p 113.
(111) Kay, B. D.; Assink, R. A. In *Better Ceramics Through Chemistry II*; Brinker, C. J., Clark, D. E., Ulrich, D. R., Eds.; Materials Research Society: Pittsburgh, PA, 1986; Vol. 73, p 157.
(112) Harris, R. K.; Knight, C. T. G.; Hull, W. E. In *Soluble Silicates*; Falcone, J. S., Ed.; ACS Symposium Series No. 194; American Chemical Society: Washington, D.C., 1982; p 79.
(113) Engelhardt, V. G.; Altenburg, W.; Hoebbel, D.; Weiker, W.; Znorg, Z. *Allgenines Journal der Chemie* **1977**, *418*, 43.
(114) Yoldas, B. E. *J. Non-Cryst. Solids* **1984**, *63*, 145.
(115) Prassas, M.; Hench, L. L. In *Ultrastructure Processing of Ceramics, Glasses and Composites*; Hench, L. L., Ulrich, D. R., Eds.; Wiley: New York, 1984; p 100.
(116) Orcel, G.; Hench, L. L. *J. Non-Cryst. Solids* **1986**, *79*, 177.
(117) Hench, L. L.; Orcel, G.; Nogues, J. L. In *Better Ceramics Through Chemistry II*; Brinker, C. J., Clark, D. E., Ulrich, D. R., Eds.; Materials Research Society: Pittsburgh, PA, 1986; Vol. 73, p 35.
(118) White, W B.; Minser, D. G. *J. Non-Cryst. Solids* **1986**, *67*, 177.
(119) Bertoluzza, A.; Fagnano, C.; Morelli, M. A.; Guglielmi, M. *J. Non-Cryst. Solids* **1982**, *48*, 117.
(120) Iler, R. K. In *Soluble Silicates*; Falcone, J. S., Ed.; Symposium Series No. 194, ACS American Chemical Society: Washington, D.C., 1982.
(121) Brinker, C. J.; Scherer, G. W. *J. Non-Cryst. Solids* **1985**, *70*, 301.
(122) Iler, R. K. In *Science of Ceramic Chemical Processing*; Hench, L. L., Ulrich, D. R., Eds.; Wiley: New York, 1986; p 3.
(123) Khan, S. A.; Rabinovich, E. M.; Prudhomme, R. K.; Sammon, M. J.; Kopylor, N. J. In *Better Ceramics Through Chemistry III*; Brinker, C. J., Clark, D. E., Ulrich, D. R., Eds.; Materials Research Society: Pittsburgh, PA, 1988; Vol. 121, p 73.
(124) Sacks, M. D.; Sheu, R. S. In *Science of Ceramic Chemical Processing*; Hench, L. L., Ulrich, D. R., Eds.; Wiley: New York, 1986; p 102.
(125) Yamane, M.; Inoue, S.; Yasumori, A. *J. Non-Cryst. Solids* **1984**, *63*, 13.
(126) Wallace, S.; Hench, L. L. In *Better Ceramics Through Chemistry*; Brinker, C. J., Clark, D. E., Ulrich, D. R., Eds.; Elsevier: New York, 1984; Vol. 32, p 47.
(127) Debsikdar, J. C. *Adv. Ceram. Mater.* **1986**, *1*, 93.
(128) Colby, M. W.; Osaka, A.; MacKenzie, J. D. *J. Non-Cryst. Solids* **1986**, *82*, 37.
(129) Klein, L. C.; Garvey, G. J. *J. Non-Cryst. Solids* **1982**, *48*, 97.
(130) Sakka, S.; Kamiya, K. *J. Non-Cryst. Solids* **1982**, *48*, 31.
(131) Lacourse, W. C. In *Better Ceramics Through Chemistry*; Brinker, C. J., Clark, D. E., Ulrich, D. R., Eds.; Materials Research Society; Elsevier: New York, 1984; Vol. 32, p 53.
(132) Sakka, S. In *Better Ceramics Through Chemistry*; Brinker, C. J., Clark, D. E., Ulrich, D. R., Eds.; Elsevier: New York, 1984; Vol. 32, p 91.
(133) Kamiya, K.; Yoko, T. *J. Mater. Sci.* **1986**, *21*, 842.
(134) Mukherjee, S. P. *Thin Solid Films Lett.* **1981**, *81*, L89.
(135) Mukherjee, S. P.; Lowdermilk, W. H. *Appl. Opt.* **1982**, *21*, 293.
(136) Sakka, S.; Kamiya, K.; Makita, K.; Yamato, Y. *J. Non-Cryst. Solids* **1984**, *63*, 223.
(137) Ling, H. C.; Yan, M. F.; Rhodes, W. W. In *Science of Ceramic Chemical Processing*; Hench, L. L., Ulrich, D. R., Eds.; Wiley: New York, 1986; p 285.
(138) Strawbridge, I.; James, P. F. *J. Non-Cryst. Solids* **1986**, *82*, 366.
(139) Hinz, P.; Dislich, H. *J. Non-Cryst. Solids* **1986**, *82*, 411.
(140) Nogami, M.; Moriya, Y. *J. Non-Cryst. Solids* **1980**, *37*, 191.
(141) Ahktar, M. M. Ph.D. Dissertation, Alfred University, New York, 1983.
(142) Mizuno, T.; Phalippou, J.; Zarzycki, *J. Glass Technol.* **1985**, *26*, 39.
(143) Mizuno, T. Ph.D. Dissertation, Université des Sciences et Techniqhes du Languedoc, Montpellier, France, 1985.
(144) Orgaz, F.; Rawson, H. *J. Non-Cryst. Solids* **1986**, *82*, 57.
(145) Guinier, A.; Fournet, G. *Small Angle Scattering of X-Rays*; Wiley: New York, 1955.
(146) Guinier, A. *X-Ray Diffraction*; Freeman: San Francisco, CA, 1963.
(147) Brumberger, H., Ed. *Small Angle X-Ray Scattering*; Gordon and Breach: New York, 1967.
(148) Keefer, K. D. *Better Ceramics Through Chemistry II*; Brinker, C. J., Clark, D. E., Ulrich, D. R., Eds.; Materials Research Society: Pittsburgh, PA, 1986; Vol. 73, p 295.
(149) Schaefer, D. W.; Martin, J. E.; Wiltzius, P. W.; Cannell, D. S. In *Kinetics of Aggregation and Gelation*; Family, F., Landau, D. P., Eds.; North Holland: Amsterdam, The Netherlands, 1984; p 71.
(150) Brinker, C. J.; Keefer, K. D.; Schaefer, D. W.; Ashley, C. S. *J. Non-Cryst. Solids* **1982**, *48*, 47.
(151) Brinker, C. J.; Keefer, K. D.; Schaefer, D. W.; Assink, R. A.; Kay, B. D.; Ashley, C. S. *J. Non-Cryst. Solids* **1984**, *63*, 45.
(152) Schaefer, D. W.; Keefer, K. D. In *Better Ceramics Through Chemistry*; Brinker, C. J., Clark, D. E., Ulrich, D. R., Eds.; Elsevier: New York, 1984; p 1.
(153) Keefer, K. D. In *Science of Ceramic Chemical Processing*; Hench, L. L., Ulrich, D. R., Eds.; Wiley: New York, 1986; p 131.
(154) Schaefer, D. W. In *Better Ceramics Through Chemistry II*; Brinker, C. J., Clark, D. E., Ulrich, D. R., Eds.; Materials Research Society: Pittsburgh, PA, 1986; Vol. 73, p 277.
(155) Schaefer, D. W.; Keefer, K. D.; Anbert, J. H.; Rand, P. B. *Science of Ceramic Chemical Processing*; Hench, L. L., Ulrich, D. R., Eds.; Wiley: New York, 1986; p 140.
(156) Orcel, G.; Gould, R. W.; Hench, L. L. In *Better Ceramics Through Chemistry II*; Brinker, C. J., Clark, D. E., Ulrich, D. R., Eds.; Materials Research Society: Pittsburgh, PA, 1986; Vol. 73, p 289.
(157) Hardman-Rhyne, K. A.; Coyle, T. D.; Lewis, E. P. Presented at the 1983 Annual Meeting of the Canadian Ceramic Society, Montreal, Quebec, Feb 20–23, 1983.
(158) Wright, A. C. *J. Non-Cryst. Solids* **1985**, *76*, 187.
(159) Zimm, B. H.; Stockmayer, W. H. *J. Chem. Phys.* **1949**, *17*, 1301.
(160) de Gennes, P.-G. *Biopolymers* **1968**, *6*, 715.
(161) Zallen, R. *The Physics of Amorphous Solids*; Wiley: New York, 1983; Chapter 4.
(162) Stauffer, D.; Coniglio, A.; Adam, M. *Adv. Polym. Sci.* **1982**, *44*, 103.
(163) Benoit, B.; Mandelbrot, W. H. *The Fractal Geometry of Nature*; Freeman and Company: New York, 1982.
(164) Abell, G. *Exploration of the Universe*, 2nd ed.; Holt, Rinehart and Winston: New York, 1969.
(165) Novotny, E. *Introduction to Stellar Atmospheres and Interiors*; Oxford University Press: New York, 1973.
(166) Witten, Jr., T. A.; Sander, L. M. *Phys. Rev. Lett.* **1981**, *47*, 1400.
(167) Witten, T. A.; Sander, L. M. *Phys. Rev. B* **1983**, *27*, 5686.
(168) Witten, T. A.; Cates, M. E. *Science* **1986**, *232*, 1607.
(169) Craievich, Aegeter, dos Santos, Woignier, Zarzycki *J. Non-Cryst. Solids* **1986**, *86*, 394.
(170) Himmel, B.; Gerber, Th.; Burger, H. *J. Non-Cryst. Solids* **1987**, *91*, 122.
(171) Bogush, G. H.; Zukoski, C. F. *Ultrastructure Processing of Advanced Ceramics*; Mackenzie, J. D., Ulrich, D. R., Eds.; Wiley: New York, 1988; p 477.
(172) Swain, C. G.; Estene, R. M., Jr.; Jones, R. H. *J. Am. Chem. Soc.* **1949**, *71*, 965.
(173) Keefer, K. D. In *Better Ceramics Through Chemistry*; Brinker, C. J., Clark, D. E., Ulrich, D. R., Eds.; Elsevier: New York, 1984; Vol. 32, p 15.
(174) Zerda, T. W.; Hoang, G. *J. Non-Cryst. Solids*, in press.
(175) Kelm, H., Ed. *High Pressure Chemistry*; Reidel: Dordrecht, 1978.
(176) van Eldik, R., Jones, J., Eds. *High Pressure Chemistry and Biochemistry*; NATO AS Series, 1987; Vol. 197.
(177) Davis, L. P.; Burggraf, L. W. In *Science of Ceramic Chemical Processing*; Hench, L. L., Ulrich, D. R., Eds.; Wiley: New York, 1986; p 400.
(178) Davis, L. P.; Burggraf, L. W. In *Ultrastructure Processing of Advanced Ceramics*; Mackenzie, J. D., Ulrich, D. R., Eds.; Wiley: New York, 1988; p 367.
(179) Davis, L. P. *Mater. Res. Soc. Symp. Proc.* **1986**, *73*, 529.
(180) Davis, L. P. *Chem. Modif. Surf.* **1986**, *1*, 157.
(181) (a) Damrauer, R.; Burggraf, L. W.; Davis, L. P.; Gordon, M. S. *J. Am. Chem. Soc.* **1988**, *110*, 6601. (b) Tandura, S. N.; Voronkov, M. G.; Alekseev, N. V. *Top. Curr. Chem.* **1986**, *131*, 99.

(182) Burggraf, L. W.; Davis, L. P. In *Better Ceramics Through Chemistry II*; Brinker, C. J., Clark, D. E., Ulrich, D. R., Eds.; Materials Research Society: Pittsburgh, PA, 1986; Vol. 73, p 529.
(183) Stewart, J. J. P. Quantum Chemistry Program Exchange, Program 455, Department of Chemistry, Indiana University, Bloomington, IN.
(184) Dewar, M. J. S.; Theil, W. *J. Am. Chem. Soc.* **1977**, *99*, 4899.
(185) Dewar, M. J. S.; Zoebisch, E. G.; Healy, E. F.; Stewardt, J. J. P. *J. Am. Chem. Soc.* **1985**, *107*, 3902.
(186) Dewar, M. J. S.; Healy, E. *Organometallics* **1982**, *1*, 1705.
(187) Frisch, M. J.; et al. GAUSSIAN86; Carnegie-Mellon Quantum Chemistry Publishing Unit, Pittsburgh, PA.
(188) Burggraf, L. W.; Davis, L. P. *Chem. Modif. Surf.* **1986**, *1*, 157.
(189) Holme, T. A.; Gordon, M. S.; Yabushita, S.; Schmidt, M. W. *Organometallics* **1984**, *3*, 583.
(190) Gordon, M. S. *J. Am. Chem. Soc.* **1982**, *104*, 4352.
(191) McKee, M. L.; Lipscomb, W. N. *J. Am. Chem. Soc.* **1981**, *103*, 4673.
(192) Davis, L. P.; Burggraf, L. W.; Gordon, M. S. *J. Am. Chem. Soc.* **1988**, *110*, 3056.
(193) West, J. K.; Wallace, S.; Hench, L. L.; Lishawa, C. R. Quantum Calculations on Sol-Gel Silica Structures. Proceedings of 4th Ultrastructure Processing of Ceramics, Glasses and Composites, Tucson, AZ, 1989.
(194) Davis, L. P.; Burggraf, L. W., personal communication, 1989.
(195) Zerner, M.; et al. Program No. 010183; Quantum Theory Project: Gainesville, FL.
(196) Alexander, J., Ed. *Colloid Chemistry*; Chemical Catalog Co.: New York, 1926; p 783.
(197) Kelts, L. W.; Armstrong, N. J. In *Better Ceramics Through Chemistry III*; Brinker, C. J., Clark, D. E., Ulrich, D. R., Eds.; Materials Research Society: Pittsburgh, PA, 1988; Vol. 121, p 519.
(198) Dorain, P. B.; Rafalko, J. J.; Feeney, J. E.; Carney, R. V.; Che, T. M. In *Better Ceramics Through Chemistry III*; Brinker, C. J., Clark, D. E., Ulrich, D. R., Eds.; Materials Research Society: Pittsburgh, PA, 1988; Vol. 121, p 523.
(199) Boulos, E. N.; Carduner, K. R.; Carter, R. O., III; Best, M. F. In *Better Ceramics Through Chemistry III*; Brinker, C. J., Clark, D. E., Ulrich, D. R., Eds.; Materials Research Society: Pittsburgh, PA, 1988; Vol. 121, p 531.
(200) Assink, R. A.; Kay, B. D. In *Better Ceramics Through Chemistry III*; Brinker, C. J., Clark, D. E., Ulrich, D. R., Eds.; Materials Research Society: Pittsburgh, PA, 1988; Vol. 121, p 25.
(201) Basil, J. D.; Lin, C.-C. In *Better Ceramics Through Chemistry III*; Brinker, C. J., Clark, D. E., Ulrich, D. R., Eds.; Materials Research Society: Pittsburgh, PA, 1988; Vol. 121, p 49.
(202) Bogush, G. H.; Dickstein, G. L.; Lewe, P.; Zukoski, K. C.; Zukoski, C. F. In *Better Ceramics Through Chemistry III*; Brinker, C. J., Clark, D. E., Ulrich, D. R., Eds.; Materials Research Society: Pittsburgh, PA, 1988; Vol. 121, p 57.
(203) McCormick, A. V.; Bell, A. T.; Radke, C. J. In *Better Ceramics Through Chemistry III*; Brinker, C. J., Clark, D. E., Ulrich, D. R., Eds.; Materials Research Society: Pittsburgh, PA, 1988; Vol. 121, p 67.
(204) Peppas, N. A.; Scranton, A. B.; Tsou, A. H.; Edwards, D. E. In *Better Ceramics Through Chemistry III*; Brinker, C. J., Clark, D. E., Ulrich, D. R., Eds.; Materials Research Society: Pittsburgh, PA, 1988; Vol. 121, p 43.
(205) Scherer, G. W. In *Better Ceramics Through Chemistry III*; Brinker, C. J., Clark, D. E., Ulrich, D. R., Eds.; Materials Research Society: Pittsburgh, PA, 1988; Vol. 121, p 179.
(206) Liu, S. *Aging of Gels*; University of Florida Internal Report, 1989.
(207) Kelts, L. W.; Effinger, N. J.; Melpolder, S. M. *J. Non-Cryst. Solids* **1986**, *83*, 353.
(208) Smith, D. M.; Glaves, C. L.; Davis, P. J.; Brinker, C. J. In *Better Ceramics Through Chemistry III*; Brinker, C. J., Clark, D. E., Ulrich, D. R., Eds.; Materials Research Society: Pittsburgh, PA, 1988; Vol. 121, p 657.
(209) Zerda, T. W.; Artaki, I.; Jonas, J. J. *J. Non-Cryst. Solids* **1986**, *81*, 365.
(210) Yoldas, B. E. *J. Mater. Sci.* **1986**, *21*, 1087.
(211) Vysotskii, Z. Z.; Strazhesko, D. N. In *Adsorption and Absorbents*; Strazhesko, D. N., Ed.; Wiley: New York, 1973; No. 1, p 55.
(212) Klimentova, Y. P.; Kiricheko, L. F.; Vysotskii, Z. Z. *Ubr. Khim. Zh.* **1970**, *26*, 49.
(213) Ponomareva, T. P.; Kontorovich, S. I.; Chekanov, N. I.; Schukin, E. D. *Kolloidn. Zh.* **1984**, *46*, 118.
(214) Alexander, G. B.; Broge, E. C.; Iler, R. K. U.S. Patent No. 2,765,242, Du Pont, 1956.
(215) Sheinfain, R. Yu.; Stas, O. P.; Neimark, I. E. *Kolloidn. Zh.* **1965**, *27*, 916.
(216) van der Grift, C. J. G.; Geus, J. W.; Barten, H.; Leferink, R. G. I.; van Miltenburg, J. C.; den Ouden, A. T. *Characterization of Porous Solids*; Elsevier: Amsterdam, 1988; p 619.
(217) Okkerse, C.; de Boer, J. H. In *Reactivity of Solids*; de Boer, J. H., Ed.; Elsevier: Amsterdam, 1960; p 240.
(218) Girgis, B. S. *Z. Phys. Chem.* **1973**, *83*, 75.
(219) Brinker, C. J. In Proceedings of 4th Ultrastructure Conference, Tucson, AZ; Wiley: New York, in press.
(220) West, J. K.; Nikles, R.; LaTorre, G. In *Better Ceramics Through Chemistry III*; Brinker, C. J., Clark, D. E., Ulrich, D. R., Eds.; Materials Research Society: Pittsburgh, PA, 1988; Vol. 121, p 219.
(221) Pardenek, S. A.; Flemming, J. W.; Klein, L. C. In *Ultrastructure Processing of Advanced Ceramics*; Mackenzie, J. D., Ulrich, D. R., Eds.; Wiley: New York, 1988; p 379.
(222) Dumas, J.; Quinson, J. F.; Bovier, C.; Baza, S.; Serughetti, J. *J. Non-Cryst. Solids* **1986**, *82*, 220.
(223) Sherwood, T. K. *Ind. Eng. Chem.* **1929**, *21*, 12.
(224) Sherwood, T. K. *Ind. Eng. Chem.* **1930**, *22*, 132.
(225) Sherwood, T. K. *Ind. Eng. Chem.* **1929**, *21*, 976.
(226) Keey, R. B. *Drying, Principles and Practice*; Pergamon Press: New York, 1972.
(227) Mujumdar, A. S., Ed. *Advances in Drying*; Hemisphere: New York, 1980; Vol. 1.
(228) Mujumdar, A. S., Ed. *Advances in Drying*; Hemisphere: New York, 1983; Vol. 2.
(229) Moore, F. *Trans. Brit. Ceram. Soc.* **1961**, *60*, 517.
(230) Whitaker, S. *Adv. Heat Transfer* **1977**, *13*, 119.
(231) Cooper, A. R. In *Ceramics Processing Before Firing*; Onoda, G. Y., Jr., Hench, L. L., Eds.; Wiley: New York, 1978; p 261.
(232) Ford, R. W. *Ceramics Drying*; Pergamon: New York, 1986.
(233) Scherer, G. W. Proceedings of IVth Ultrastructure Conference, Tucson, AZ; Wiley: New York, 1989.
(234) Kawaguchi, T.; Jura, J.; Taneda, N.; Hishikura, H.; Kokubu, Y. *J. Non-Cryst. Solids* **1986**, *82*, 50.
(235) Dwivedi, R. K. *J. Mater. Sci. Lett.* **1986**, *5*, 373.
(236) Macey, H. H. *Trans. Brit. Ceram. Soc.* **1942**, *41*, 73.
(237) Wilson, M. J. R. Drying Kinetics of Pure Silica Xerogels. Masters Theses, University of Florida, Gainesville, FL, 1989.
(238) Wilson, M. J. R.; Hench, L. L. Real Time Monitoring of Silica Gel Drying Behavior. Proceedings of 4th International Conference on Ultrastructure Processing of Ceramics, Glasses, and Composites; Tucson, AZ, 1989.
(239) Wilson, M. J. R.; Hench, L. L. Drying of Gel Silica Monoliths. Submitted to *J. Non-Cryst. Solids*.
(240) Clews, F. H. *Heavy Clay Technology*; Academic Press: New York, 1969.
(241) Whitaker, S. In *Advances in Drying*; Mujumdar, A. S., Ed.; Hemisphere: New York, 1980; Vol. 1, p 23.
(242) Fortes, M.; Okos, M. R. In *Advances in Drying*; Mujumdar, A. S., Ed.; Hemisphere: New York, 1980; Vol. 1, p 119.
(243) Bruin, S.; Luyben, K. Ch. A. M. In *Advances in Drying*; Mujamdar, a. S., Ed.; Hemisphere: New York, 1980; Vol. 1, p 155.
(244) van Brakel, J. In *Advances in Drying*; Mujumdar, A. S., Ed.; Hemisphere: New York, 1980; Vol. 1, p 217.
(245) Wallace, S.; Hench, L. L. In *Better Ceramics Through Chemistry III*; Brinker, C. J., Clark, D. E., Ulrich, D. R., Eds.; Materials Research Society: Pittsburgh, PA, 1988; Vol. 121, p 355.
(246) Wallace, S.; Hench, L. L. In *Ultrastructure Processing of Advanced Ceramics*; Mackenzie, J. D., Ulrich, D. R., Eds.; Wiley: New York, 1988; p 873.
(247) Wallace, S.; Hench, L. L. In Proceedings of 4th Ultrastructure Conference, 1989, Tucson, AZ; Wiley: New York, in press.
(248) Klier, K.; Zettlemoyer, A. C. *J. Colloid Interface Sci.* **1977**, *58*, 216.
(249) Guerin, V. These de Docteur Ingenier, Mulhouse, France, 1983.
(250) Zhuravlev, L. T. *Langmuir* **1987**, *3*, 316.
(251) Vasconcelos, W. Topological Analysis of Densification of Silica Gels. Ph.D. Dissertation, University of Florida, Gainesville, FL, 1989.
(252) Wallace, S. Structure of Silica Gel Monoliths and Water. Ph.D. Dissertation, University of Florida, Gainesville, FL, 1990.
(253) Pfeifer, P.; Avnir, D.; Farin, D. *J. Stat. Phys.* **1984**, *36*, 699.
(254) Rojanski, D.; Farin, D.; Avnir, D. *Phys. Rev. Lett.* **1986**, *56*, 2505.
(255) Shaw, T. M. In *Better Ceramics Through Chemistry II*; Brinker, C. J., Clark, D. E., Ulrich, D. R., Eds.; Materials Research Society: Pittsburgh, PA, 1986; Vol. 73, p 215.
(256) Susa, K.; Matsuyama, I.; Saton, S.; Suganuma, T. *J. Non-Cryst. Solids* **1986**, *79*, 165.
(257) Hair, M. L.; Hertle, W. *J. Phys. Chem.* **1968**, *72*, 2372.
(258) Kiselev, A. V.; Lygin, V. I. *Infrared Spectra of Surface Compounds*; Keter Publishing House Jerusalem Ltd.; Wiley: New York, 1975.
(259) Snyder, L. R.; Ward, J. W. *J. Phys. Chem.* **1966**, *70*, 3941.
(260) Hench, L. L.; Wang, S. H. The Sol-Gel Glass Transformation of Silica. *Phase Transform.*, in press.

(261) Young, G. J. *J. Colloid Sci.* **1958**, *13*, 67.
(262) Benesi, H. A.; Jones, A. C. *J. Phys. Chem.* **1957**, *63*, 179.
(263) Hockey, J. A.; Pethica, B. A. *Trans. Faraday Soc.* **1961**, *57*, 2247.
(264) Kieselev, A. V. *Structure and Properties of Porous Materials*; Colston Papers; Butterworth: London, 1958; Vol. 10, p 195.
(265) McDonald, R. S. *J. Phys. Chem.* **1958**, *62*, 1168.
(266) Wang, S. H. Sol–Gel Derived Silica Optics. Ph.D. Dissertation, University of Florida, Gainesville, FL, 1988.
(267) Phalippou, J.; Woignier, T.; Zarzycki, J. In *Ultrastructure Processing of Ceramics, Glasses and Composites*; Hench, L. L., ulrich, D. R., Eds.; Wiley: New York, 1984; p 70.
(268) Hair, M. L. *Infrared Spectroscopy in Surface Chemistry*; Dekker: New York, 1967.
(269) Anderson, J. H., Jr.; Wickersheim, K. A. *Surf. Sci.* **1964**, *2*, 252.
(270) Peri, J. B. *J. Phys. Chem.* **1966**, *70*, 2937.
(271) Cant, N. W.; Little, L. H. *Can. J. Chem.* **1965**, *43*, 1252.
(272) Cant, N. W.; Little, L. H. *Can. J. Chem.* **1964**, *42*, 802.
(273) Hair, M. L.; Chapman, I. D. *J. Am. Ceram. Soc.* **1966**, *49*, 651.
(274) Elmer, T. H.; Chapman, I. D.; Nordberg, M. E. *J. Phys. Chem.* **1962**, *66*, 1517.
(275) Keck, D. B.; Maurer, R. D.; Schultz, P. C. *Appl. Phys. Lett.* **1973**, *22*, 307.
(276) Basila, M. R. *J. Chem. Phys.* **1961**, *35*, 1151.
(277) Davydov, V. Y.; Zhuravelev; Kiselev, A. V. *Trans. Faraday Soc.* **1964**, *60*, 2254.
(278) Zhu, B. F.; Wang, F.; Hench, L. L. Dilatometry of Gel Silica. Proceedings of 4th Ultrastructure Processing of Ceramics, Glasses and Composites, Tucson, AZ, 1989.
(279) Brinker, C. J.; Bunker, B. C.; Tallant, D. R.; Ward, K. J. *J. Chim. Phys.* **1986**, *83*, 851.
(280) Brinker, C. J.; Tallant, D. R.; Roth, E. P.; Ashley, C. S. *Mater. Res. Soc. Symp.* **1986**, *61*, 387.
(281) Tallant, D. R.; Bunker, B. C.; Brinker, C. J.; Balfe, C. A. In *Better Ceramics Through Chemistry II*; Brinker, C. J., Clar, D. E., Ulrich, D. R., Eds.; Materials Research Society: Pittsburgh, PA, 1986; Vol. 73, p 261.
(282) Brinker, C. J.; Kirkpatrick, R. J.; Tallant, D. R.; Bunker, B. C.; Montez, B. *J. Non-Cryst. Solids* **1988**, *99*, 418.
(283) Brinker, C. J.; Brow, R. K.f Tallant, D. R.; Kirkpatrick, R. *Mater. Res. Soc. Symp.* **1988**, *105*, 289.
(284) O'Keffe, M.: Gibbs, G. V. *J. Chem. Phys.* **1984**, *81*, 876.
(285) Galeener, F. L. *Solid State Commun.* **1982**, *44*, 1037.
(286) Brinker, C. J.; Tallant, D. R.; Roth, E. P.; Ashley, C. S. *J. Non-Cryst. Solids* **1986**, *82*, 117.
(287) Wallace, S.; Hench, L. L., private communication, 1989.
(288) West, J. K.; Zhu, B. F.; Cheng, Y. C.; Hench, L. L. Theoretical and Experimental Studies on Water Adsorption Onto Sol–Gel Silica. In press.
(289) Takahashi, K. *J. Chem. Soc., Faraday Trans. 1* **1982**, *78*, 2059.
(290) Zerner, M. C.; Loew, G. H.; Kirchner, R. F.; Mueller-Westerhoff, U. T. *J. Am. Chem. Soc.* **1980**, *102*, 589.
(291) Mukherjee, S. P.; Zarzycki, J.; Traverse, J. P. *J. Non-Cryst. Solids* **1976**, *11*, 341.
(292) Decottignies, M.; Phalippou, J.; Zarzycki, J. *C. R. Acad. Sci.* **1977**, *285*, C265.
(293) Decottignies, M.; Mukherjee, S.; Phalippou, J.; Zarzycki, J. *C. R. Acad. Sci.* **1977**, *285*, C289.
(294) Decottignies, M.; Phalippou, J.; Zarzycki, J. *J. Mater. Sci.* **1978**, *13*, 2605.
(295) Jabra, R.; Phalippou, J.; Zarzycki, J. *Rev. Chim. Miner.* **1979**, *16*, 245.
(296) Jabra, R.; Phalippou, J.; Zarzycki, J. *J. Non-Cryst. Solids* **1980**, *42*, 489.
(297) Klein, L. C.; Gallo, T. A.; Garvey, G. J. *J. Non-Cryst. Solids* **1984**, *63*, 23.
(298) Kawaguchi, T.; Hishikura, H.; Iura, J.; Kokubu, Y. *J. Non-Cryst. Solids* **1984**, *63*, 61.
(299) Klein, L. C.; Garvey, G. J. In *Ultrastructure Processing of Ceramics, Glasses and Composites*; Hench, L. L., Ulrich, D. R., Eds.; Wiley: New York, 1984; p 88.
(300) Krol, D. M.; van Lierop, J. G. *J. Non-Cryst. Solids* **1984**, *63*, 131.
(301) Yamane, M.; Aso, S.; Sakano, T. *J. Mater. Sci.* **1979**, *14*, 607.
(302) Matsuyama, I.; Susa, K.; Satoh, S.; Suganuma, T. *J. Am. Ceram. Bull.* **1984**, *63*, 1408.
(303) Gallo, T. A.; Klein, L. C. *J. Non-Cryst. Solids* **1986**, *82*, 198.
(304) Quinson, J. F.; Dumas, J.; Serughetti, J. *Proceedings of the 3rd International Conference on Non-Crystalline Solids*; Janot, C., Wright, A. F., Eds.; Physique: Paris, 1985.
(305) Duran, A.; Serna, C.; Fornes, V.; Fernandez Navarro, J. M. *J. Non-Cryst. Solids* **1986**, *82*, 69.
(306) Gallo, T. A.; Brinker, C. J.; Klein, L. C.; Scherer, G. W. In *Better Ceramics Through Chemistry*; Brinker, C. J., Clark, D. E., Ulrich, D. R., Eds.; Materials Research Society: Elsevier: New York, 1985; p 85.
(307) Brinker, C. J.; Roth, E. P.; Tallant, D. R.; Scherer, G. W. In *Science of Ceramic Chemical Processing*; Hench, L. L., Ulrich, D. R., Eds.; Wiley: New York, 1986; p 37.
(308) Phalippou, J.; Prassas, M.; Zarzycki, J. *Verres Refract.* **1981**, *35*, 975.
(309) Yamane, M.; Okano, S. *Yogyo-Kyokai-Shi* **1979**, *87*, 56.
(310) Gottardi, V.; Guglielmi, M.; Bertoluzza, A.; Magano, C.; Morelli, M. A. *J. Non-Cryst. Solids* **1984**, *63*, 71.
(311) Brinker, C. J.; Roth, E. P.; Scherer, G. W.; Tallant, D. R. *J. Non-Cryst. Solids* **1985**, *71*, 171.
(312) Brinker, C. J.; Scherer, G. W.; Roth, E. P. *J. Non-Cryst. Solids* **1985**, *72*, 345.
(313) Brinker, C. J.; Tallant, D. R.; Roth, E. P.; Ashley, C. H. In *Materials Research Society Symposium*; Elsevier: New York, 1986; Vol. 61, p 387.
(314) Frenkel, J. *J. Phys.* **1945**, *9*, 385.
(315) Scherer, G. W. *J. Am. Ceram. Soc.* **1977**, *60*, 236.
(316) Mackenzie, J. D.; Shuttleworth, R. *Proc. Phys. Soc., London* **1949**, *62*, 833.
(317) Scherer, G. W.; Brinker, C. J.; Roth, E. P. *J. Non-Cryst. Solids* **1985**, *72*, 369.
(318) Rhines, F. N. *Plansee Proc., 3rd Seminar, Reutte, Tyrol* **1958**, 58.
(319) Rhines, F. N.; DeHoff, R. T.; Kronsbein, J. *A Topological Study of the Sintering Process*; Final Report for the US Atomic Energy Commission, 1969.
(320) Rhines, F. N.; DeHoff, R. T. In *Sintering and Homogeneous Catalysis*; Kuczynski, G. C., Miller, A. E., Sargent, G. A., Eds.; Plenum: New York, 1984; p 49.
(321) DeHoff, R. T. In *Quantitative Microscopy*; DeHoff, R. T., Rhines, F. N., Eds.; McGraw-Hill: New York, 1968; p 291.
(322) DeHoff, R. T. In *Encyclopedia of Materials Science and Engineering*; Bever, M. B., Ed.; Pergamon: Oxford, 1986; p 4633.
(323) Hench, L. L.; Vasconcelos, W. Structure Properties Relations in Gel Silica and Gel Glass Monoliths. *Ann. Rev. Mater. Sci.*, in press.
(324) Flory, P. J. In *Science of Ceramic Chemical Processing*; Hench, L. L., Ulrich, D. R., Eds.; Wiley: New York, 1986; p 415.
(325) Pierre, A. C. Proceedings of 4th International Conference on Ultrastructure Processing of Ceramic, Glasses, and Composites; Tucson, AZ, 1989.
(326) Gottardi, V.; Guglielmi, M.; Bertolugza, A.; Fagnano, C.; Morelli, M. A. *J. Non-Cryst. Solids* **1982**, *48*, 117; **1984**, *63*, 71.
(327) Krol, D. M.; van Lierop, J. G. *J. Non-Cryst. Solids* **1984**, *63*, 131.
(328) Krol, D. M.; Mulder, C. A. M.; van Lierop, J. G. *J. Non-Cryst. Solids* **1986**, *86*, 241.
(329) Mulder, C. A. M.; Damin, A. A. J. M. *J. Non-Cryst. Solids* **1987**, *93*, 387; **1987**, *95/96*, 303.
(330) Rousset, J. L.; Duval, E.; Boukenter, A.; Champagnon, B.; Monteil, A.; Serughetti, J.; Dumas, J. *J. Non-Cryst. Solids* **1988**, *107*, 27.
(331) Vacher, R. In *Annual Review of Materials Science*; Huggins, R. A., Giordmaine, J. A., Wachtman, J. B., Jr., Eds.; Annual Reviews, Inc.: Palo Alto, CA, 1989; p 509.
(332) Shoup, R.; Hagy, H. *Opt. News*, Paper FE2; Optical Society of America: Orlando, FL, 1989; p A-93.
(333) Bachman, P. K.; Geittner, P.; Krafizynk, E.; Lydtin, H.; Romanowski, G. *Ceram. Bull.* **1989**, *68*(10), 1826.
(334) Birchall, J. D. In *New Trends in Bio-Inorganic Chemistry*; Williams, R. J. P., DaSilva, J. R. R. F., Eds.; Academic Press: New York, 1978; p 210.
(335) Williams, R. J. P. *Silicon Biochemistry*; CIBA Foundation Symposium 121; Wiley: New York, 1986.
(336) Carlisle, E. *J. Nutr.* **1976**, *106*(4), 478.
(337) Hench, L. L. *J. Biomed. Mater. Res.* **1989**, *23*, 685.